ELECTROCHEMICAL PROMOTION OF PT CATALYSTS FOR GAS PHASE REACTIONS

PAR

Arnaud JACCOUD

ingénieur chimiste diplômé EPF
de nationalité suisse et originaire de Chexbres (VD)

EPFL

ÉCOLE POLYTECHNIQUE
FÉDÉRALE DE LAUSANNE

Suisse
2007

Remerciements

Par ces quelques lignes, j'aimerais exprimer toute ma reconnaissance à mon Directeur de thèse, le Professeur Christos Comninellis pour m'avoir accueilli dans son groupe de recherche. Il a toujours été là pour m'écouter, me conseiller et sans lui, je n'aurais sans doute jamais commencé une thèse à l'EPFL.

J'aimerais également remercier chaleureusement mon co-Directeur de thèse, György Fóti pour son aide inestimable. Il a su m'encourager, en faisant preuve de beaucoup de patience et sans lui, j'aurais sans doute terminé ma thèse, mais beaucoup plus tard…

I would like to thank the other members of the jury, Prof. U. Von Stockar, Prof. I. Riess, Prof. C. G. Vayenas and Prof. V. Hatzimanikatis. I wish to address my very special gratitude to Prof. Vayenas for its precious encouragements and advices.

In addition, many thanks go to Prof. M. A. Rodrigo and Prof. L. Gauckler for their very useful collaboration and expertise.

Ce travail a été possible grâce à l'aide de Carole, Stéphanie, Méri, Alexandre et Costas. Je tiens également à remercier Mme Margot, G. Bovard, J.-C. Rapit, Eddy, PAP, H. Jotterand et N. Xanthopoulos pour leur disponibilité et leur bonne humeur.

Merci à tous les chimistes, et pas si chimistes que ça, que j'ai croisés au GGEC, dans les couloirs de l'EPFL et aux fêtes. Alain (p'tite pause à l'Arcad'?), Guillaume (St-Malo et adaptateur 12V), Carole, Bahaa (collègue Roustom), Mariam (monday night fever), Flop, Carla et Oliv.
Merci également à Aga, Gabriele, Erika, Julian, Stéphane, Meryem, Cyril, Mickaël, Pietro, César, Lassiné, Ivan, David, Jojo, Elena, Béatrice, Ilaria, Justyna et Lahsen qui ont su donner au labo une ambiance chaleureuse.

J'en profite pour remercier ceux avec qui j'ai passé des journées sur la neige et des soirées au B'Bar (R.I.P.) : Payot (tartiflette au p'tit déj' et night session aux Crosets), Ahriel (le visual alchemist), Kiki (mondial du snowscout aux Diables), Stef, Steph, Baudin, Léona, Stef, Pamela et Guegré (encore merci pour le squat et les bons délires), Mic, Raph, Fenek,

Leresche, Edy, Yogi, Thomas, Lambert, Jules et aussi ceux du team, des Diables, de Villars et des Crosets.

Aux scouts, Looping (ma määän Lumpi), Murdock (Breilll), Nat (Loutre), Camille (les Posses reprezent), Dom, Knopf (Hutchinson), Pomme, Juan et Sophie.

A Vincent (couz'), Maureen (ceinture noire), Géraldine (disco fever), Sylvie (bullshit et piscola), Cléo (marcassin) et Giz (viva BCN).

A mes colocs, Bibu (Capitaine Palonnier), Eliz (Reine du château), DJ Greengiant (Royal Flush), GR ! (42,195 km), Webb (Krrr), DJ Mitch (Nobel Prize) et Martino (Bang Bang).

Aux autres "morgiens": Saugy (son qui frue), Alexandra (clash de tartes aux pommes), Moody (body rockin'), Latifeh (save the world), Amjad (10m de Belerive à 3am), Rakel (mais bouffez-le!), Ader, Gaël, Céline, Ya (till late), Karlito et Tranbert.

A mes parents, pour m'avoir toujours soutenu et donné de quoi passer les meilleures années de ma vie, pour m'avoir permis de voyager, de rider et d'aller faire des cabanes dans la forêt.

A mes grands-parents pour leur soutient, leurs encouragements et pour m'attraper quand je me fais croquer par des animaux sauvages.

A mes frèros, Alexandre pour m'avoir montré ce qui compte vraiment dans une vie (de teenager) : les ollies, les backflips, Run DMC, se déguiser en Starsky et chiller en cox rose.
Et Maxime pour toutes les incroyables sessions (Rathvel powpow, les doublettes au glacier), les Fluo Flash Fun, les kilomètres de route tracés ensemble, les documentaires animaliers, les rodeos backs, les stickers BS7 et "Très Chasse" à 3 heures du mat'.

Merci de tout cœur

Abstract

The subject of this work is the study of the electrochemical promotion of catalysis (EPOC), also called non-Faradaic electrochemical modification of catalytic activity (NEMCA). In this phenomenon, application of small currents or potentials on catalysts in contact with solid electrolytes leads to very pronounced strongly non-Faradaic and reversible changes in catalytic activity and selectivity.

This work concerns the system composed of platinum film electrodes, deposited on the YSZ electrolyte (ZrO_2 doped with 8% Y_2O_3), in contact with an oxygen containing atmosphere (the $O_{2(g)}$,Pt/YSZ system).

The aim of this work was to focus on two points in the phenomenon of EPOC: 1) The nature of the species present on the surface of the catalyst and their impact on the catalytic activity. 2) The phenomenon of permanent promotion of catalysis (P-EPOC), for which the catalytic rate enhancement is not totally reversible, leading to a long lasting activated state.

The Pt electrodes were prepared via three different methods (sputtering, thermal decomposition and screen-printing) and, as expected, the resulting microstructure, observed by scanning electron microscopy (SEM), was found to depend greatly on the preparation technique. The electrochemical response of each electrode was characterized by the technique of cyclic voltammetry. Due to the occurrence of different site-related electrochemical reactions, the voltammogram shape was highly influenced by the microstructure of the Pt/YSZ contact.

Based on the preliminary studies, the cermet electrode was chosen for additional electrochemical experiments, using chronoamperometry, chronopotentiometry, cyclic voltammetry, steady state polarization and impedance spectroscopy. The results of all these techniques suggest that under anodic polarization, two parallel reactions take place. The first reaction is the oxygen evolution, giving rise to a steady state current under a constant applied potential. The other reaction is the oxygen storage (oxygen injection) in the form of Pt-O species. This second process gives rise to a time dependant current under a constant applied potential, and is therefore responsible for the pseudocapacitive behavior of the electrode. Moreover, linear sweep voltammetry measurements indicated that, by application of an anodic potential, at least three types of Pt-O species were stored, following distinct kinetics. Based on the amount of stored Pt-O and on the corresponding storage kinetics, they were attributed to three different locations on the electrode:

1) at the Pt/YSZ interface, 2) diffusing from the tpb toward the Pt/gas interface, 3) diffusing from the Pt/YSZ interface toward the bulk of the platinum electrode.

It has been shown that the Pt film exhibited various activity states toward the catalytic oxidation of ethylene, depending on the oxygen species present at its surface. As evidenced by XPS measurements and in agreement with the thermodynamic data for the given system, the inactive (deactivated) state has been attributed to the formation of surface platinum oxide at $T > 550°C$. Decreasing the reaction temperature to $525°C$ caused the slow spontaneous reactivation of the catalyst and several days were necessary to reach the active state, where most of the catalyst was present in its metallic state. The catalyst activity recovery could be accelerated by the application of anodic potential pulses. In agreement with the mechanism of EPOC, this was explained by the oxide destabilizing effect of the anodically produced $O^{\delta-}$ species.

Anodic polarization also caused reversible electrochemical promotion of catalysis at unusual high temperature ($600°C$). In addition, very intriguing catalytic relaxation transients were observed after prolonged anodic polarization times. Indeed, it was found that enhanced catalytic activity could be maintained for up to 10 hours after current interruption.

Combination of these latter results, the related literature, the state of the art model of EPOC, and the results obtained by electrochemical techniques led to the proposition of an original model based on the processes of Pt-O storage/release at various locations of the $O_{2(g)}$,Pt/YSZ system.

According to this model, anodic polarization produces $O^{\delta-}$ back-spillover species, promoting the catalytic activity, in agreement with the mechanism of EPOC. In parallel, hidden oxygen species are stored at the Pt/YSZ interface and diffuse toward the Pt phase. When the polarization is switched off, these hidden oxygen species diffuse to the gas-exposed surface and cause non-Faradaic promotion, as back-spillover $O^{\delta-}$ do. The large amount of stored charge and its slow diffusion controlled emergence causes the rate enhancement to last for hours.

Keywords

Version abrégée

Le sujet de ce travail est l'étude de la promotion électrochimique de la catalyse (EPOC), également appelée la modification électrochimique non-Faradique de l'activité catalytique (NEMCA). Dans ce phénomène, l'application de courants ou potentiels faibles à des catalyseurs en contact avec un électrolyte solide conduit à d'importants effets sur leur activité catalytique et leur sélectivité. Ces effets sont souvent réversibles et fortement non-Faradiques.

Ce travail traite du système composé d'électrodes, sous forme de films de platine, déposés sur l'électrolyte YSZ (ZrO_2 dopé par 8% Y_2O_3), en contact avec une atmosphère contenant de l'oxygène (le système $O_{2(g)}$,Pt/YSZ).

Le but de ce travail était de se concentrer sur deux points du phénomène : 1) la nature des espèces présentes sur la surface du catalyseur et leur impact sur l'activité catalytique. 2) le phénomène de promotion permanente de la catalyse (P-EPOC), lors duquel l'augmentation de la vitesse de réaction catalytique n'est pas totalement réversible et conduit à des états activés persistants.

Les électrodes de platine ont été préparées selon trois méthodes (pulvérisation, décomposition thermique et sérigraphie) et, comme prévu, la méthode de déposition de l'électrode a eu une grande influence sur sa microstructure. Celle-ci a été observée par microscopie électronique à balayage (SEM). Le comportement électrochimique de chaque électrode a été caractérisé par voltamétrie cyclique. Dû au fait que des réactions électrochimiques se produisent à des sites géométriquement différents de l'électrode, la forme des voltamogrammes était fortement influencée par sa microstructure. Sur la base de ces études préliminaires, l'électrode de type "cermet" a été choisie pour d'autres mesures électrochimiques (chronoamperométrie, chronopotentiométrie, voltamétrie cyclique, polarisation stationnaire et spectrométrie d'impédance). Les résultats de toutes ces techniques indiquent que deux réactions électrochimiques parallèles se produisent sous polarisation anodique. La première réaction est le dégagement d'oxygène, générant un courant stationnaire par l'application d'un potentiel constant. L'autre réaction est le stockage d'oxygène (injection d'oxygène) sous la forme d'une espèce Pt-O. Cette second réaction génère un courant transitoire par l'application d'un potentiel constant. Elle est responsable du comportement pseudocapacitif de l'électrode.

De plus, des mesures de voltamétrie à balayage linéaire ont montré que par l'application d'un potentiel anodique, au moins trois types d'espèces Pt-O étaient stockées, suivant des

cinétiques différentes. En se basant sur les quantités de Pt-O stockés et sur les différentes cinétique de stockage, ces espèces furent attribuées à trois emplacements de l'électrode ; 1) à l'interface Pt/YSZ, 2) diffusant de l'interface triple (tpb) vers l'interface Pt/gaz, 3) diffusant de l'interface Pt/YSZ vers l'intérieur de l'électrode platine.

Nous avons observés différents états d'activité du film de platine pour l'oxydation catalytique de l'éthylène. Ils furent liés aux différentes espèces d'oxygène présentes à sa surface. En accord avec les mesures XPS et avec les données thermodynamiques du système, l'état désactivé a été attribué à la formation d'oxydes de platine à la surface à $T > 550°C$. Le fait de diminuer la température à 525°C, a causé la lente réactivation spontanée du catalyseur et plusieurs jours ont été nécessaires pour atteindre l'état activé, où la surface du catalyseur était principalement métallique. La réactivation du catalyseur a pu être accélérée par l'application d'impulsions de potentiel anodique. En accord avec le mécanisme de la promotion électrochimique, cela a été expliqué par le fait que les espèces $O^{\delta-}$, produites anodiquement, tendent à déstabiliser l'oxyde.

L'application d'une polarisation anodique a également provoqué la promotion électrochimique réversible jusqu'à des températures étonnamment élevées (600°C). De plus, de très intriguant transitoires de relaxation ont été observés après des longs temps de polarisation anodique. En effet, une activité catalytique promue a ainsi pu être maintenue plus de 10 heures après avoir coupé le courant.

En combinant ces résultats, les données bibliographiques, le model actuel de la promotion électrochimique, et les mesures électrochimiques, nous avons proposé un modèle basé sur les processus de stockage/déstockage de Pt-O à différents emplacement du système $O_{2(g)}$,Pt/YSZ.

Selon le modèle proposé, la polarisation anodique produit des espèces *back-spillover* $O^{\delta-}$, qui promeuvent l'activité catalytique, en accord avec le mécanisme classique de la promotion électrochimique. En parallèle, des espèces Pt-O sont stockées à l'interface Pt/YSZ et diffusent vers la phase de Pt. Quand le polarisation est coupée, ces espèces cachées diffusent vers la surface exposée au gaz et causent une promotion non-Faradique, comme le font les *back-spillovers* $O^{\delta-}$. Le nombre important d'espèces stockées et leur lente émergence, contrôlée par la diffusion, conduisent à une promotion de l'activité catalytique qui dure plusieurs heures.

Mots clés

Promotion électrochimique de la catalyse (EPOC), Electrodes de platine; électrolyte solide; YSZ; EPOC permanent; voltamétrie cyclique; chronoamperométrie; stockage d'oxygène; oxydes de platine.

Contents

CHAPTER 1
Introduction, motivations and objectives

The subject of this thesis is the electrochemical promotion of catalysis (EPOC) also called non-Faradaic electrochemical modification of catalytic activity (NEMCA). In this phenomenon, application of small currents or potentials on catalysts in contact with solid electrolytes leads to very pronounced strongly non-Faradaic and reversible changes in catalytic activity and selectivity. In other terms, it is the modification of the catalytic activity of a material (a metal or a metal oxide), in contact with a solid electrolyte, by the application of an electrical polarization.

This theoretically challenging phenomenon was discovered in the 1980s by C. G. Vayenas and co-workers. It is an interdisciplinary subject involving at least five different fields: catalysis, surface science, electrochemistry, solid-state ionics and chemical reaction engineering. Today, several research groups all over the world are studying this effect, and it has been demonstrated that it is not limited to any particular electrolyte, conductive catalyst, or type of reaction [1]. Recently, the practical utilization of EPOC in automotive exhaust units was encouraged by the successful tests of a monolithic type electrochemically promoted catalytic reactor (MEPR) for hydrocarbon oxidation and lean burn NO reduction [2, 3].

EPOC has been extensively studied during the last decade, bringing new challenges, but also new insight into the fields of heterogeneous catalysis, solid-state electrochemistry and surface science. In particular, investigations into the mechanism and origin of EPOC have already made an enormous contribution to the understanding of related phenomena in heterogeneous catalysis, such as promotion and metal-support interactions. It has been established that promotion and electrochemical promotion are both linked by the phenomena of spillover and back-spillover.

These studies led to the development of a model interpreting the origin of the phenomenon. The state of the art mechanism of EPOC is based on the promoting effect of electrochemically produced species, back-spilling over the catalyst surface, altering its work function, the latter being a key property in heterogeneous catalysis. The prefix "back" means that the species spills from the support toward the metal surface, in contrast to the original spillover phenomenon found in heterogeneous catalysis. This mechanism of EPOC allowed interpreting many results on various catalyst materials, supported by different electrolyte types. However, some aspects of the phenomenon of EPOC are still ambiguous and constitute challenges for fundamental research in the fields concerned.

The present work focuses on two of these issues:

1)   The nature of the species present on the surface of the catalyst and their impact on the catalytic activity. In the present case of YSZ supported Pt films, the involved species are oxygen atoms of different kinds: oxidic, chemisorbed or back-spillover. These oxygen species can originate directly from the gas phase via chemisorption or they can be produced via electrochemical reactions.

2)   The phenomenon of permanent promotion of catalysis (P-EPOC), for which the catalytic rate enhancement is not totally reversible, leading to a permanent activated state. The permanent phenomenon has been reported for various catalyst materials [4-9] supported by the YSZ electrolyte. However, its mechanism is not fully understood and hardly interpreted by the mechanism of EPOC.

This work constitutes part of the investigations that have been conducted in our laboratory over the last decade [5, 8, 10-21]. It concerns the system composed of platinum film electrodes, deposited on the YSZ electrolyte, in contact with an oxygen containing atmosphere (the $O_{2(g)}$,Pt/YSZ system). It is probably the most widely studied system in

solid-state electrochemistry, due to its use in devices such as solid oxide fuel cells and gas sensors.

The abundant literature on this system, along with the original results presented in this work, will aim to clarify the two ambiguous issues.

In chapter 2, bibliography on these key issues is presented. It focuses on the different oxygen species reported to be found on the platinum surface, and on their effects on catalysis. In particular, we concentrate on the surface platinum oxides and their still unclear nature and effects. In addition, literature dealing with the redox reactions occurring on the $O_{2(g)}$,Pt/YSZ system under polarization is reviewed. It focuses on the diversity of the proposed mechanisms and kinetics. Finally, literature on the phenomenon of EPOC and its mechanism is summarized, with particular attention to the permanent phenomenon.

In chapter 3, preliminary studies using scanning electron microscopy (SEM) are conducted to investigate the effect of the electrode preparation on the resulting microstructure. In addition, cyclic voltammetry in 20kPa O_2 at 450°C is used to evaluate the influence of the microstructure on the electrochemical response of the electrode. Cyclic voltammetry should reveal the typical features of the $O_{2(g)}$,Pt/YSZ system in the form of current peaks in the voltammogram.

In chapter 4, various electrochemical techniques are performed on the system to study its response to anodic and cathodic polarization. These techniques are chronoamperometry, chronopotentiometry, cyclic voltammetry, steady state polarization and impedance spectroscopy. Both the transient and the steady state electrochemical responses are discussed in order to propose a global reaction mechanism. In particular, emphasis is placed on the effect of prolonged anodic polarization (hours).

In chapter 5, ethylene is added to the gas mixture and the catalytic activity of the YSZ supported Pt surface toward ethylene oxidation is measured. The presence of various oxygen species on the Pt film surface is expected to have a strong impact on the global catalytic activity, especially under the influence of electrical polarization.

Chapter 6 reviews the principal outcomes of the thesis, focusing on the link between the results and on their originality. In addition, some major perspectives are proposed.

1.1   References

1   C. G. Vayenas, S. Bebelis, C. Pliangos, S. Brosda, D. Tsiplakides, Electrochemical Activation of Catalysis: Promotion, Electrochemical Promotion, and Metal-Support Interactions (Kluwer Academic / Plenum Publishers, New York, 2001)

2   D. Tsiplakides, S. Balomenou, A. Katsaounis, D. Archonta, C. Koutsodontis, C. G. Vayenas, Catal. Today 100 (2005) 133

3   S. P. Balomenou, D. Tsiplakides, A. Katsaounis, S. Brosda, A. Hammad, G. Foti, C. Comninellis, S. Thiemann-Handler, B. Cramer, C. G. Vayenas, Solid State Ionics 177 (2006) 2201

4   E. A. Baranova, G. Foti, C. Comninellis, Electrochem. Comm. 6 (2004) 389

5   G. Foti, O. Lavanchy, C. Comninellis, J. Appl. Electrochem. 30 (2000) 1223

6   J. Nicole, C. Comninellis, Solid State Ionics 136-137 (2000) 687

7   J. Nicole, C. Comninellis, Proceedings of The 1997 Joint International Meeting 97-2 (1997)

8   S. Wodiunig, Electrochemical Promotion of RuO2 Catalysts for the Gas Phase Combustion of Ethylene, Thesis Nr. 2138, Ecole Polytechnique Fédérale, Lausanne (2000)

9   S. Wodiunig, C. Comninellis, C. Mousty, Proceedings of The 1997 Joint International Meeting 97-2 (1997)

10   E. Varkaraki, J. Nicole, E. Plattner, C. Comninellis, C. G. Vayenas, J. Appl. Electrochem. 25 (1995) 978

11   S. Wodiunig, C. Comninellis, C. Mousty, in: Energy and Electrochemical Processing for a Cleaner Environment, 97-28, (The Electrochemical Society Proceedings Series, Pennington, 1997), 147

12   J. Nicole, C. Comninellis, Proceedings of Symposium on Energy and Electrochemical Processing for a Cleaner Environment 97-28 (1997) 495

13   G. Fóti, S. Wodiunig, C. Comninellis, Curr. Topics Electrochem. 7 (2000) 1

14   G. Foti, I. Bolzonella, J. Eaves, C. Comninellis, Chimia 56 (2002) 137

15   G. Foti, V. Stankovic, I. Bolzonella, C. Comninellis, J. Electroanal. Chem. 532 (2002) 191

16   G. Foti, I. Bolzonella, D. Bachelin, C. Comninellis, J. Appl. Electrochem. 34 (2004) 9

17   E. A. Baranova, A. Thursfield, S. Brosda, G. Fóti, C. Comninellis, C. G. Vayenas, J. Electrochem. Soc. 152 (2005)

18   J. Nicole, Etude de la promotion électrochimique de l'oxydation catalytique de l'éthylène sur des oxydes métalliques, Thesis Nr. 1933, EPFL, Lausanne (1999)

19   E. Varkaraki, Electrochemical promotion of an IrO2 catalyst for the gas phase oxidation of ethylene, Thesis Nr. 1455, EPFL, Lausanne (1995)

20   E. A. Baranova, Chemical and Electrochemical Promotion of Supported Rh Catalyst, Thesis Nr. 3245, EPFL, Lausanne (2005)

21   I. Bolzonella, Electrochemical Promotion of Rhodium Catalyst. Application to Nitrogen Monoxide Reduction, Thesis Nr. 2743, Ecole Polytechnique Fédérale, Lausanne (2003)

CHAPTER 2
Bibliography
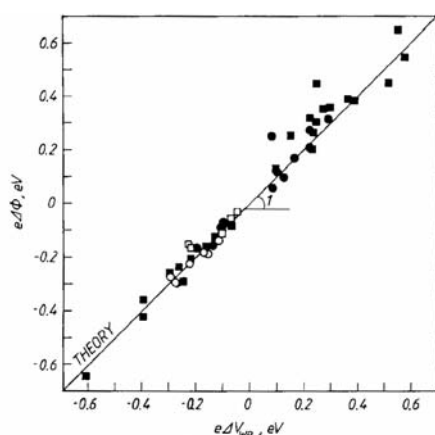
In this chapter, we review relevant literature on the electrochemistry of the system consisting of a metal film deposited on the YSZ solid electrolyte (the $O_{2(g)}$,M/YSZ system) with particular emphasis on the case where platinum is used as metal. Various paths for the redox reaction of oxygen, taking place on this system, are presented. The location of the electrochemical reaction site (ERS) and the nature of the rate-determining step (RDS) are discussed.

We also review literature on the main electrochemical techniques used in this work (chronoamperometry and cyclic voltammetry) and the relevant results reported on the $O_{2(g)}$,Pt/YSZ system.

The state of the art in the theory of electrochemical promotion of catalysis (EPOC) is presented. Particular attention is given to the origin of the effect, its mechanism, and the phenomenon of permanent EPOC.

The last section concerns the various oxygen species found on the platinum surface and their effect on the catalytic activity. This includes different forms of surface platinum oxides, chemisorbed oxygen, and the anodically produced back-spillover species.

2.1 The $O_{2(g)}$,M/YSZ system

The $O_{2(g)}$,M/YSZ system is composed of three phases. M represents the metallic electron-conducting phase (electrode). The electrode is in intimate contact with YSZ, an O^{2-}-conducting solid electrolyte (ZrO_2, doped with 8mol% Y_2O_3). These two solid phases are surrounded by a gaseous atmosphere containing molecular oxygen $O_{2(g)}$. As illustrated in Fig. 1, the system features three interfaces (metal/electrolyte, gas/metal and gas/electrolyte) and one triple phase boundary (tpb) where the three interfaces meet.
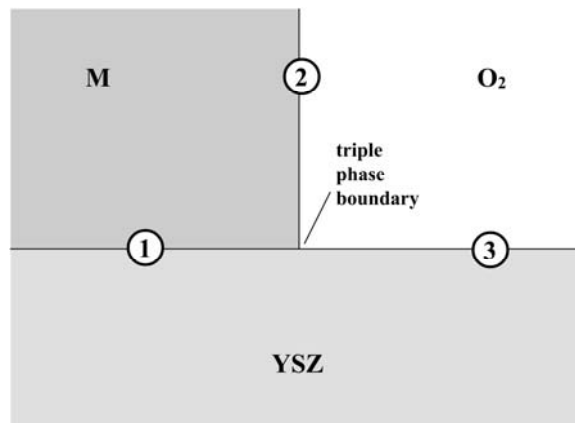
Fig. 1   Simplified scheme of the phases and interfaces of the $O_{2(g)}$,M/YSZ system. ①: Metal/electrolyte interface, ② : Metal/gas interface, ③ : gas/electrolyte interface.

Systems where yttria stabilized zirconia (YSZ) is used as the solid electrolyte are certainly the most studied in the field of high temperature solid electrochemistry. This interest is motivated by the common usage of such systems in gas sensors [1-5], gas pumps [6, 7], solid oxide fuel cells (SOFCs) [8], electrolysis cells [9, 10] and electrochemically promoted catalysts (EPOC) [11].

In these devices, the $O_{2(g)}$,M/YSZ system is used as an electrode for the electrochemical oxygen exchange reaction (eq. 2.1).

$$\tfrac{1}{2}O_{2\,(g)} + V_{O(YSZ)} + 2e^-_{(M)} \rightleftarrows O^{2-}_{(YSZ)} \qquad\qquad 2.1$$
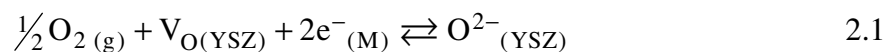
where O^{2-} is the lattice oxygen and V_O, the oxygen vacancy site, in the solid electrolyte (YSZ). O_2 is molecular oxygen in the gas phase and e^- is an electron on the metal electrode.

Electrodes can be prepared by deposition of a metallic film on the YSZ support using various techniques [12-14]. In this type of electrode, the extent of the tpb and of the M/YSZ interface are restricted to the surface of the YSZ support (see Fig. 2 a). However, by deposition of metal/YSZ mixtures on the solid electrolyte support, so-called "cermet" electrodes can be obtained [15-19]. Due to the preparation procedure, cermet electrodes feature a high dispersion of the solid electrolyte phase into the metal phase. For this reason, the tpb and the M/YSZ interface are not restricted to the surface of the YSZ support but extend into the deposited film (see Fig. 2 b). Consequently, this type of electrode offers an increased number of tpb and M/YSZ sites compared to the metallic film type (a). Since some electrochemical reactions, the oxygen exchange reaction 2.1 in particular, are thought to occur on such sites, cermet electrodes usually give better performances. For this reason, they are widely used in applications where high electrode performance (low resistance) is a key issue, e.g. gas sensors and SOFCs [2, 15-18].

Fig. 2   Schematic representation of an electrode film prepared by deposition of a metal (a) and a metal/electrolyte mixture (b). The black dots represent the sites at the tpb. The black lines represent the sites at the M/YSZ interface.
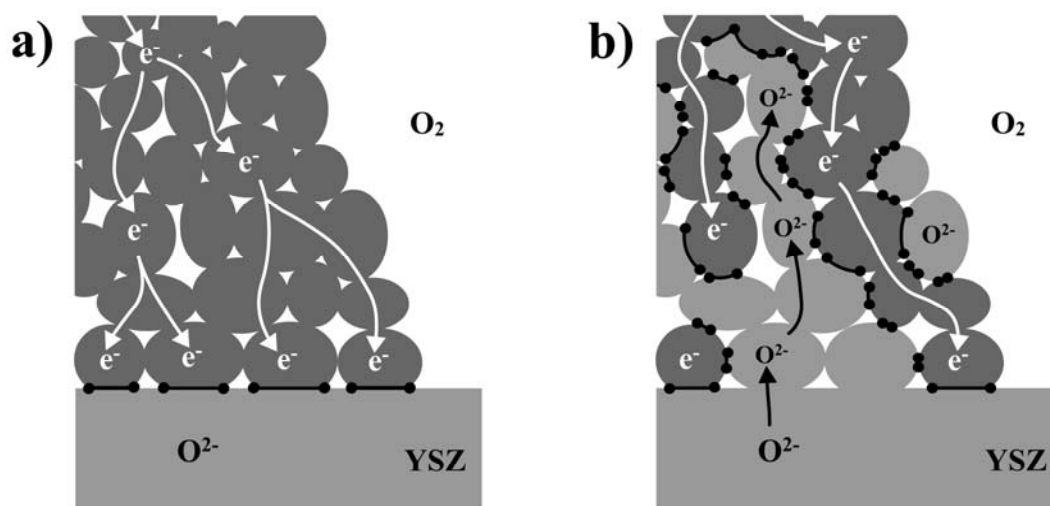
Out of a variety of metals and composite materials employed as electrodes on YSZ, platinum has always been of particular interest due to its good electrocatalytic properties. Indeed, the $O_{2(g)}$,Pt/YSZ system is the most widely studied in solid electrochemistry. Nevertheless, despite decades of investigation [7, 10, 13, 15, 18, 20-57], numerous aspects of the electrochemical reactions occurring in this system are still controversial and subject to discussion, especially on the questions of the electrochemical reactions sites (ERS) and the rate determining steps (RDS).

2.1.1 The reaction paths in the $O_{2(g)}$,M/YSZ system

Determination of the reaction mechanism of the oxygen redox reaction (eq. 2.1) and, in particular, the site of the electrochemical reaction (ERS) is not straightforward and no clear agreement is found in literature. The mechanism is reported to depend on many factors, such as the experimental temperature, oxygen partial pressure and applied polarization. However, it is also found to depend on the electrode preparation method, its type, its microstructure, and the choice of electrode material.

Over the years, various mechanisms have been proposed for the electrochemical oxygen exchange reaction (eq. 2.1), some of which are schematically depicted in Fig. 3. The figure represents the reaction in the cathodic direction (oxygen reduction reaction). Identical reverse paths are found for the anodic case.

The gaseous diffusion and the adsorption of oxygen are steps found in every path shown in Fig. 3. In path (a), also called "surface process" [58], gaseous diffusion and adsorption of oxygen is followed by diffusion of adsorbed oxygen species on the gas exposed electrode surface toward the tpb, where the electrochemical reaction takes place. The reduced oxygen O^{2-} enters the solid electrolyte by association with an oxygen vacancy V_O. Locating the ERS at the tpb is straightforward in the sense that it is the only geometric location directly accessible to all reactants and products of the electrochemical oxygen exchange reaction 2.1.

(a)

(b)

(c)

(d)

(e)
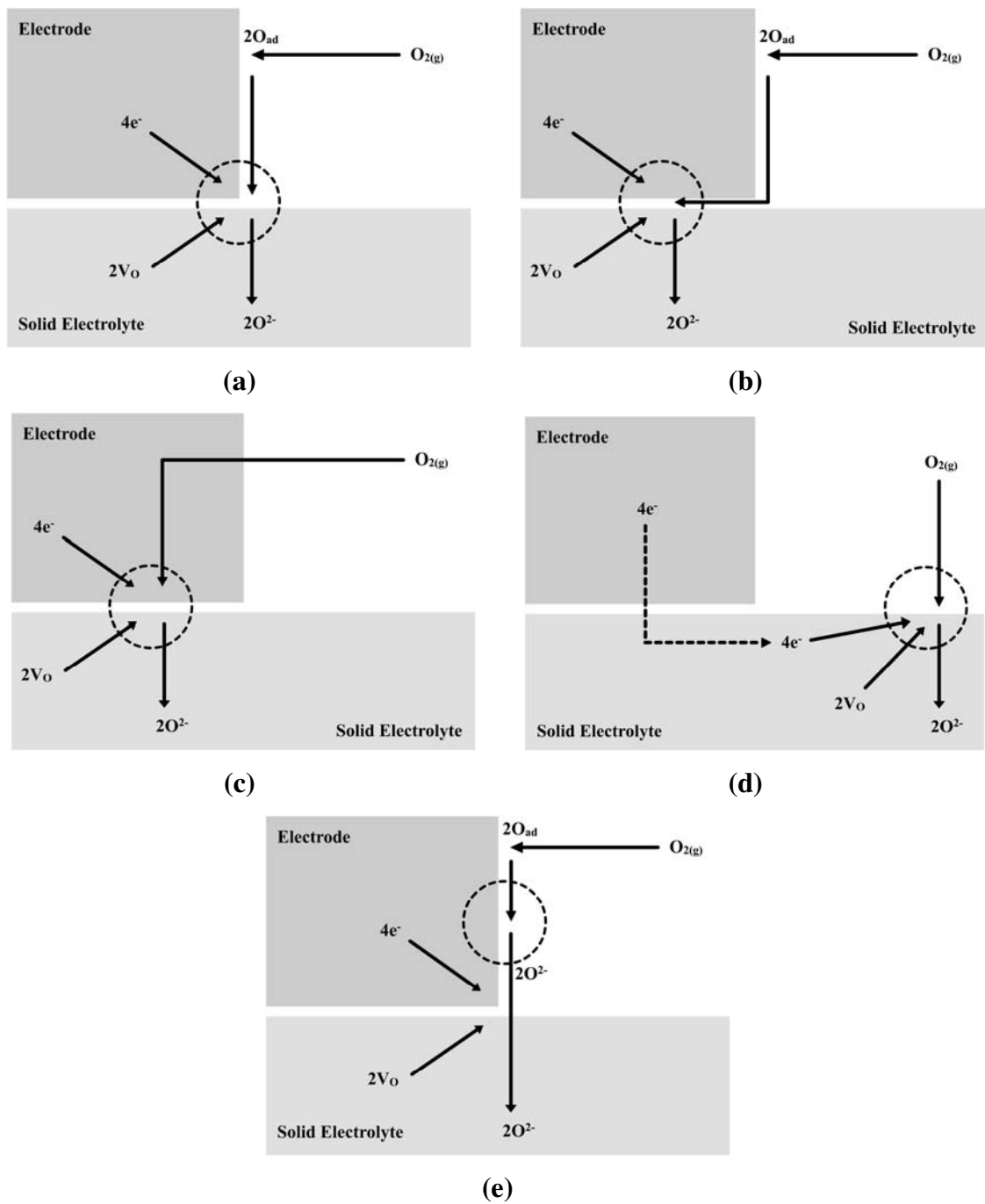
Fig. 3   Possible pathways for the oxygen exchange reaction (eq. 2.1) (cathodic case): (a) dissociative adsorption on the electrode and surface diffusion to the electrochemical reaction site at the tpb, (b) adsorption and diffusion to the reaction sites at the electrode/electrolyte interface, (c) dissolution in the electrode and bulk diffusion to the interface, (d) adsorption and reaction on the electrolyte, (e) adsorption and electron transfer at the electrode/gas interface

Since the charge transfer takes place at the triple phase boundary, its length, l_{tpb}, is one of the most important factors influencing the electrode performance. For the $O_{2(g)}$,Pt/YSZ system, where path (a) is of outmost importance, l_{tpb} has been found to have a direct influence on the polarization resistance R_p [40, 59] :

$$R_p \propto l_{tpb}^{-1}$$
$$2.2$$

For this reason, the $O_{2(g)}$,Pt/YSZ electrode is sometimes called a "tpb-electrode" [60].

Since the triple phase boundary is geometrically represented by a line, hence with zero width, the site of the electrochemical reaction (ERS) is often reported to extend toward an adjacent interface. The charge transfer step has been suggested to proceed at different interfaces: electrode/electrolyte, electrolyte/gas, and electrode/gas (schemes (b) – (e) in Fig. 3).

In path (b), the ERS is located at the interface between the electrode and the electrolyte. This mechanism has been reported in various papers [7, 47, 61-63]. The electrode/electrolyte interface is a very favorable place for the electrochemical step of an electrode process. Indeed, the electron exchange may take place over the entire electrolyte/electrode interface instead of being confined to the tpb line. However, for this path to proceed, one must consider the relation between the rate of oxygen diffusion along the electrolyte/electrode interface and the rate of the electron transfer step.

For the $O_{2(g)}$,Pt/YSZ system, where the diffusion of oxygen along the interface has been found to be possible but at a limited rate [64], the accumulation of oxygen at the Pt/YSZ interface by anodic polarization is thought to produce surface platinum oxide [20, 59, 65, 66]. This oxide layer acts as a passivation layer, causing an extra resistance at the Pt/YSZ interface.

In contrast, if the charge transfer is slow with respect to the oxygen diffusion along the Pt/YSZ interface, extra charge transfer sites are available at this interface and the ERS is extended (path (b)).

In summary, the relationship between the rates of mass transfer (oxygen diffusion) and charge transfer (electron exchange) is determining for the spread of the ERS toward the

electrolyte/electrode interface. Consequently, different electrode morphologies give rise to different polarization behaviors [61, 67].

Path (c) in Fig. 3 represents the case where oxygen is provided to the ERS (the electrolyte/electrode interface) by bulk diffusion of oxygen through the electrode. This process, called "electrode process" [58] can occur in the case of electrode metals in which oxygen is soluble (Ag for instance) or in the case of mixed ionic-electronic conductivity electrodes [68]. Given the low solubility and diffusivity of oxygen in bulk Pt [69], Rh, Pd, and Au, the applicability of this mechanism is strongly limited.

Path (d) represents the case where the ERS is located at the gas/electrolyte interface. This path, called "electrolyte process" [58], is suggested in various papers [46, 64]. Significant electronic conductivity in the solid electrolyte must be assumed from this path to proceed. In YSZ however, the high percentage of Y_2O_3 generates an ionic conductivity orders of magnitude superior to the hole and electron conductivities at common experimental oxygen partial pressures [70]. Therefore, it can be assumed to be a purely ionic conductor and, in most cases, the occurrence of path (d) on the $O_{2(g)}$,Pt/YSZ system is impeded by a lack of electronic conductivity in the electrolyte. However, local partial reduction of YSZ, by application of a strong cathodic current or a low O_2 partial pressure, can produce significant electronic conductivity and lead to a mixed ionic-electronic conductor (MIEC) [5, 64]. The mixed conductivity can also be achieved by implantation of an electronic conductor in the near surface YSZ layers [46, 58, 71]. In both cases, due to the mixed conductivity, the reaction path (d) may take place and improve the electrode performances [30, 46, 72]. This is a key issue in the improvement of high temperature SOFC cells and gas sensors [73].

In path (e), the electron transfer occurs at the electrode/gas interface. For this mechanism to occur, we assume the presence of oxygen atoms in a reduced form at this interface. Diffusion of such species at the gas exposed platinum surface is discussed in various works and, in particular, in the field of electrochemical promotion of catalysis (EPOC) [11]. In the phenomenon of EPOC, the flooding of the electrode/gas interface by these oxygen species causes the modification of the catalyst work function and, consequently, a change of its activity. Apart from works on the electrochemical promotion of catalysis,

other authors discuss the extension of the electrochemical reaction site over the gas exposed electrode surface. In his model, Mitterdorfer et al. consider that the ERS extends from the tpb to a certain distance on the electrode/gas interface [50].

2.1.2   The rate-determining step in the electrochemical oxygen exchange reaction

A variety of kinetic studies have been performed over the last three decades, and many models have been proposed to describe the mechanism of the oxygen exchange reaction [6, 7, 47, 61, 63, 67, 74-78].

In the case of the $O_{2(g)}$,Pt/YSZ system, literature discussing the nature of the rate determining step of the reaction is abundant, but not unanimous. To date, no consensus has emerged concerning the details of the reaction mechanism. The differences in the proposed mechanisms can be attributed to variations in the electrode morphology, temperature and O_2 partial pressure used.

It is generally accepted that any step of the electrochemical oxygen exchange reaction on Pt electrodes can be rate determining.

First, the gas phase diffusion of O_2 from the gaseous phase of the reactor to the micropores of the electrode has been found to be rate limiting in a few studies [13, 55, 79]. The rate of gas phase diffusion is influenced by the electrode microstructure amongst other factors [21, 54]. In general, the overall rate has been found to be controlled by gaseous diffusion under the following conditions: i) low oxygen partial pressure (below ~10^{-5} atm), ii) high polarization ($|\eta|$ > ~200 mV), iii) with particularly thick electrodes, iv) at high temperature (above ~800°C).

Dissociative adsorption is known to be the common mode of adsorption for oxygen on most transition metals at high temperatures [80-82]. This step has also been suggested to contribute to the limitation of the reaction rate [12, 46], especially under 500°C [47, 81, 83].

Once adsorbed on the gas exposed platinum surface, O_{ad} species may diffuse toward the ERS, as shown in Fig. 3 (paths a, b and e). Many claim the diffusion of O_{ad} as the rate determining step [7, 47, 52, 55, 83]. This step is also influenced by the microstructure of

the electrode and its surface state. At temperatures below 500°C, this step is thought to be impeded due to its high activation energy [7, 47].

The diffusion of oxygen in the electrode/electrolyte interface, as shown by path b in Fig. 3, has been found to be rate determining in a few papers [61, 62, 75]. The relation between the oxygen diffusion rate at this interface and the charge transfer rate determines the extent of the ERS toward the solid-solid interface [84].

The rate of the electron transfer steps is usually assumed to depend exponentially on the applied potential according to a Butler-Volmer kinetic law [85, 86]. For this reason, it may be rate limiting at small overpotential values, i.e. at near open-circuit potentials [49, 51]. However, when higher $|\eta|$ values are applied, the rate-determining step (RDS) may switch from a charge transfer step to a non-electroactivated step.

One may note that the rate-determining step for a certain electrode in given experimental conditions may be different under cathodic and anodic polarization. This is due to the nature of the phase in which the reactant (oxygen) is found, i.e. a gas for the cathodic case and a solid for the anodic case.

2.1.3 Chronoamperometry and cyclic voltammetry of the $O_{2(g)}$,Pt/YSZ system

Most of the studies mentioned above, dealing with the mechanisms and kinetics of the electrochemical oxygen exchange reaction 2.1, are based on steady state polarization curves and impedance spectroscopy. However, many other electrochemical methods, initially developed in the field of liquid electrochemistry, can be used successfully to gather knowledge on solid electrochemistry systems. Chronoamperometry, for instance, is a powerful technique, which enables the kinetic study of charging/discharging processes occurring at electrodes (pseudocapacitance). However, only few papers deal with chronoamperometric measurements on the $O_{2(g)}$,Pt/YSZ system. A paper by Kenjo et al. [87] claims that, under anodic polarization, the first electron transfer step ($O^{2-} \rightarrow O^{-} + e^{-}$) is of pure charge transfer type and gives rise to a classical double layer capacitance. It also speculates that the second electron transfer step ($O^{-} \rightarrow O + e^{-}$) involves a concentration polarization due to the accumulation of oxygen atoms at the Pt/YSZ interface

(pseudocapacitance). As seen on Fig. 4, the transient current behaviors of the two capacitive processes are separated on the basis of the two distinct rates of current decay. The pseudocapacitive process (high capacitance) is characterized by a decay rate much slower than the fast double layer capacitive process (low capacitance).
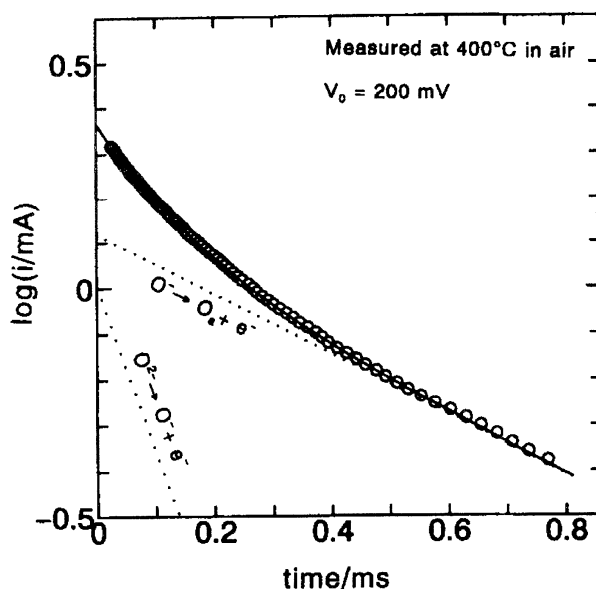
Fig. 4   Current decay curve for the $O_{2(g)}$,Pt/YSZ system. Open circles indicate the experimental data and the solid line, the best-fit theoretical curve calculated considering a double layer capacitive process for the first transferred electron r and a pseudocapacitive process for the second transferred electron [87].

Linear sweep voltammetry and cyclic voltammetry are also well-suited techniques for in situ non-steady state investigation of solid-state electrochemical systems. Developed originally for the study of liquid phase electrochemistry, they were used to investigate, for instance, the behavior of platinum electrodes in aqueous H_2SO_4 [88-91]. These studies demonstrated the Pt-O site exchange mechanism, a key step in the platinum oxide growth at these electrodes. Later, the techniques of voltammetry were adapted to high temperature solid electrochemistry [20, 59, 65, 66, 92, 93], and several papers dealing with voltammetric characterization of the $O_{2(g)}$,Pt/YSZ system have appeared, reporting various peaks observed during the potential scans.

The occurrence of one anodic and one cathodic peak in the cyclic voltammogram of the $O_{2(g)}$,Pt/YSZ system (see Fig. 5) has been reported in literature in a wide range of temperature and oxygen partial pressures with electrode prepared by sputtering [94] but also using Pt pastes and other preparation methods [20, 59, 92, 95].
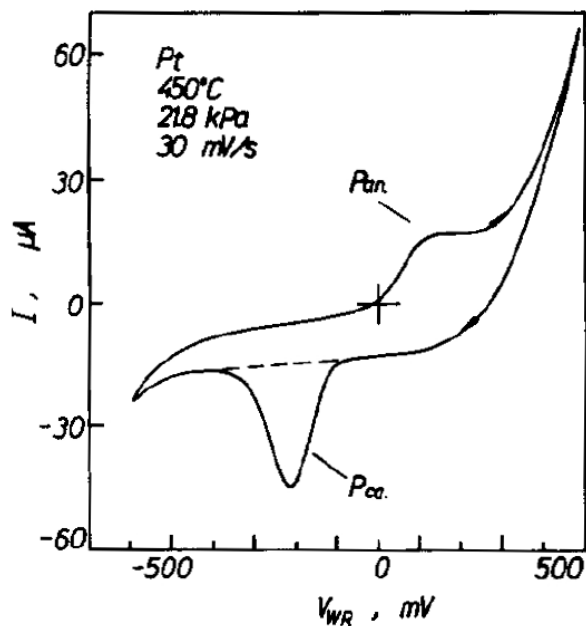
Fig. 5   Cathodic and anodic peaks in the voltammogram of the $O_{2(g)}$,Pt/YSZ system in 21.8 kPa O_2 atmosphere [92].

Fig. 6   Linear potential scan of the $O_{2(g)}$,Pt/YSZ system. Influence of the holding time t_h at the potential $E_h = 300$ mV. $pO_2 = 0.1$ kPa [92].

All papers agree that the first peak corresponds to the reduction of a Pt-O compound. However, the nature of this compound is still subject to controversy. It has been attributed
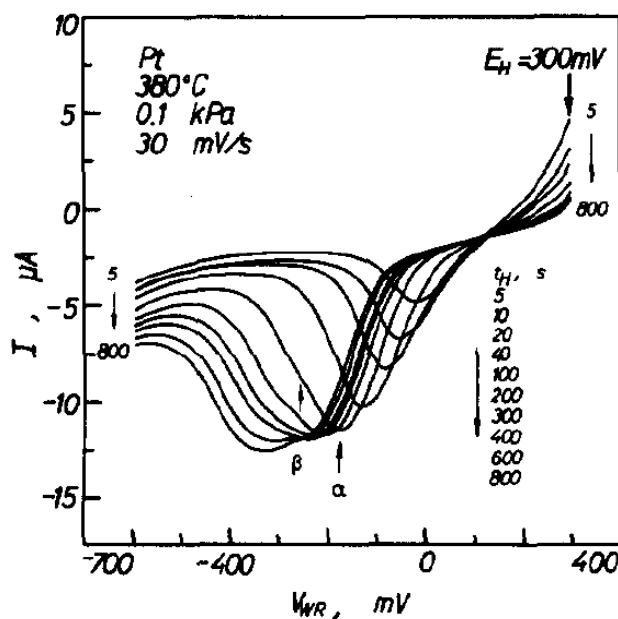
to oxygen atoms adsorbed at the tpb [92] or to platinum oxide formed at the Pt/YSZ interface [20, 59, 65, 66, 92, 96].

The observation of a second peak (see Fig. 6), often poorly defined, in the voltammogram of the $O_{2(g)}$,Pt/YSZ system has also been reported in several papers [20, 65, 66, 92, 96]. As found in aqueous electrochemistry [91], the observation of multiple cathodic peaks after prolonged anodic polarization is thought to depend mainly on the microstructure and chemical state of the electrode, hence on its history. Again, various interpretations are proposed for the observation of the second peak. These interpretations invoke the back-spillover oxygen [66, 92], platinum oxides [92] or a rearranged type of platinum oxide [20, 66].

2.2   Electrochemical promotion of catalysis

In the late 1980s, it has been discovered that the use of solid electrolyte cells offers some interesting possibilities in the area of heterogeneous catalysis. The early results have been given by Vayenas and co-workers [11, 97-99] who have shown that the catalytic activity of metal catalysts deposited on solid electrolytes can be altered in a dramatic manner by applying potential or current to the catalyst. Later, it has been shown in our laboratory [100-103] that this effect can be extended to oxide catalyst, thus the catalytic activity of iridium oxide films for the combustion of ethylene can be increased by up to a factor 10 via anodic polarization.

Today, the electrochemical promotion of catalysis (EPOC), also known as non-Faradaic electrochemical modification of catalytic activity (NEMCA), is a general phenomenon, which has been demonstrated for many different catalytic reactions over different metal [11, 104] and metal oxide catalysts [102, 105] by using several solid electrolytes [11, 104, 106]. This phenomenon has been investigated also by a number of other groups [22, 23, 41, 105, 107-114] and brought new theoretical challenges to the field of modern electrochemistry and surface science [115, 116].

Although the phenomenon of electrochemical promotion of catalysis has been observed on many catalytic processes, with usually quite good results, there has been so far no large-scale commercial utilization. However, a monolithic type electrochemically promoted

catalytic reactor (MEPR) has been recently designed, constructed, and tested for the practical utilization in automotive exhaust units [117, 118]. It has proved its efficiency for the oxidation of hydrocarbons and the reduction of NO in lean burn conditions. These promising results encourage the practical application of EPOC in common catalytic devices.

2.2.1 Phenomenon and mechanism

The basic setup used to observe the effect on O^{2-} conducting solid electrolytes is shown in Fig. 7 for the case of catalytic ethylene oxidation in presence of oxygen. The porous, electropromoted catalyst film also serves as the working electrode in the solid-electrolyte cell.

Catalytic Oxidation   Electrochemical Oxidation

$C_2H_4 + 3O_2 \rightarrow 2CO_2 + 2H_2O$ $C_2H_4 + 6O^{2-} \rightarrow 12e^- + 2CO_2 + 2H_2O$

catalyst

YSZ $O^{2-}\uparrow$ $O^{2-}\uparrow$ $O^{2-}\uparrow$

gold

$O_2 \rightarrow 2O^{2-} + 2e^-$

Gas mixture $C_2H_4 + O_2$
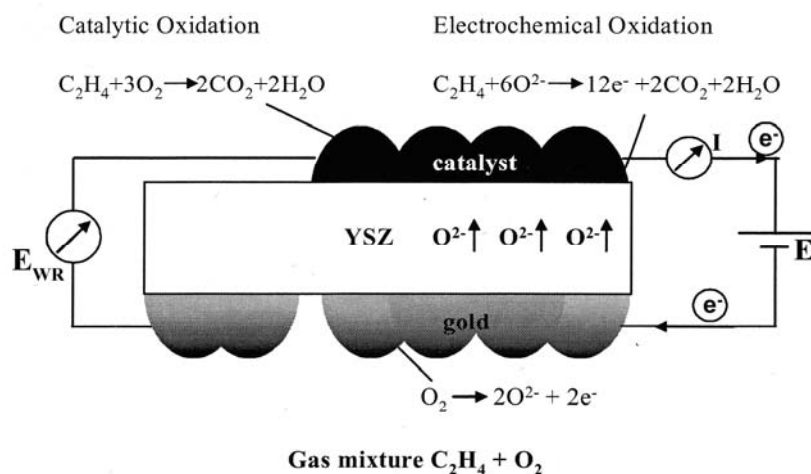
Fig. 7   Scheme of the electrochemical cell used in experiments of electrochemical promotion of catalysis with an O^{2-} conducting solid electrolyte.

Fig. 8 shows the behavior of the catalytic rate versus time during a typical electrochemical promotion experiment. Under open-circuit conditions ($I = 0$), a catalytic rate r_0 is measured. Application of an electrical current I or a potential difference between the working and the reference electrode, E_{WR}, gives rise to changes in the catalytic rate r. These changes are often found to be non-Faradaic ($\Delta r >> I/2F$). The rate of the catalytic reaction r can become up to 200 times larger than the open circuit rate r_0 [11, 97, 119]. The electrochemically induced rate increase is entirely reversible in most cases. After current interruption, the rate usually reaches back to the initial rate r_0.

The phenomenon of electrochemical promotion can be characterized by various parameters:

1)   The rate enhancement ratio ρ:

$$\rho = r/r_0 \qquad\qquad 2.3$$

where r is the electropromoted catalytic rate and r_0 is the unpromoted (open-circuit) catalytic rate before polarization.

2)   The Faradaic efficiency Λ:

$$\Lambda = \Delta r_{catalytic}/(I/2F) \qquad\qquad 2.4$$

where $\Delta r_{catalytic}$ is the polarization-induced change in catalytic rate, I is the applied current and F is Faraday's constant.

Fig. 8   Reversible electrochemical promotion experiment. Catalytic rate transient caused by the application of a current step. After current interruption, the rate tends to its initial open circuit r_0 value.

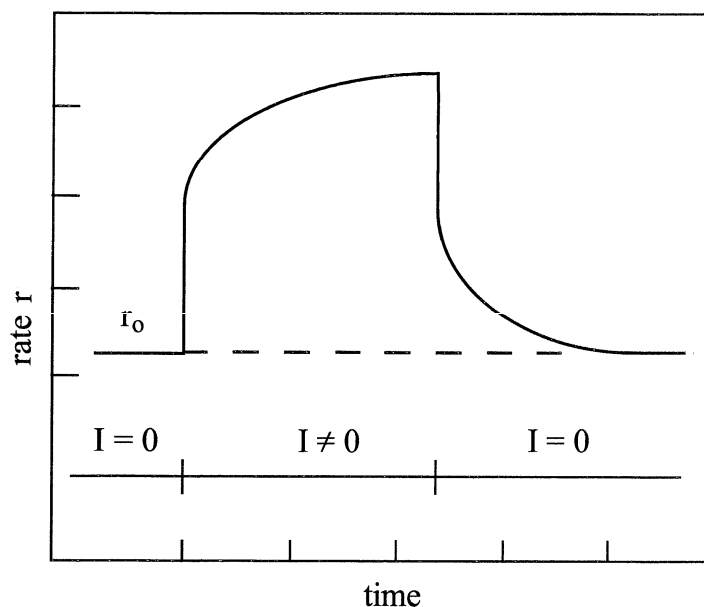The generally admitted mechanism of electrochemical promotion, illustrated in Fig. 9 is based on the effect of promoting species originating from the solid electrolyte and back-spilling over the catalyst gas exposed surface via the tpb. In the example of anodic polarization of the catalyst, the solid electrolyte functions as donor supplying $O^{\delta-}$ ions to the catalyst, functioning as acceptor. In such conditions, it was demonstrated that two types of adsorbed oxygen species exist [120] : one type is the catalytically active species adsorbed from the gas phase and the other is back-spillover oxygen $O^{\delta-}$ from the solid electrolyte, which acts as a sacrificial promoter [11, 97]. Back-spillover species may indeed be consumed in electrochemical reactions (oxygen evolution and/or oxidation of adsorbed reactants). In recent papers [112, 113], it has been postulated that partially impeded step in the oxygen path from gaseous O_2 to adsorbed $O^{\delta-}$ results in the equilibration of the electrochemical potentials between the adsorbed $O^{\delta-}$ species, the electron in Pt and YSZ lattice oxygen O^{2-}. The $O^{\delta-}$ coverage over the platinum electrode is therefore controlled by the applied voltage with respect to the reference electrode.

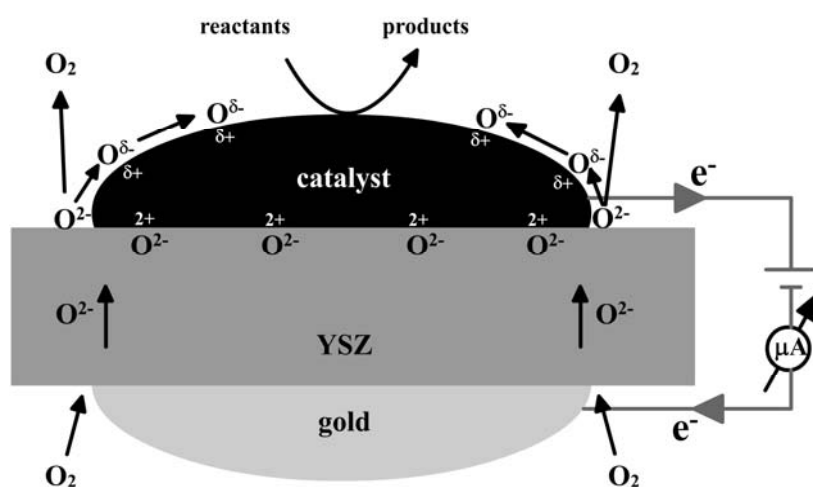Fig. 9   Schematic representation of the mechanism of electrochemical promotion by an applied anodic current via back-spillover of charged promoting species

The existence of back-spillover oxygen ions at a gas exposed catalyst surface was demonstrated by XPS measurements [121]. These oxygen species could not be detected under open-circuit conditions, but they were found in abundance after anodic polarization

of the catalyst/solid-electrolyte interface. Back-spillover oxygen and chemisorbed oxygen may be clearly distinguished also by temperature-programmed desorption (TPD) [122]. It was shown that oxygen adsorbed from the gas phase desorbs at a lower temperature, hence is more reactive, than the oxygen species generated electrochemically.

During their diffusion, the oxygen ions are accompanied by their compensating mirror charges in the catalyst, forming a dipole. When these dipoles spread out, an overall neutral, effective double layer is built up at the gas exposed catalyst surface. This causes changes in the catalyst work function. As shown in Fig. 10, the changes in work function have been found to vary with the applied potential with a one to one relation [121]. The effect of the change in the catalyst's work function is the modification of the binding strength of chemisorbed reactants and intermediates, thus giving rise to changes in the catalytic activity [11].
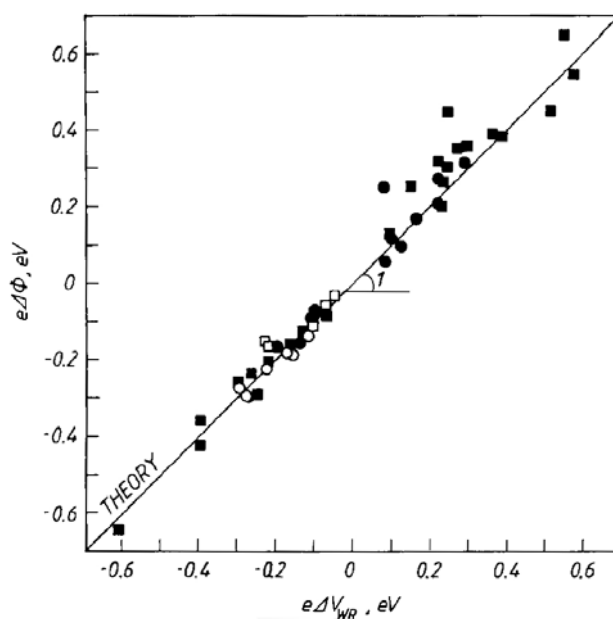
Fig. 10   Effect of catalyst-electrode potential on the work function of the gas exposed catalyst-electrode surface in varying gas compositions. Open symbols: open circuit operation. Closed symbols: closed circuit operation [121].

2.2.2 Permanent EPOC

After the discovery of this phenomenon by the group of Vayenas et al, we have reported in the late 1990s for the first time, the so-called "permanent electrochemical promotion" (P-EPOC). Indeed, despite that the phenomenon of EPOC is generally completely

reversible (see Fig. 8), permanent (irreversible) EPOC has been observed under certain conditions. Technically, electrochemical promotion is called permanent if the open-circuit reaction rate after current interruption remains different from the value before current application. Presumably, the effect of electrochemical promotion may appear to be partially irreversible when the particular catalyst can exist in various oxidation states, giving rise to distinct catalytic activity states.

In order to describe quantitatively the irreversible character of the promotion, a "permanent" rate enhancement ratio, γ, is used [11, 123, 124]:

$$\gamma = r'/r_0 \qquad\qquad 2.5$$

Where r_0 and r' denote the open-circuit catalytic rate before and after the polarization pulse, respectively.

Fig. 11 schematizes the non-reversible catalytic rate transient caused by the application of a galvanostatic polarization. Upon current interruption, the rate decreases rapidly at first, followed by a slow decrease to a new steady-state value r'.
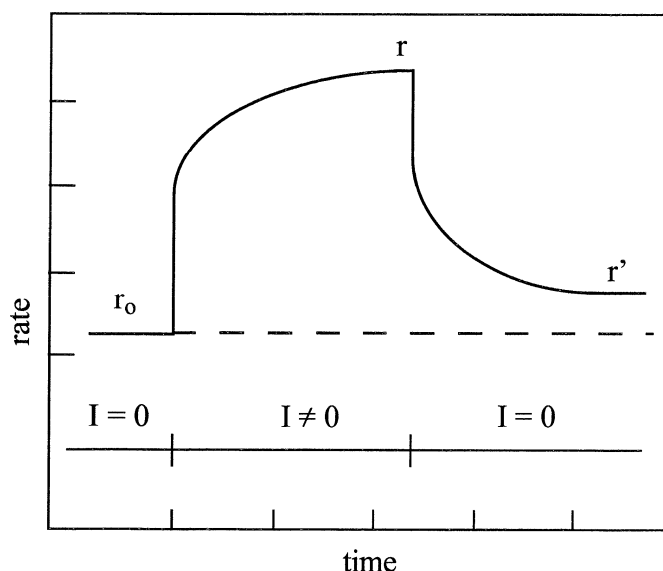
Fig. 11   Non-reversible electrochemical promotion experiment. Catalytic rate transient caused by the application of a current step. After current interruption, the rate tends to another open circuit stationary rate r'.

The permanent electrochemical promotion of catalysis was first reported by Nicole on IrO$_2$ catalysts [123-126]. Fig. 12 shows the transient rate response to an applied anodic current step during ethylene combustion on an IrO$_2$ catalyst film deposited on YSZ [123]. Initially, the circuit is open ($I = 0$) and the unpromoted catalytic reaction rate is low. At $t = 0$, the current step is applied between the catalyst (working electrode) and the counter-electrode. The reaction rate increases rapidly at the beginning and, within the few minutes of current flow, reaches a value about eight times higher than the initial rate. After this rapid increase, the rate increases much more slowly to a value 13 times higher than the initial open-circuit rate.

Upon current interruption, the rate decreases rapidly at first and then slowly tends to a new stationary value, about three times higher than the initial rate measured prior to application of the current ($\gamma = 3$).
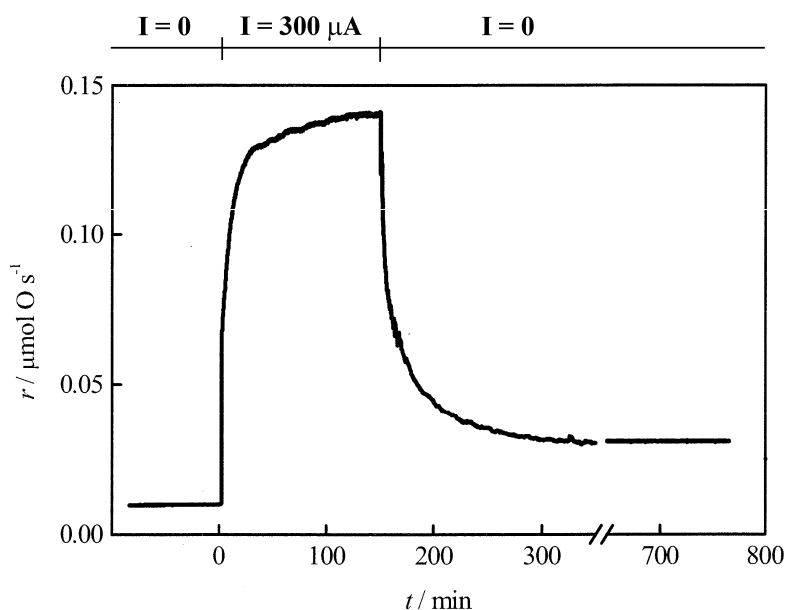
Fig. 12   Permanent EP. Polarization and relaxation transient of the rate of ethylene combustion on IrO$_2$/YSZ catalyst due to a 300 μA current application for 120 minutes. Catalyst: IrO$_2$, $T = 380°C$, $pO_2 = 17$ kPa, $pC_2H_4 = 140$ Pa [126].

The permanent rate enhancement factor γ has been found to depend on the duration of the current application, reaching a maximum plateau for polarization times of about 90 minutes (Fig. 13). These results suggest that the electrochemical activation of IrO$_2$ is a

two-stage process. It consists of a rapid reversible stage ($\gamma = 1$ for very short polarization times) followed by a slow irreversible stage, where the increase in catalytic activity persists after interruption of the current ($\gamma > 1$). It is evident that the slow process is responsible for the permanent effect.

The permanent activation of the catalyst was explained by the formation of an electrochemically produced higher oxide state $IrO_{2+\delta}$ upon anodic polarization. This oxide forms by the interaction between the catalyst and the electrochemically produced oxygen ions diffusing on the catalyst surface. In situ catalyst work function measurements showed that the permanent activity gain was linked to a permanent increase in the work function.
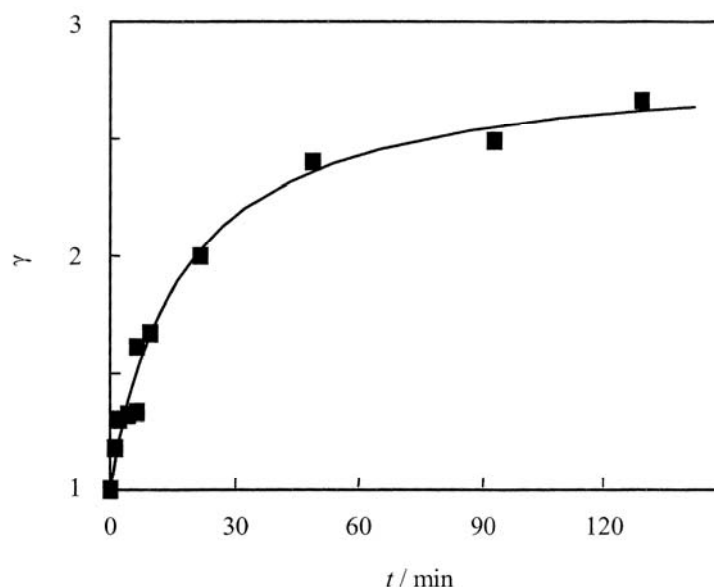
Fig. 13   Influence of the duration of the current application, t, on the permanent enhancement factor γ (see eq. 2.5). Experimental conditions as in Fig. 12 [126].

The permanent EPOC has also been observed in the reduction of NO by C_3H_6 using rhodium catalysts in oxidizing environment [127, 128]. As shown by Fóti et al., the measurements were performed in a slightly oxidizing gas mixture (0.1 kPa C_3H_6; 0.1 kPa NO; 0.5 kPa O_2) at $T = 300°C$ [127]. In this composition, a one-hour heating treatment at 400°C resulted in a strong deactivation of the catalyst due to partial oxidation of the rhodium surface; the new steady state catalytic activity at 300°C was about 90% lower than prior to the heat treatment. Under open circuit conditions, no spontaneous reactivation occurred at 300°C.

After the pretreatment, a great permanent effect was observed at 300°C. The observed permanent activation was interpreted as a consequence of the oxidation state change of the catalyst surface. According to this interpretation, a Rh catalyst with an initial active metallic surface will only exhibit a reversible promotion effect, which will disappear totally after the interruption of the polarization application. In contrast, an initially oxidized catalyst will exhibit, after a sufficiently long polarization period, a permanent activation, which will persist for days in the slightly oxidizing gas mixture.
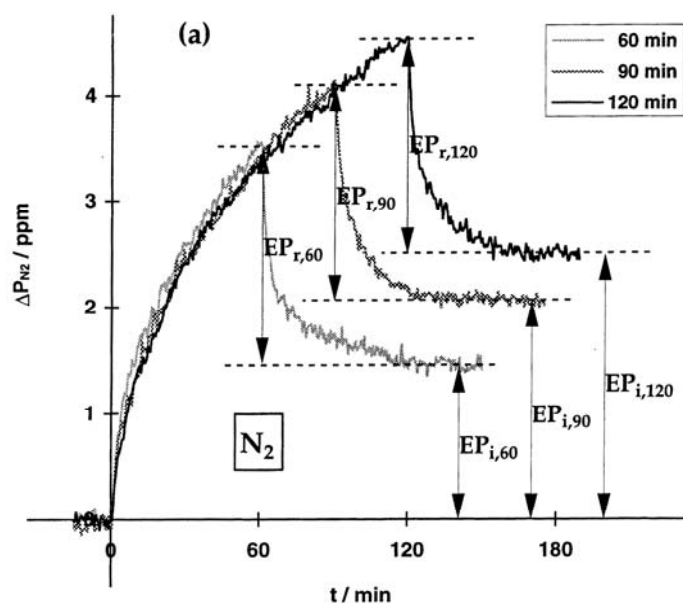
Fig. 14   Effect of the polarization time on the reversibility of the electrochemical promotion of a Rh/YSZ catalyst. Gas: 1000 ppm C_3H_6, 1000 ppm NO and 5000 ppm O_2. T = 300°C. ΔP_{N2} is the N_2 production increase during polarization, with respect to the open circuit value. The 5µA current has been applied at t = 0 and interrupted at t = 60, 90 and 120 min. EP_r and EP_i are the reversible and irreversible transient parts, respectively [127].

According to Fóti, the promoting effect of the current passing through the cell can be considered as the sum of a totally reversible effect EP_r and a permanent effect EP_i, the latter depending highly of the polarization time (see Fig. 14). According to the paper, the reversible effect EP_r is probably due to the accumulation, on the gas exposed catalyst surface, of promoting species diffusing from the solid electrolyte according to the back-spillover model. This effect vanishes after the interruption of the current application. The irreversible effect EP_i is due to a stabilization of the reduced state of the Rh catalyst

surface. The latter can be achieved through the weakening of the Rh-O link, assisted by the anodic polarization, as observed for platinum oxides [129].
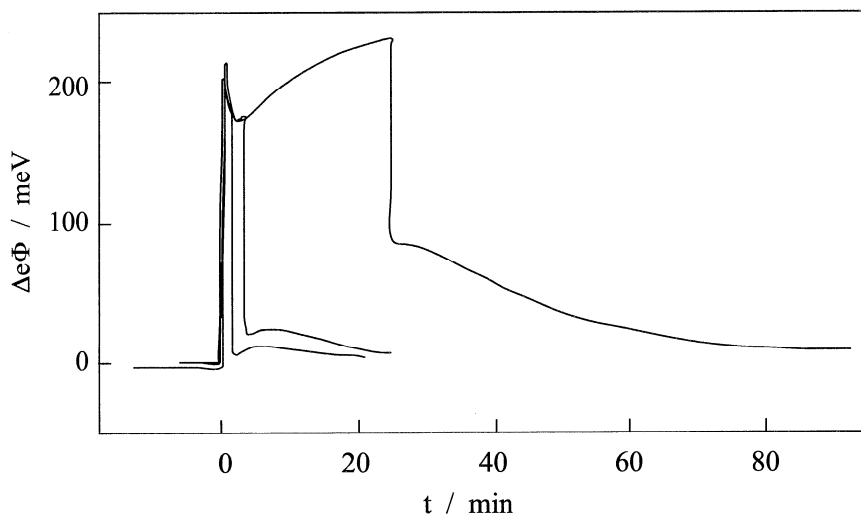
Fig. 15   Temporal evolution of the work function difference $\Delta e\Phi$ for different current application durations: 2 min, 5 min and 23 min. Galvanostatic step of 50 μA, $T = 380$ °C, $pC_2H_4 = 114$ Pa, $pO_2 = 17.7$ kPa [130, 131].

The work function change $\Delta(e\Phi)$ of a RuO_2 catalyst has been measured during the electrochemical promotion of the catalytic ethylene oxidation by the application of an anodic polarization [130, 132]. As mentioned above, the work function measurement provides insight into the migration of promoting species toward the gas exposed catalyst surface and into the consequent catalytic activity. Fig. 15, shows the influence of the duration of the 50 μA current application on the work function change $\Delta(e\Phi)$ with time. The work function transients observed during anodic polarization are composed of different steps. First, a sharp increase just after the current application ($t = 0$), then, a sharp decrease and a slow increase toward a plateau value. The initial jump in work function is associated with the back-spillover of promoting species on the surface region easily accessible, close to the triple phase boundary (tpb). The slow work function increase toward the plateau value is attributed to the diffusion of the promoting species over the entire gas exposed catalyst surface. Particular attention must be drawn to the relaxation kinetics, after the interruption of the current application. After longer polarization, more time is needed to reach a steady state value. Indeed, more than 60 minutes are necessary

after a 23 minute polarization. Since work function has direct incidence on the catalytic activity, the relaxation transient of the latter also depends on the polarization time.

2.3   The platinum oxide and other Pt-O species

The platinum oxygen interactions have been studied extensively over decades. In particular, research on platinum oxide has been motivated by the use of Pt in many heterogeneous catalytic systems, such as 3-way catalyst for exhaust gas treatment. Studies have shown that surface Pt oxides layers may grow in the presence of oxygen under certain conditions.

$$Pt_{(surf.)} + \frac{x}{2} O_{2\ (g)} \rightleftarrows PtO_{x\ (surf.)} \qquad\qquad 2.6$$
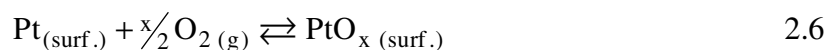
The term "PtO_X" is used to refer to platinum oxides of ill-defined stoichiometry. Indeed, many different Pt/O ratios have been reported for surface and bulk oxides (α-PtO_2, PtO, Pt_3O_4, Pt_2O) [66, 133-138]. "Oxygen solid solution in Pt" or "high oxygen concentration Pt" are also used to refer to the Pt oxide layer [139-142], suggesting the lack of properly defined stoichiometry and, sometimes, the observation of various coexisting species [138].

2.3.1   The thermodynamics and kinetics of Pt oxidation

For the oxidation to occur, both thermodynamic and kinetic requirements must be met. For the thermodynamic side, a model developed for the oxidation of noble metals [143] suggests that there is a critical O_{ad} coverage at which the transition between chemisorbed oxygen and the oxide film occurs; and that this oxygen coverage is thermodynamically, rather than kinetically, determined. Below this critical coverage, the Gibbs free energy ΔG_f of chemisorbed oxygen formation is more favorable (more negative) than the free energy of the oxide film formation. The high Gibbs free energy of the oxide formation is due to the energy cost for distorting the substrate lattice and breaking metal bonds required for oxygen incorporation. However, as the oxygen coverage increases, the repulsive interactions between the adsorbed oxygen atoms increase the value of the free energy of the chemisorbed oxygen formation to the level of the oxide film formation. Oxidation may occur. At this point, the two phases (Pt and Pt oxide) coexist at the surface and further increasing the oxygen partial pressure extends the oxide phase over the entire surface.

Indeed, above the critical coverage value, the occupation of subsurface (oxidic) sites becomes more favorable compared to continued filling of surface (chemisorption) sites.

The reader may note that in conditions where the oxygen penetration into the first Pt layers is thermodynamically favorable, the resulting subsurface oxygen finds itself in a more stable state. Consequently, in order to reverse the process (Pt oxide reduction), extra energy will have to be provided. Experimentally, in temperature programmed desorption experiments, the oxide is found to dissociate at higher temperatures than the chemisorbed oxygen [144]. In electrochemical experiments, a more negative overpotential has to be applied for the reduction of oxides with respect to adsorbed oxygen species [66, 88].
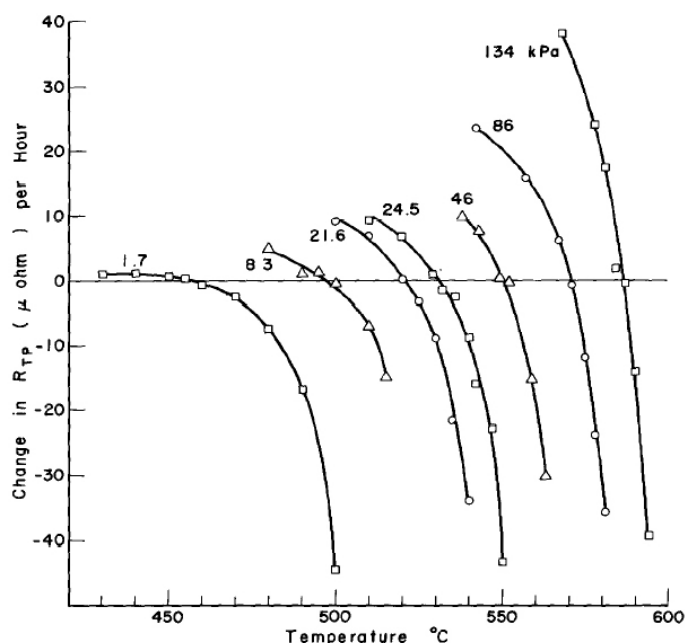
Fig. 16   Isobaric rate of oxide growth on a Pt wire as a function of temperature. The O_2 pressure used for each isobar curve is given on the graph in kPa. Negative rates indicate oxide dissociation. [145]

A study based on high precision electrical resistance measurements of polycrystalline platinum wires allowed accurate in situ measurement of the oxide layer thickness for varying conditions of O_2 pressure and temperature. The rate of the oxide layer growth and decrease are shown in for various pressures and temperatures (Fig. 16 and Fig. 17). The results show that oxides are formed upon heat treatment in presence of O_2, but they are destabilized by high temperature. As an example, the oxide species starts dissociating at $T > 525°C$ in contact with the oxygen partial pressure $pO_2 = 21$ kPa (see Fig. 16).
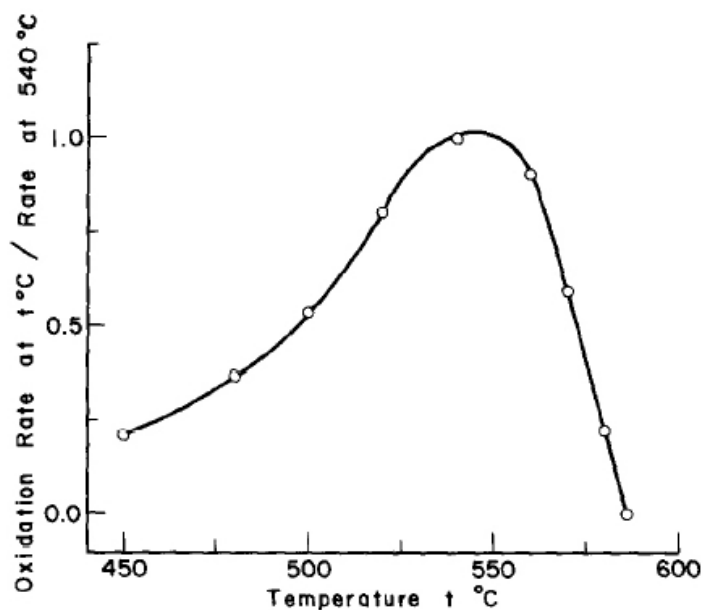
Fig. 17   Isobaric changes in the normalized oxidation rate on the surface of Pt wires as a function temperature, for an O_2 pressure of 132 kPa. [145]

Based on these kinetic measurements, Berry calculated ΔH and ΔS values for the formation of surface Pt oxides [145]. Comparable thermodynamic values were later determined by Vayenas et al. [136]. These were based on the observation of oscillation in the catalytic oxidation of ethylene over YSZ supported Pt [133]. These values were later confirmed [134]. Using the ΔH and ΔS values, one may calculate the oxygen partial pressure $pO_2{}^*$ in equilibrium with the surface oxide at any given temperature T:

$$\ln \frac{p_{O_2}{}^*}{p^\circ} = \frac{\Delta H - T \cdot \Delta S}{RT} \qquad\qquad 2.7$$

If the experimental oxygen partial pressure pO_2 is higher than $pO_2{}^*$, the oxidation is thermodynamically favored. In the opposite case ($pO_2 < pO_2{}^*$), the dissociation of the oxide is thermodynamically favored. Consequently, eq. 2.7 gives the pO_2 and T conditions at the limit of the oxide stability domain. This domain is represented in Fig. 18 using the ΔH and ΔS values given by Berry in [145] and by Vayenas in [136]. The figure suggests that as temperature increases, the minimum oxygen partial pressure of the oxide stability domain also increases.

Despite the good correlation of ΔH and ΔS values between the two papers considering the difference in the manner in which they were measured, the domain between the two lines is considerable. It suggests that the stability domain of the oxide is extended to higher temperatures in the case of YSZ supported Pt films (Vayenas) with respect to unsupported Pt wires (Berry). This underlines the influence of the support and of the geometry on the oxide stability [134, 137, 138].
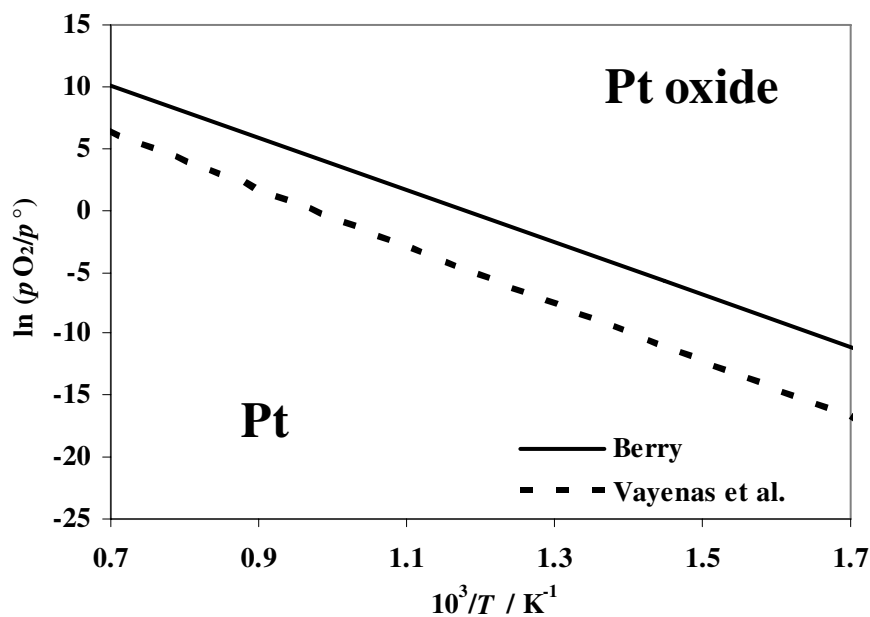
Fig. 18   Stability domain of surface platinum oxide (Berry [145] and Vayenas et al. [136]), $p° = 100$ kPa.

Fig. 17 illustrates the effect of temperature on the rate of the oxide growth. At low temperatures ($T < 510°C$), the oxidation is thermodynamically favored i.e. the experimental oxygen partial pressure ($pO_2 = 132$ kPa) is much higher than pO_2^* given by equation 2.7. However, the oxide growth rate is kinetically limited by the low temperature. At high temperatures ($T > 560°C$), although faster kinetics are possible, the oxide growth rate drops because pO_2^* approaches po_2 and the oxide formation becomes less favorable. Around $T = 590°C$, the oxide stability limit is reached. Consequently, the growth rate is zero. At moderate temperatures ($T \approx 550°C$), the influences of the kinetic and thermodynamic effects give rise to a maximum.

Concerning the kinetics of Pt oxide formation/dissociation, the transition between chemisorbed oxygen and the oxide has been reported to be blocked at low temperature [139, 141, 146]. In particular, Salmerón et al. [139] evidenced that oxide layers, once formed, are stable indefinitely below 400°C - 500°C beyond the stability limit predicted by thermodynamics. This is caused by the very slow rate of decomposition, controlled by diffusion of oxygen from the bulk of the metal to its surface, where desorption takes place. Indeed, diffusion of oxygen inside platinum is known to be a very slow process, associated with a high activation energy [69]. The kinetically blocked diffusion of oxygen can therefore creates metastable states, which do not correspond to the thermodynamic predictions.

2.3.2   The chemisorbed oxygen and the high temperature Pt oxide

Based on measurements of thermal desorption spectroscopy and various physical surface analysis [134, 137, 141, 142, 146, 147], the presence of two oxygen species on Pt having very distinct characteristics has been reported: These species are designated as the chemisorbed oxygen and the oxide (or subsurface oxygen) [141, 148].

First, the chemisorbed oxygen atom O_{ad}, sometimes called atomic β state [81, 145], is found to be the main adsorbate from room temperature to 400 °C. It is formed when exposing at $T < 525$ °C and desorbs completely around 725 °C. It is located at the top platinum layer [141]. It is very reactive and can be removed by reaction with H_2 or CO even at room temperature. It is found to have a positive effect on the work function (+0.5 eV).

Then, at $T > 525$ °C, the subsurface oxide is formed by penetration of adsorbed oxygen atoms under the top layers, the latter consisting only of Pt atoms [141]. This "non reactive" species desorbs at $T > 1000$ °C and is not removed by H_2 or CO, even at 725°C. It has a negative effect on work function (-1 eV) [149], increasing the binding energy of H_2 and CO. It exhibits a low catalytic oxidation activity toward $CH_4 + O_2$. However, this reported high temperature subsurface oxide is controversial because it subsists at temperatures much higher than predicted by the thermodynamic values given by Berry (Fig. 18, Fig. 16 and Fig. 17). Therefore, it has been thought to be related to impurities in Pt [150-152]. Yet, oxide formation far from the stability domain has also been reported on high purity single crystals of platinum [139].

The characteristics of these two species are summarized in Table 1.

Table 1   Characteristics of the chemisorbed oxygen and the oxide
            (extracted from [141])

	"Chemisorbed" oxygen	"Oxide"
Generation by O_2 exposure at	T < 800 K	T > 800 K
Desorption	Slowly at T > 550 K, completely at 1000 K	Slow decomposition at 1200 K
Reaction with H_2 and CO	Removed even at room temperature, "reactive"	Not removed even at 1000 K, "non-reactive"
Work function changes with respect to clean Pt	+ 0.5 eV	-1 eV

2.3.3   The oxygen incorporation mechanism

A mechanism for the formation of subsurface oxygen has been proposed by Lauterbach et al. [149]. It is illustrated by Fig. 19 (steps 1 to 3). On the left part of the first figure, (step 1), the platinum (1x1) phase is represented covered by chemisorbed oxygen atoms (black circles). On the right, the platinum is in the form of a clean hex phase. When the platinum covered by chemisorbed oxygen layer is heated up, the Pt atoms may thermally fluctuate far from their equilibrium position. A Pt atom at the border of the (1x1) region, covered with chemisorbed oxygen, is incorporated into the hex phase. At the same time, the oxygen atom bonds to the second layer, as shown in step 2. For the chemisorbed oxygen, the binding energies before and after this process are the same. Because the Pt atoms in the hex-phase are more stable than in the (1x1) phase, the Pt atoms caught in the hex phase are stabilized. Both the Pt atom phase transition and the transfer of oxygen into the second layer proceed (step 3). Consequently, the transition front moves into the oxygen covered (1x1) area. In the final stage of the conversion, the whole surface should be in the hexagonal phase. According to this model, for the subsurface oxygen to be formed as described above, both (1x1) and hex islands must be found on the platinum surface.
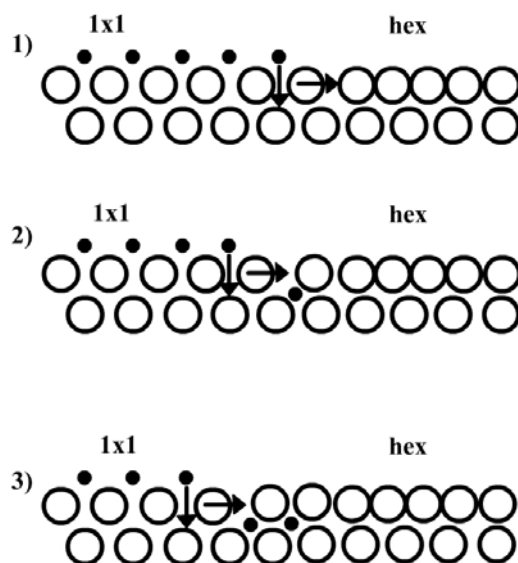
Fig. 19   Three steps of the mechanism of oxygen incorporation into the Pt subsurface layer. Model proposed by Lauterbach et al. [149]. Pt and O atoms are represented by open and filled circles, respectively.

2.3.4   Pt oxidation and catalytic activity

The presence of oxides on the surface of a Pt catalyst is known to have a major influence on its activity. Indeed, oxides have been found to cause the deactivation of the Pt catalyst toward the oxidation of CO and hydrocarbons [133, 136, 148, 153]. However, the oxide can also participate in the process of hydrocarbon oxidation. Indeed, as shown in reaction 2.8, the hydrocarbon RH can react with surface Pt oxide and produce carbon dioxide, water and a reduced Pt site. This suggests that the presence of hydrocarbons may help the reduction of a deactivated oxidized catalyst, leading to an active catalytic surface (activity recovery).

$$PtO_{X\,(surf.)} + RH \longrightarrow Pt_{(surf.)} + CO_2 + H_2O \qquad\qquad 2.8$$

2.3.5   Electrochemically produced oxygen species

As presented above in section 2.2, yet another type of oxygen is produced upon anodic polarization of the YSZ supported Pt electrode (Fig. 9). Once produced at the triple phase boundary, this strongly bonded $O^{\delta-}$ species is known to back-spill over the Pt surface. This justifies that it is sometimes mentioned as "back-spillover oxide ions $O^{\delta-}$" [11].
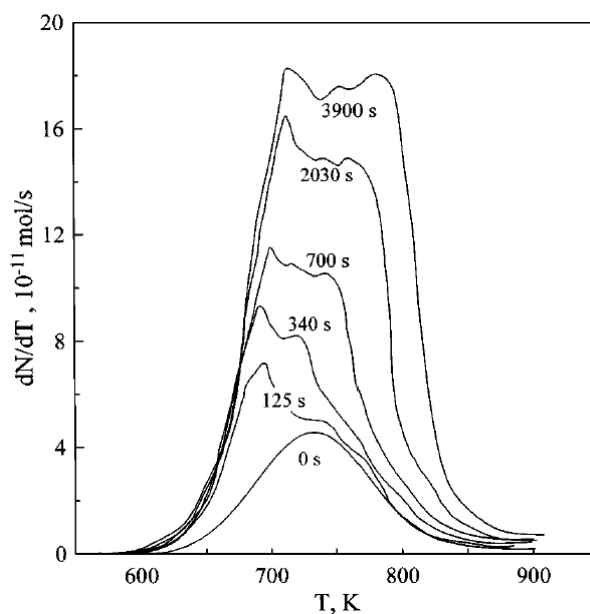
Fig. 20   Thermal desorbtion spectra of oxygen on a Pt film deposited on YSZ after gaseous oxygen adsorption at 673 K and an O_2 pressure of $4 \cdot 10^{-6}$ Torr for 1800 s followed by electrochemical O^{2-} supply ($I = 15$ μA) for various time periods. [122]

As shown in the TPD and XPS spectra (Fig. 20 and Fig. 21 respectively), the anodic polarization produces the $O^{\delta-}$ species, which has a different behavior than the chemisorbed oxygen originating from the gas. TPD measurements (Fig. 20) show that the back-spillover species appears progressively with increasing anodic polarization duration. In addition, it desorbs at a temperature 30 K higher than the oxygen formed via gaseous adsorption without polarization (0 s curve). This indicates that it is more strongly bonded to the Pt. The figure also shows that the presence of the $O^{\delta-}$ weakens the bond of the chemisorbed oxygen species of gaseous origin. This is evidenced by the lower desorption temperature (- 40 – 50 K) of the chemisorbed oxygen upon anodic polarization. XPS measurements (Fig. 21) show that the anodically produced $O^{\delta-}$ species has a very low bonding energy (~ 528.8 eV), indicating that it is very oxidic and carries a strong negative charge [11]. In summary, the exact nature of this species is still ambiguous as its characteristics differ from those of both the chemisorbed oxygen and the oxide.
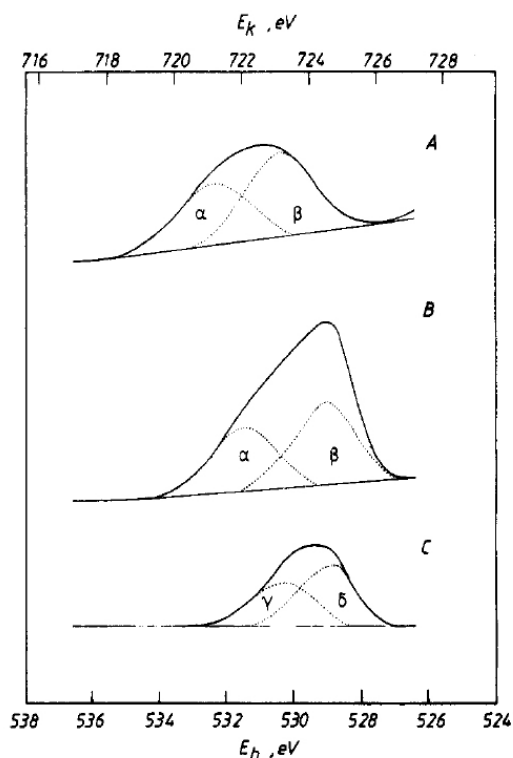
Fig. 21   Effect of electrochemical O^{2-} pumping on the O 1s spectrum of Pt/YSZ (A-C). XPS spectra at 400°C (A) $\Delta E_{WR} = 0$, $I = 0$; (B) $\Delta E_{WR} = 1.2$ V, $I = 40$ μA; (C) O 1s difference spectrum [154].

In summary, despite extended studies on the interactions between platinum and oxygen, recent papers [140, 148] suggest that the issue of platinum oxide is still ambiguous and matter to discussion. This concerns in particular the differentiation between adsorbed oxygen, subsurface oxygen and surface oxides and their respective stoichiometries. Moreover, an additional species, produced by anodic polarization, is known to back-spill over the catalyst surface (Fig. 9).

2.4   Aim of the work

Considering the relevant literature reviewed in this chapter, it was decided that the investigations of this present work should aim to clarify the effect of polarization on the reversible and permanent promotion of catalysis on YSZ supported Pt films. The chosen promoted chemical reaction is the catalytic oxidation of hydrocarbons. As discussed in this chapter, the measured catalytic activity is expected to reflect the state of the Pt catalyst and, in particular, the nature of the oxygen species present at its surface. Therefore, the study of the electrochemical promotion must be accompanied by the study of these oxygen

species. They consist of the chemisorbed oxygen originating from the gas phase, the platinum oxides, and the electrochemically produced back-spillover oxygen. However, one should also consider the oxygen species present at other interfaces of the $O_{2(g)}$,Pt/YSZ system. To gather knowledge on these species and how they interact, various electrochemical techniques should be used. Amongst them, linear sweep voltammetry and chronoamperometry, known to be precious tools for the in situ study of the electrochemical reactions in non steady state conditions, should be exploited.

2.5   References

1   T. Kawai, N. Hayakawa, T. Yamada, US Pat. 5,433,830, Method of Activating Zirconia Oxygen Sensor, 1995

2   Takao Murase, T. Yoshimura, US Pat. 5130002, Method of processing oxygen concentration sensor by applying AC current, and the thus processed sensor, 1992

3   H. K. O. Yasushi, US Pat. 4,702,816, Oxygen concentration detection system 1987

4   J. H. Visser, E. M. Logothetis, L. Rimai, R. E. Soltis, US Pat. 5281313, Selective combustible sensor and method, 1994

5   H. D. Wiemhofer, Solid State Ionics 75 (1995) 167

6   C. Deportes, Electrochimie des solides (Presses Universitaires de Grenoble, 1994)

7   J. Mizusaki, K. Amano, S. Yamauchi, K. Fueki, Solid State Ionics 22 (1987) 313

8   K. V. Kordesch, J. C. T. De Olivera, in: Ullmann's Encyclopedia of Industrial Chemistry, A12, (Wiley, New York, 1989

9   E. C. Subbarao, Solid Electrolytes and their Applications (Plenum Press, New York, 1980)

10   G. Tao, K. R. Sridhar, C. L. Chan, Solid State Ionics 175 (2004) 615

11   C. G. Vayenas, S. Bebelis, C. Pliangos, S. Brosda, D. Tsiplakides, Electrochemical Activation of Catalysis: Promotion, Electrochemical Promotion, and Metal-Support Interactions (Kluwer Academic / Plenum Publishers, New York, 2001)

12   J. E. Bauerle, J. Phys. Chem. Solids 30 (1969) 2657

13   T. H. Etsell, S. N. Flengas, J. Electrochem. Soc. 118 (1971) 1890

14   S. Pizzini, M. Bianchi, P. Colombo, S. Torchio, J. Appl. Electrochem. 3 (1973) 153

15   D. T. Dimitrov, C. D. Dushkin, Central European Journal of Chemistry 3 (2005) 605

16   P. Costamagna, M. Panizza, G. Cerisola, A. Barbucci, Electrochim. Acta 47 (2002) 1079

17   P. Costamagna, P. Costa, E. Arato, Electrochim. Acta 43 (1998) 967

18   A. Barbucci, R. Bozzo, G. Cerisola, P. Costamagna, Electrochim. Acta 47 (2002) 2183

19   L. Bultel, P. Vernoux, F. Gaillard, C. Roux, E. Siebert, Solid State Ionics 176 (2005) 793

20   Tsaofang Chao, K. J. Walsh, P. S. Fedkiw, Solid State Ionics 47 (1991) 277

21   S. P. Yoon, S. W. Nam, S.-G. Kim, S.-A. Hong, S.-H. Hyun, J. Power Sources 115 (2003) 27

22   P. E. Tsiakaras, S. L. Douvartzides, A. K. Demin, V. A. Sobyanin, Solid State Ionics 152-153 (2002) 721

23   P. Vernoux, F. Gaillard, L. Bultel, E. Siebert, M. Primet, J. Catal. 208 (2002) 412

24   A. Katsaounis, Z. Nikopoulou, X. E. Verykios, C. G. Vayenas, J. Catal. 222 (2004) 192

25   Y.-Z. Chen, B.-J. Liaw, C.-F. Kao, J.-C. Kuo, Appl. Catal. A 217 (2001) 23

26   J. Poppe, S. Völkening, A. Schaak, J. Janek, R. Imbihl, Phys. Chem. Chem. Phys. 1 (2000) 5241

27   A. Kaloyannis, C. A. Pliangos, I. V. Yentekakis, C. G. Vayenas, Ionics 1 (1995) 159

28   L. Bay, T. Jacobsen, Solid State Ionics 93 (1997) 201

29   W.-F. Zhang, P. Schmidt-Zhang, U. Guth, Solid State Ionics 169 (2004) 121

30   S. N. Shkerin, Russ. J. Electrochem. 39 (2003) 863

31   M. G. H. M. Hendriks, B. A. Boukamp, J. E. ten Elshof, W. E. van Zyl, H. Verweij, Solid State Ionics 146 (2002) 123

32   T. Jacobsen, L. Bay, Electrochim. Acta 47 (2002) 2177

33   S. Sridhar, V. Stancovski, U. Pal, Solid State Ionics 100 (1997) 17

34   A. Katsaounis, Z. Nikopoulou, X. E. Verykios, C. G. Vayenas, J. Catal. 226 (2004) 197

35   N. Kotsionopoulos, S. Bebelis, J. Appl. Electrochem. 35 (2005) 1253

36   L. Bultel, C. Roux, E. Siebert, P. Vernoux, F. Gaillard, Solid State Ionics 166 (2004) 183

37   C. Kokkofitis, G. Karagiannakis, S. Zisekas, M. Stoukides, J. Catal. 234 (2005) 476

38   J. Nowotny, T. Bak, C. C. Sorrell, Adv. Appl. Ceram. 104 (2005) 214

39   R. Todorovska, N. Petrova, D. Todorovsky, Appl. Surf. Sci. 252 (2005) 1266

40   R. Radhakrishnan, A. V. Virkar, S. C. Singhal, J. Electrochem. Soc. 152 (2005)

41   X. Li, F. Gaillard, P. Vernoux, Ionics 11 (2005) 103

42   S. Bredikhin, G. Abrosimova, A. Aronin, K. Hamamoto, Y. Fujishiro, S. Katayama, M. Awano, J. Electrochem. Soc. 151 (2004)

43   J. W. Jian, B. C. Yang, Y. K. Zhang, Wuji Cailiao Xuebao/Journal of Inorganic Materials 19 (2004) 93

44   O. Sze Nga Sum, E. Djurado, T. Pagnier, N. Rosman, C. Roux, E. Siebert, Solid State Ionics 176 (2005) 2599

45   J. Poppe, A. Schaak, J. Janek, R. Imbihl, Berichte der Bunsen-Gesellschaft 102 (1998) 1019

46   E. J. L. Schouler, M. Kleitz, J. Electrochem. Soc. 134 (1987) 1045

47   J. Mizusaki, K. Amano, S. Yamauchi, K. Fueki, Solid State Ionics 22 (1987) 323

48   J. Sasaki, J. Mizusaki, S. Yamauchi, K. Fueki, Solid State Ionics 3-4 (1981) 531

49   A. Mitterdorfer, L. J. Gauckler, Solid State Ionics 120 (1999) 211

50   A. Mitterdorfer, L. J. Gauckler, Solid State Ionics 117 (1999) 187

51   A. Mitterdorfer, L. J. Gauckler, Solid State Ionics 117 (1999) 203

52   M. J. Verkerk, M. W. J. Hammink, A. J. Burggraaf, J. Electrochem. Soc. 130 (1983) 70

53   R. J. Brook, W. L. Pelzmann, F. A. Kroger, J. Electrochem. Soc. 118 (1971) 185

54   S. P. Yoon, S. W. Nam, J. Han, T.-H. Lim, S.-A. Hong, S.-H. Hyun, Solid State Ionics 166 (2004) 1

55   T. M. Gur, I. D. Raistrick, R. A. Huggins, J. Electrochem. Soc. 127 (1980) 2620

56   D. Braunshtein, D. S. Tannhauser, J. Riess, J. Electrochem. Soc. 128 (1981) 82

57   J. L. Gland, Surf. Sci. 93 (1980) 487

58   E. Siebert, Electrochim. Acta 39 (1994) 1621

59   T. Kenjo, Y. Yamakoshi, K. Wada, J. Electrochem. Soc. 140 (1993) 2151

60   M. Mogensen, S. Skaarup, Solid State Ionics 86-88 (1996) 1151

61   D. Y. Wang, A. S. Nowick, J. Electrochem. Soc. 128 (1981) 55

62   G. B. Barbi, Ber. Bunsenges. Phys. Chem. Chem. Phys. 99 (1995) 741

63   N. L. Robertson, J. N. Michaels, J. Electrochem. Soc. 137 (1990) 129

64   W. Gopel, H. D. Wiemhofer, Ber. Bunsenges. Phys. Chem. 94 (1990) 981

65   M. W. Breiter, K. Leeb, G. Fafilek, J. Electroanal. Chem. 434 (1997) 129

66   A. Jaccoud, G. Foti, C. Comninellis, Electrochim. Acta 51 (2006) 1264

67   D. Y. Wang, A. S. Nowick, J. Electrochem. Soc. 126 (1979) 1155

68   J. Fleig, J. Power Sources 105 (2002) 228

69   L. R. Velho, R. W. Bartlett, Metallurgical Transactions 3 (1972) 65

70   J.-H. Park, R. N. Blumenthal, J. Electrochem. Soc. 136 (1989) 2867

71   B. A. van Hassel, B. A. Boukamp, A. J. Burggraaf, Solid State Ionics 53-56 (1992) 890

72   S. N. Shkerin, Russ. J. Electrochem. 40 (2004) 510

73   I. Riess, Solid State Ionics 52 (1992) 127

74   B. C. Nguyen, L. M. Rincon-Rubio, D. M. Mason, J. Electrochem. Soc. 133 (1986) 1860

75   M. V. Perfilyev, Solid State Ionics 9-10 (1983) 765

76   B. A. van Hassel, B. A. Boukamp, A. J. Burggraaf, Solid State Ionics 48 (1991) 155

77   O. J. Velle, T. Norby, P. Kofstad, Solid State Ionics 47 (1991) 161

78   C. Athanasiou, G. Karagiannakis, S. Zisekas, M. Stoukides, Solid State Ionics 136-137 (2000) 873

79   D. Braunshtein, D. S. Tannhauser, I. Riess, J. Electrochem. Soc. 128 (1981) 82

80   J. R. Anderson, in: (Academic Press, New York, 1975), 13

81   Y. K. Peng, P. T. Dawson, Can. J. Chem. 52 (1974) 3507

82   H. Okamoto, G. Kawamura, T. Kudo, Electrochim. Acta 28 (1983) 379

83   B. L. Kuzin, M. A. Komarov, Solid State Ionics 39 (1990) 163

84   E. A. Baranova, Chemical and Electrochemical Promotion of Supported Rh Catalyst, Thesis Nr. 3245, EPFL, Lausanne (2005)

85   J. Bockris, A. Reddy, Modern Electrochemistry (Plenum Press, New York, 1970)

86   A. J. Bard, L. R. Faulkner, Electrochemical Methods: Fundamentals and Applications (Wiley, New York, 1980)

87   T. Kenjo, N. Shiroichi, Electrochim. Acta 42 (1997) 3461

88   H. Angerstein - Kozlowska, B. E. Conway, W. B. A. Sharp, J. Electroanal. Chem. 43 (1973) 9

89   K. J. Vetter, J. W. Schultze, J. Electroanal. Chem. 34 (1972) 131

90   G. Jerkiewicz, G. Vatankhah, J. Lessard, M. P. Soriaga, Y.-S. Park, Electrochim. Acta 49 (2004) 1451

91   L. D. Burke, M. B. C. Roche, J. Electroanal. Chem. 137 (1982) 175

92   J. Yi, A. Kaloyannis, C. G. Vayenas, Electrochim. Acta 38 (1993) 2533

93   P. A. van Manen, R. Weewer, H. W. de Wit, J. Electrochem. Soc. 139 (1992) 1130

94   G. Fafilek, K. Leeb, M. W. Breiter, Solid State Ionics 86-88 (1996) 1415

95   C. G. Vayenas, A. Ioannides, S. Bebelis, J. Catal. 129 (1991) 67

96   E. Varkaraki, Electrochemical promotion of an IrO_2 catalyst for the gas phase oxidation of ethylene, Thesis Nr. 1455, EPFL, Lausanne (1995)

97   C. G. Vayenas, M. M. Jaksic, S. I. Bebelis, S. G. Neophytides, in: Modern Aspects of Electrochemistry, 29, (Plenum Press, New York, 1996), 57

98   J. Pritchard, Nature 343 (1990) 592

99   C. G. Vayenas, S. Bebelis, Ladas.S, Nature 343 (1990) 625

100   E. Varkaraki, J. Nicole, E. Plattner, C. Comninellis, C. G. Vayenas, J. Appl. Electrochem. 25 (1995) 978

101   J. Nicole, C. Comninellis, Proceedings of Contemporary Trends in Electrochemical Engineering (1996) 1

102   J. Nicole, C. Comninellis, Solid State Ionics 136-137 (2000) 687

103   J. Nicole, C. Comninellis, Proceedings of The 1997 Joint International Meeting 97-2 (1997)

104   C. G. Vayenas, S. I. Bebelis, Solid State Ionics 94 (1997) 267

105   S. Wodiunig, V. Patsis, C. Comninellis, Solid State Ionics 136-137 (2000) 813

106   S. Bebelis, M. Makri, A. Buekenhoudt, J. Luyten, S. Brosda, P. Petrolekas, C. Pliangos, C. G. Vayenas, Solid State Ionics 129 (2000) 33

107   E. P. M. Leiva, C. G. Sánchez, J. Solid State Electrochem. 7 (2003) 588

108   V. D. Belyaev, T. I. Politova, V. A. Sobyanin, Solid State Ionics 136-137 (2000) 721

109   E. D. Wachsman, P. Jayaweera, G. Krishnan, A. Sanjurjo, Solid State Ionics 136-137 (2000) 775

110   J. Janek, B. Luerßen, R. Imbihl, M. Rohnke, Phys. Chem. Chem. Phys. 2 (2000) 1935

111   G. Foti, I. Bolzonella, J. Eaves, C. Comninellis, Chimia 56 (2002) 137

112   J. Fleig, J. Jamnik, J. Electrochem. Soc. 152 (2005) E138

113   I. Riess, Solid State Ionics 176 (2005) 1667

114   A. Piram, X. Li, F. Gaillard, C. Lopez, A. Billard, P. Vernoux, Ionics 11 (2005) 327

115   M. Stoukides, C. G. Vayenas, J. Catal. 70 (1981) 137

116   C. G. Vayenas, S. Bebelis, S. Neophytides, J. Phys. Chem. 92 (1988) 5083

117   D. Tsiplakides, S. Balomenou, A. Katsaounis, D. Archonta, C. Koutsodontis, C. G. Vayenas, Catal. Today 100 (2005) 133

118   S. P. Balomenou, D. Tsiplakides, A. Katsaounis, S. Brosda, A. Hammad, G. Foti, C. Comninellis, S. Thiemann-Handler, B. Cramer, C. G. Vayenas, Solid State Ionics 177 (2006) 2201

119   C. G. Vayenas, S. Brosda, C. Pliangos, J. Catal. 216 (2003) 487

120   C. G. Vayenas, Solid State Ionics 168 (2004) 321

121   S. Ladas, S. Bebelis, C. G. Vayenas, Surf. Sci. 251/252 (1991) 1062

122   S. Neophytides, D. Tsiplakides, C. G. Vayenas, J. Catal. 178 (1998) 414

123   J. Nicole, D. T. Tsiplakides, S. Wodiunig, C. Comninellis, J. Electrochem. Soc. 144 (1997) L312

124   J. Nicole, C. Comninellis, J. Appl. Electrochem. 28 (1998) 223

125   D. Tsiplakides, J. Nicole, C. G. Vayenas, C. Comninellis, J. Electrochem. Soc. 145 (1998) 905

126   J. Nicole, Etude de la promotion électrochimique de l'oxydation catalytique de l'éthylène sur des oxydes métalliques, Thesis Nr. 1933, EPFL, Lausanne (1999)

127   G. Foti, O. Lavanchy, C. Comninellis, J. Appl. Electrochem. 30 (2000) 1223

128   I. Bolzonella, Electrochemical Promotion of Rhodium Catalyst. Application to Nitrogen Monoxide Reduction, Thesis Nr. 2743, Ecole Polytechnique Fédérale, Lausanne (2003)

129   S. G. Neophytides, C. G. Vayenas, J. Phys. Chem. 99 (1995) 17063

130   S. Wodiunig, Electrochemical Promotion of RuO_2 Catalysts for the Gas Phase Combustion of Ethylene, Thesis Nr. 2138, Ecole Polytechnique Fédérale, Lausanne (2000)

131   S. Wodiunig, C. Comninellis, C. Mousty, Proceedings of The 1997 Joint International Meeting 97-2 (1997)

132   S. Wodiunig, C. Comninellis, C. Mousty, in: Energy and Electrochemical Processing for a Cleaner Environment, 97-28, (The Electrochemical Society Proceedings Series, Pennington, 1997), 147

133   C. G. Vayenas, C. Georgakis, J. Michaels, J. Tormo, J. Catal. 67 (1981) 348

134   C.-B. Wang, H.-K. Lin, S.-N. Hsu, T.-H. Huang, H.-C. Chiu, J. Molec. Catal. A 188 (2002) 201

135   C.-C. Hu, K.-Y. Liu, Electrochim. Acta 45 (2000) 3063

136   C. G. Vayenas, J. N. Michaels, Surf. Sci. 120 (1982) L405

137   C.-B. Wang, C.-T. Yeh, J. Catal. 178 (1998) 450

138   C.-P. Hwang, C.-T. Yeh, J. Catal. 182 (1999) 48

139   M. Salmeron, L. Brewer, G. A. Somorjai, Surf. Sci. 112 (1981) 207

140   C. R. Parkinson, M. Walker, C. F. McConville, Surf. Sci. 545 (2003) 19

141   H. Niehus, G. Comsa, Surf. Sci. 93 (1980) L147

142   J. L. Gland, B. A. Sexton, G. B. Fisher, Surf. Sci. 95 (1980) 587

143   C. I. Carlisle, T. Fujimoto, W. S. Sim, D. A. King, Surf. Sci. 470 (2000) 15

144   C. P. Hwang, C. T. Yeh, J. Molec. Catal. A 112 (1996) 295

145   R. J. Berry, Surf. Sci. 76 (1978) 415

146   R. Ducros, R. P. Merrill, Surf. Sci. 55 (1976) 227

147   T. Matsushima, D. B. Almy, J. M. White, Surf. Sci. 67 (1977) 89

148   J. Dicke, H. H. Rotermund, J. Lauterbach, Surf. Sci. 454-456 (2000) 352

149   J. Lauterbach, K. Asakura, H. H. Rotermund, Surf. Sci. 313 (1994) 52

150   H. P. Bonzel, A. M. Franken, G. Pirug, Surf. Sci. 104 (1981) 625

151   H. Niehus, G. Comsa, Surf. Sci. 102 (1981) L14

152   P. Legare, L. Hilaire, G. Maire, Surf. Sci. 141 (1984) 604

153   C. G. Vayenas, B. Lee, J. Michaels, J. Catal. 66 (1980) 36

154   S. Ladas, S. Kennou, S. Bebelis, C. G. Vayenas, J. Phys. Chem. 97 (1993) 8845

CHAPTER 3

Preliminary studies on the $O_{2(g)}$,Pt/YSZ system
Influence of the electrode preparation method

The chapter presents and discusses the characterization via electrochemical measurements and scanning electron microscopy (SEM) of platinum electrodes prepared by three different methods. The electrodes have been deposited by sputtering, by thermal decomposition of a Pt salt and by screen-printing of a paste composed of Pt and YSZ particles.
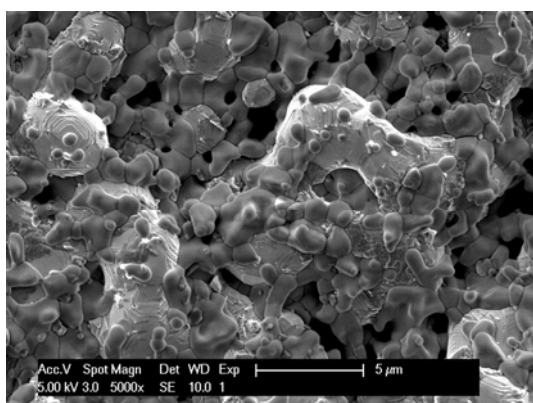
The results evidence significant variations of the electrochemical response (cyclic voltammogram) for the different preparation methods, hence different microstructures, revealed by SEM. The variations of the electrochemical response with the observed microstructure is discussed in terms of electrochemical processes, assumed to occur at the $O_{2(g)}$,Pt/YSZ system. The most promising results are obtained with the cermet electrode prepared by screen-printing of a paste containing Pt and YSZ particles.

3.1 Introduction

Reproducibility problems are often encountered with the $O_{2(g)}$,Pt/YSZ system. The importance of the preparation procedure has been discussed or mentioned in papers dealing with electrochemical promotion of catalysis [1, 2], cyclic voltammetry [3-6] and analysis of the electrode resistances [7-10]. Although the general chemical composition of the electrode components is identical, the preparation method can have a great influence on the results and the interpretations. It is explained by the fact that the microstructure has an important impact on the electrode behavior and the former is usually highly affected by the preparation and aging effects [7-13].

The $O_{2(g)}$,Pt/YSZ system is usually used as an electrode for the electrochemical oxygen exchange reaction. The overall reaction can be written

$$O^{2-}_{(YSZ)} \rightleftarrows \tfrac{1}{2} O_{2(gas)} + 2e^-$$

3.1
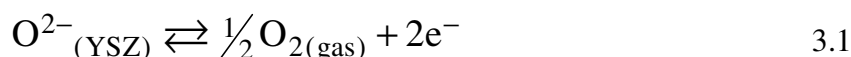
Where O^{2-} is the mobile oxygen on a lattice site of YSZ, e^- is an electron located on the Pt electrode and O_2 is molecular oxygen. Due to the heterogeneous origin of the species taking place in this reaction, the only location where it can occur is the vicinity of the triple phase boundary (tpb), even though extension of the reaction site toward binary interfaces are sometimes mentioned.

However, as it is discussed in literature [4-6, 14, 15] and as it will be seen in details in the subsequent chapter, additional electrochemical reactions may also occur at the solid/solid interface between the Pt and the YSZ phases, giving rise to a pseudocapacitive behavior.

The goal of the preliminary studies, presented in this chapter, is to compare the electrochemical response of electrodes prepared by three different methods (sputtering, thermal decomposition and screen-printing). Cyclic voltammetry is known to be a sensitive electrochemical method and will therefore be used to characterize the electrochemical behavior of the electrodes. The voltammogram shape is expected to depend on the geometrical (microstructure) and chemical state of the electrode. Along with cyclic voltammetry, scanning electron microscopy (SEM) is also used in this work to give the apparent microscale morphology of each electrode.

3.2   Experimental

3.2.1   Electrodes prepared by sputtering

The sputtered platinum electrode was deposited onto the YSZ substrate by magnetron sputtering technique in inert atmosphere at room temperature. Direct current (dc) mode was used with a discharge of 330 V at an argon pressure of 10^{-2} mbar. Under these conditions, the deposition rate was 0.09 nm s^{-1} on the YSZ pellet, as determined by profilometric measurement (Alphastep, Model 500) of the film thickness on smooth silicon samples processed simultaneously. A 200 nm thick Pt electrode was deposited on a 10 x 15 x 1 mm YSZ 8%mol pellet (Technox 802, Dynamic Ceramic Ltd) (Fig. 1). The electrode size is 7 x 5 mm giving a geometric surface of 0.35 cm^2. Platinum counter and reference electrodes have been deposited on the reverse side of the pellet using the same sputtering procedure. The working and counter electrodes were located in a symmetrical face-to-face arrangement on the opposite sides of the YSZ pellet. This geometry ensured a symmetrical current and potential distribution in the cell [16]. Before carrying out the first electrochemical studies, the cell was let in the measuring condition ($T = 450°C$, $pO_2 = 20$ kPa in He) for two days to achieve stabilization. After having completed a series of voltammetric measurements, a heat treatment has been carried out at 700°C in the same atmosphere during 4 hours in order to alter the electrode microstructure. Another series of electrochemical studies were performed after the heat treatment.
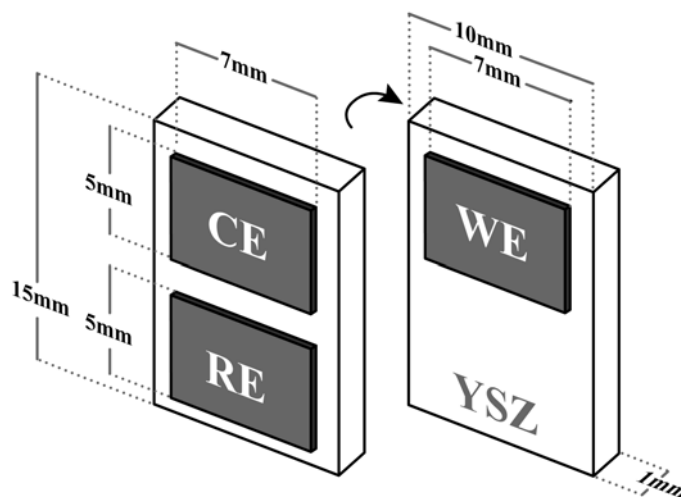

Fig. 1   Placement and dimensions of the Pt electrodes prepared by sputtering and by thermal decomposition of Pt salt. WE: working electrode; CE: counter electrode; RE: reference electrode.

3.2.2   Electrodes prepared by thermal decomposition of H_2PtCl_6

The electrodes were prepared by thermal decomposition of a 0.1 M solution of hexachloroplatinic acid (H_2PtCl_6 x $(H_2O)_6$) in isopropanol. 12 µl of solution was deposited on each delimited electrode surface, dried under infrared lamp and decomposed at 500°C during 30 minutes in air. This step was repeated seven times. All three electrodes were prepared following the same procedure. The electrochemical cell was then annealed at 1150°C during two hours in air. The YSZ pellet, the electrode locations and dimensions are identical to the cell equipped with sputtered electrodes described above (Fig. 1).

3.2.3   Electrode prepared by screen-printing of a paste composed of Pt and YSZ particles

This three-electrode electrochemical cell has been provided by Bosch GmbH. All electrodes were prepared using a paste composed of : $65\%_w$ of 1µm particle size platinum powder, $11\%_w$ of 1 µm particle size YSZ (8 mol% Y_2O_3 in ZrO_2) and $24\%_w$ of a polyvinyl pyrrolidone solution (2% in isopropanol). The paste was screen printed on a 1.3 mm thick YSZ pellet in the shape of 2 x 4 mm rectangles and sintered at 1400°C in air to give a film thickness of 15 µm (Fig. 2). The resulting cermet electrode is composed of 62 $\%_{vol}$ of platinum and 38 $\%_{vol}$ of YSZ and has a geometric surface area of 0.08 cm^2.

3.2.4   The measurements

The SEM images were obtained using a JEOL JMS-6300-F scanning electron microscope. The reactor for electrochemical measurements, shown in Fig. 2, was of single-chamber type where all electrodes were exposed to the same atmosphere. It consisted of a quartz tube of 90 ml volume closed with a stainless steel cap. The single-pellet three-electrode cell was simply suspended in the reactor with the three gold wires serving as electrical contacts to the electrodes. The temperature in the reactor was measured with a K-type (NiCr-Ni) thermocouple placed in proximity of the surface of the working electrode. Gold wires and thermocouple were led out the reactor through a four-hole alumina tube (*Degussa*). The reactor was put into a furnace (*XVA271, Horst*) equipped with a heat control system (*HT30, Horst*). Measurements were carried out at 450°C under continuous gas flow of 200 ml min^{-1} fed by mass flow controllers (*F/201C and E-5514-FA, Bronkhorst*). The gas source was a *Carbagas* certified standard of O_2 (99.95%) supplied as

a 20% mixture in He (99.996%). Dilution was made with He (99.996%). All electrochemical measurements and data acquisition were made using a scanning potentiostat (*Autolab, Model PGSTAT30, Eco Chemie*). Unless otherwise specified, the potential of the working electrode, E_{WR}, is given with respect to the reference electrode exposed to oxygen partial pressure of 20 kPa.
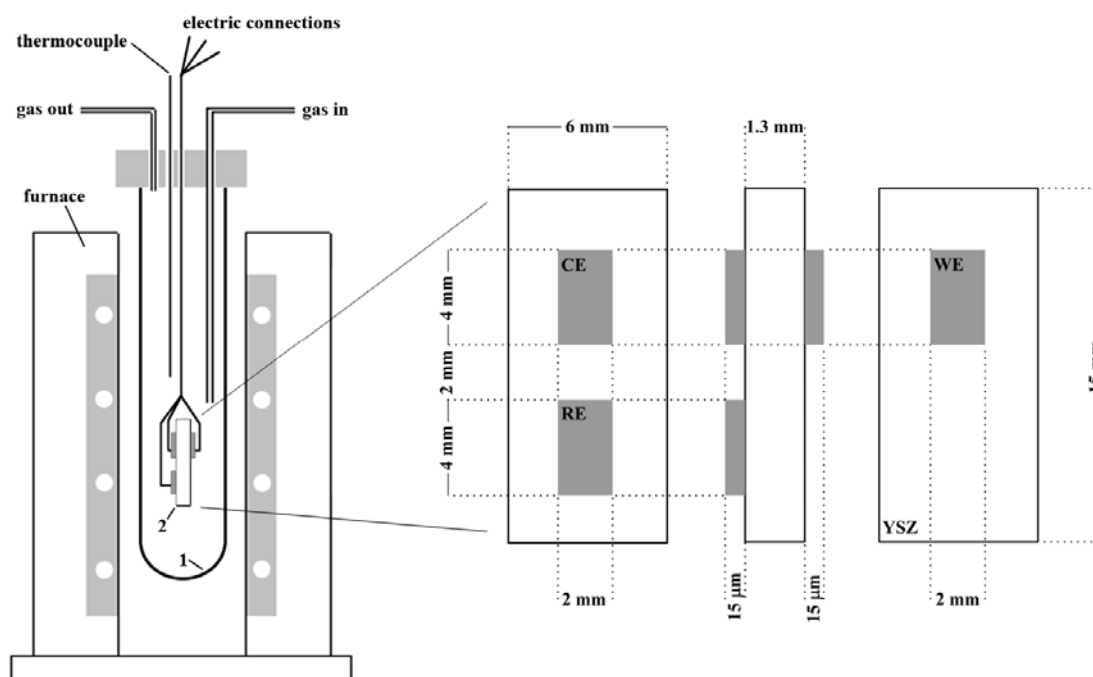
Fig. 2   Scheme of the experimental setup and the electrochemical cell equipped with cermet electrodes. 1: quartz tube; 2: electrochemical cell.

The overpotential η for the O_2/O^{2-} redox couple is defined as $\eta = E_{WR} - E_{WR\ eq}$, where $E_{WR\ eq}$ is the potential difference between the working and the reference electrode at equilibrium (open circuit potential).

Since the working and the reference electrode are identical and exposed to the same gas composition, $E_{WR\ eq}$ is zero. The overpotential η is therefore simply given by $\eta = E_{WR}$.

3.3 Results

3.3.1 Scanning electron microscopy

Electrode prepared by sputtering

Fig. 3 shows the SEM image of the electrode prepared by sputtering. The platinum is found in the form of a compact amorphous film, with no apparent porosity. It follows the topography of the YSZ substrate.

Fig. 3   SEM image of the sputtered Pt electrode before the 700°C heat treatment

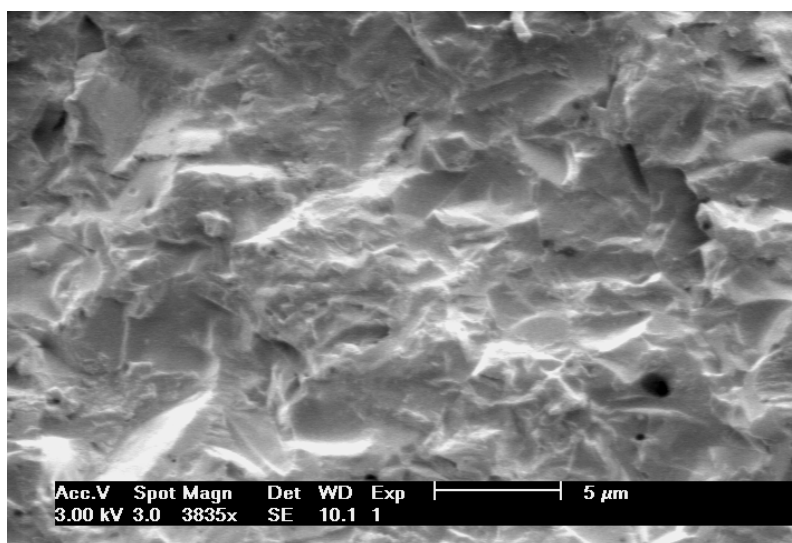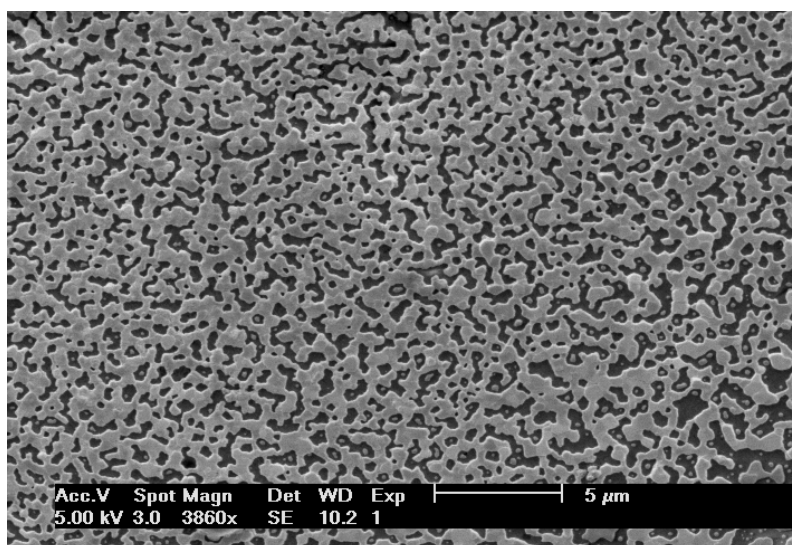Fig. 4   SEM image of the sputtered Pt electrode after the 4 hour heat treatment in $pO_2 = 20$ kPa (in He) at $T = 700$°C

Fig. 4 shows the microstructure of the sputtered electrode after the 4 hour heat treatment at 700°C in 20 kPa O_2. A continuous amorphous platinum network (light grey on the image) with pores of the size of a few hundred nm to 1 µm lays on the YSZ substrate (black).

Electrode prepared by thermal decomposition of H_2PtCl_6

The microstructure of the electrode prepared by thermal decomposition of H_2PtCl_6 (Fig. 5) is characterized by a continuous platinum network formed by micrometer scale crystallites.
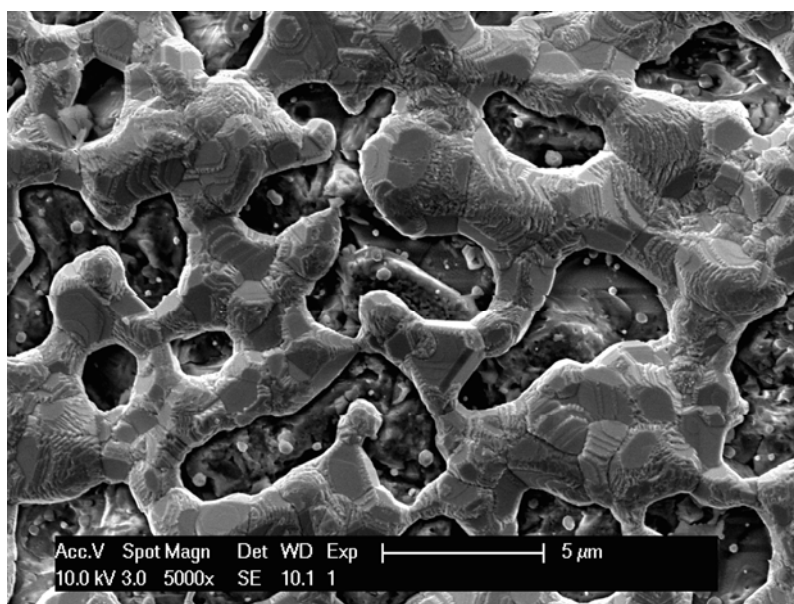
Fig. 5   SEM image of the platinum film (light grey) and the YSZ solid electrolyte (dark grey) on the electrode prepared by thermal decomposition of H_2PtCl_6

Electrode prepared by screen-printing of a paste composed of Pt and YSZ particles

The microstructure of the cermet electrode prepared by screen printing is shown in Fig. 6. It consists of a continuous network of platinum composed of crystallites of a few µm. The continuity of the platinum network is confirmed by the electrical conductivity of the film at ambient temperature. The YSZ network, composed of 1 µm particles, appears darker on the image and seems continuous.
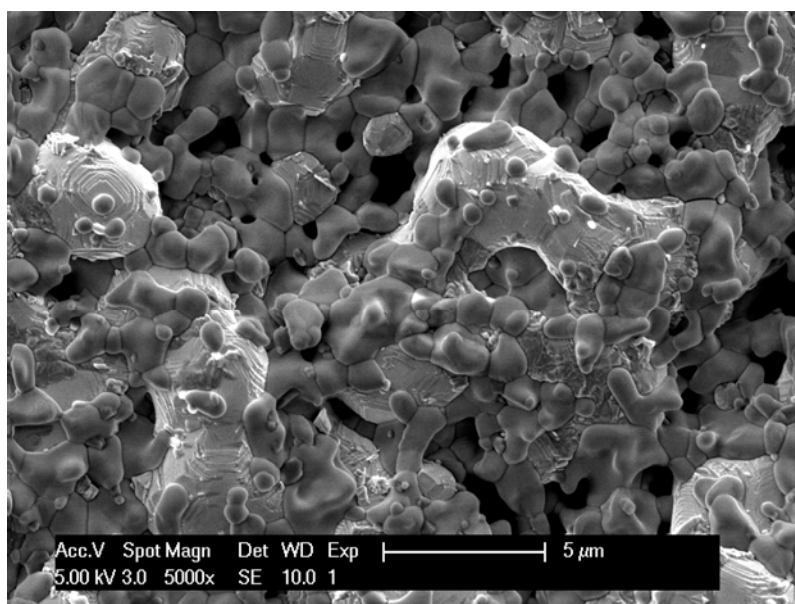
Fig. 6   SEM image of the electrode prepared by screen-printing of a paste composed of Pt (light grey) and YSZ (dark grey) particles.

3.3.2   Cyclic voltammetry

Electrode prepared by sputtering
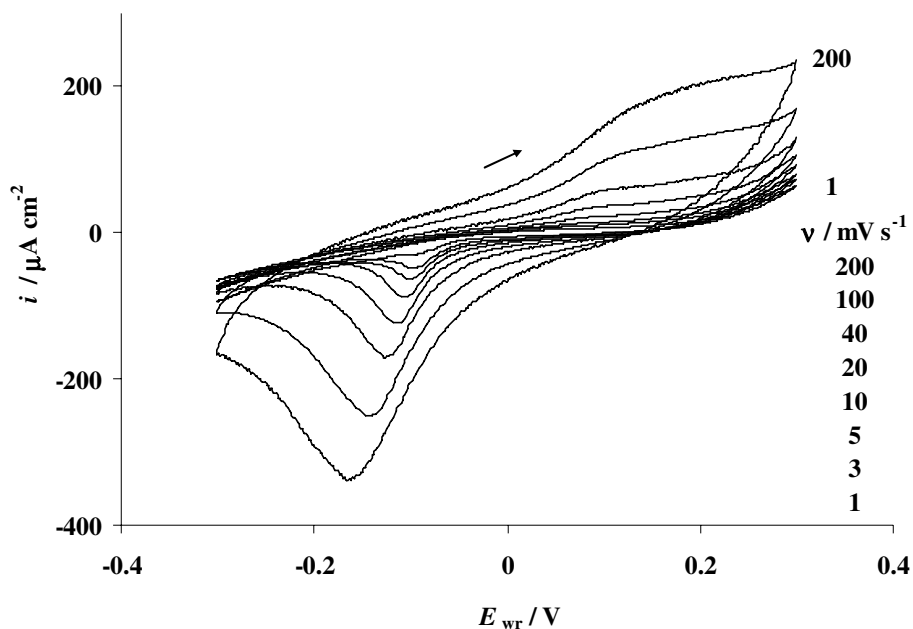
Fig. 7   Cyclic voltammetry with the electrode prepared by sputtering before the heat treatment. Effect of the scan rate v. $T = 450°C$; $pO_2 = 20$ kPa. The current density i is calculated with respect to the geometric area of the electrode.

Fig. 7 shows the effect of the potential scan rate on the voltammogram of the sputtered electrode before the heat treatment. These voltammograms feature an anodic wave and a cathodic peak. At low scan rates ν, the cathodic peak appears at $E_{WR} = -0.1$ V. As the rate increases, the peak current grows and the peak potentials shifts toward lower values, up to $E_{WR} = -0.15$ V. The anodic wave appears at $E_{WR} = 0.1$ V. It is more pronounced as the scan rate increases.
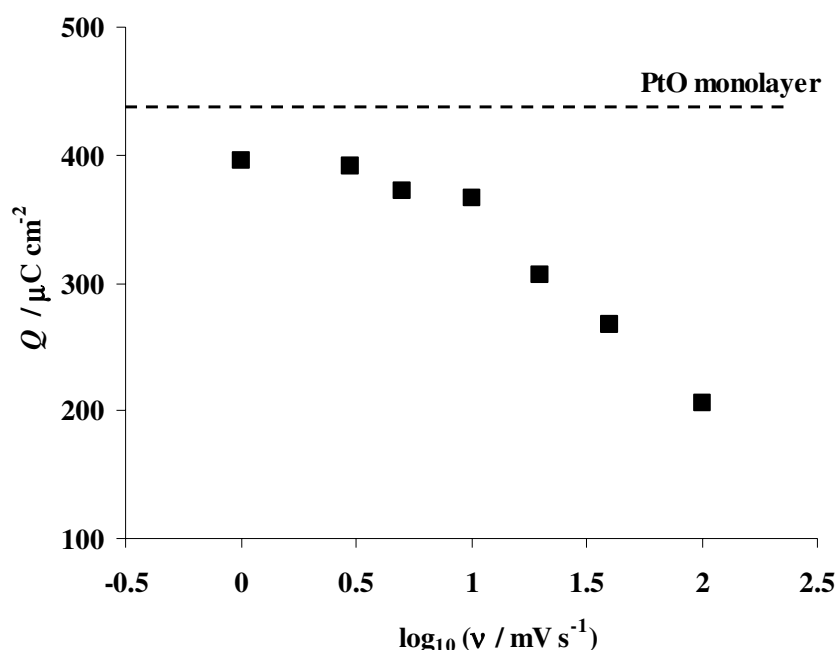
Fig. 8   Charge density Q, obtained by integration of the cathodic peak in the voltammograms of Fig. 7, as a function of the decimal logarithm of the scan rate, ν. Charge density Q is calculated with respect to the geometric area of the electrode.

Integration of the cathodic peak appearing in the voltammograms of Fig. 7 gives a charge density Q. Fig. 8 shows the integrated charge density Q as a function of the scan rate in a decimal logarithmic scale. The charge density, calculated with respect to the geometric area of the electrode, is found to increase as the potential scan rate decreases. For low scan rates, it tends to approximately 400 $\mu C\ cm^{-2}$.

Fig. 9 shows the effect of the potential scan rate on the voltammogram of the sputtered electrode after the heat treatment. Unlike for the untreated sputtered electrode (Fig. 7), no

distinct cathodic or anodic peak is observed. Moreover, the scan rate dependency is weak and the anodic-cathodic behaviors are almost symmetrical. At low scan rate, the heat-treated electrode (Fig. 9) is over three times more active than before heat treatment (Fig. 7).
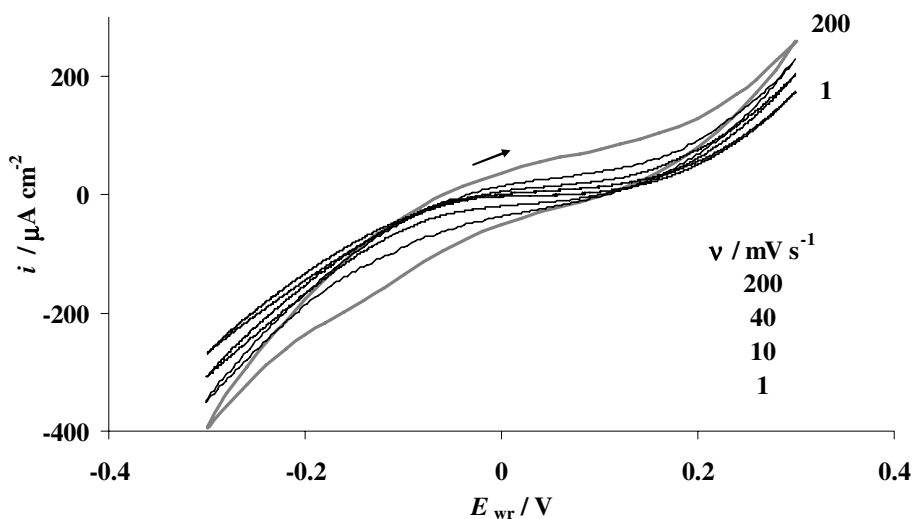
Fig. 9   Cyclic voltammetry with the electrode prepared by sputtering followed by the 4 hour heat treatment at $T = 700°C$ in 20 kPa O_2. Effect of the scan rate v. $T = 450°C$; $pO_2 = 20$ kPa. The current density i is calculated with respect to the geometric area of the electrode.

Electrode prepared by thermal decomposition of H_2PtCl_6

Fig. 10 shows the effect of the potential scan rate on the voltammogram of the electrode prepared by thermal decomposition of H_2PtCl_6. These voltammograms, featuring an anodic wave and a cathodic peak, are very similar to those obtained with the sputtered electrode before the heat treatment (Fig. 7). Indeed, despite their very distinct electrode preparation methods, the peaks, their potentials, and the way they vary with the scan rate are almost identical. As for the sputtered electrode, the cathodic peak of the voltammograms of Fig. 10 has been integrated. The calculated charge density Q increases and tends to 260 μC cm^{-2} as the scan rate decreases.
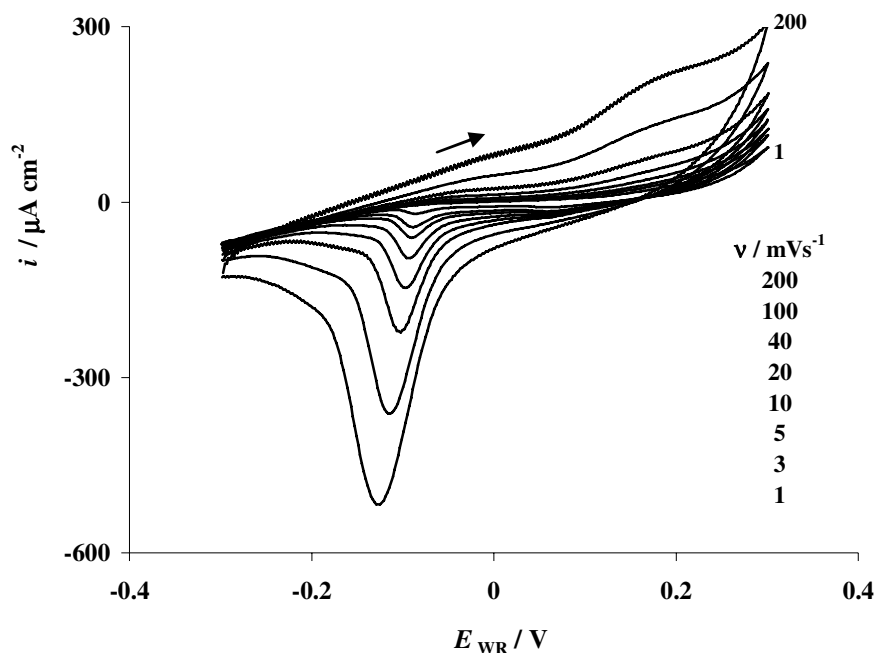
Fig. 10   Cyclic voltammetry with the electrode prepared by thermal decomposition of H_2PtCl_6. Effect of the scan rate v. $T = 450°C$; $pO_2 = 20$ kPa. The current density i is calculated with respect to the geometric area of the electrode.

Electrode prepared by screen-printing of a paste composed of Pt and YSZ particles

Fig. 11 shows the effect of the potential scan rate on the voltammogram of the cermet electrode prepared using a paste composed of Pt and YSZ particles. These voltammograms feature no distinct anodic peak or wave. However, two cathodic peaks are observed. Distinction of the peaks is made easier as the scan rate decreases. The potential of the first peak is in the range of the peaks found for the two other electrode preparations (see Fig. 7 and Fig. 10). The second peak, however, appears at lower potentials, beyond $E_{WR} = -0.2$ V at high scan rates.

As in Fig. 7 and Fig. 10, increasing the scan rate causes the growth of the peak current and the shift toward lower E_{WR}.
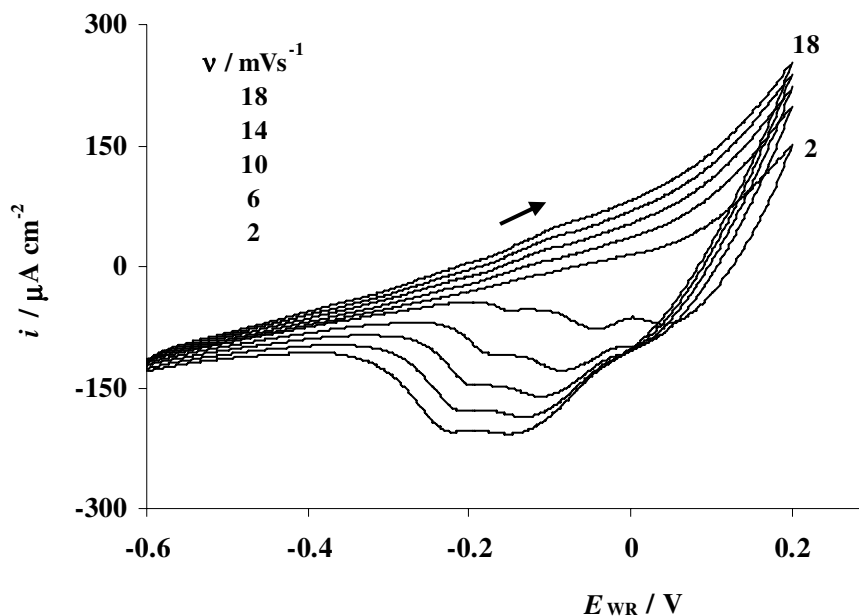
Fig. 11   Cyclic voltammetry with the cermet electrode prepared using a Pt/YSZ paste. Effect of the scan rate v. $T = 450°C$; $pO_2 = 20$ kPa. The current density i is calculated with respect to the geometric area of the electrode.

3.4   Discussion

Scanning electron microscopy of the electrode prepared by sputtering (Fig. 3) shows that the platinum layer is very compact, with no apparent porosity. This characteristic is usually encountered for the sputtering deposition technique [13, 17]. The 4 hour heat treatment at 700°C causes the alteration of the Pt film microstructure. Indeed, under the influence of high temperature, the films tends to and create porosity through the formation of agglomerates [17]. This is a clear indication that the sputtered electrode is not stable if not treated at high temperature. Concerning the electrochemical response of the electrode before and after the heat treatment, studied by cyclic voltammetry, the behavior changes radically. The voltammogram of the untreated compact film shows a distinct cathodic peak and an anodic wave, which may indicate the occurrence of a pseudocapacitive behavior. This means that an electrochemical reaction may take place and cause the storage of charges on the electrode.

The occurrence of an anodic and a cathodic peak has been reported in literature with electrode prepared by sputtering [18] but also using a Pt paste and other preparation methods [4, 6, 15, 19]. In all papers, these peaks are related to charging/discharging

processes involving a Pt-O compound of various natures, remaining on the electrode surface.

Fig. 8 shows that the charge involved in the cathodic peaks increases with decreasing scan rate. This tendency is expected given that, at lower rates, more time is conceded to store charges. The value of the corresponding charge density Q seems to saturate at approximately 400 μC cm^{-2}, slightly below the value of a Pt-O monolayer [20]. This result tends to confirm the conclusion of the paper written by Kenjo et al. [15] speculating that the cathodic peak is due to the reduction of an anodically formed oxygen monolayer at the Pt/YSZ interface.

In contrast to the untreated electrode, cyclic voltammetry on the heat-treated porous electrode (Fig. 9) shows no pseudocapacitive behavior, i.e. no peak and a low scan rate dependency. This dramatic change of behavior could be due to the modification of the electrode microstructure, shown by SEM (Fig. 4). Indeed, the creation of pores, consequently, the creation of tpb sites, may favor the electrochemical oxygen exchange reaction 3.1. In this reaction, $O_{2(g)}$ and $O^{2-}_{(YSZ)}$ are free to diffuse away from the electrochemical reaction site and therefore cannot cause charge storage (the pseudocapacitive behavior).

SEM images of the electrode prepared by thermal decomposition of H_2PtCl_6 at 1150°C (Fig. 5) features pores and Pt agglomerates of bigger size than for the heat-treated sputtered electrode (Fig. 4). This is certainly due to the higher treatment temperature. Cyclic voltammetry indicates that, despite the very different preparation procedures, the electrochemical behavior of this electrode is very similar to the untreated compact sputtered electrode (Fig. 7 and Fig. 10). This may indicate that the nature of the contact between the platinum film and the YSZ support is similar, i.e. an intimate contact with only a low porosity. It has been shown that increasing the sintering temperature causes the Pt/YSZ contact surface to be increased [15].

The main most intriguing result obtained with the cermet electrode prepared by screen-printing of a paste containing Pt and YSZ particles is the appearance of a second peak in cyclic voltammetry. Indeed, the appearance of a second peak in the voltammograms of the $O_{2(g)}$,Pt/YSZ system is not systematically reported in literature [3-6, 15]. It is thought to be

related to the electrode preparation procedure, its high sintering temperature and the high dispersion of the Pt and YSZ phases. By analogy, in liquid electrochemistry, the appearance of multipeaks with platinum electrodes has been found to depend on the initial electrode microstructure and history [21].

To give an overview of the relation between the preparation procedure, microstructure and electrochemical behavior (using cyclic voltammetry), data from literature and results presented in this chapter allows drawing general trends. For electrodes prepared using paste [4-6, 15], pressed point [5], pressed foil or chloroplatinic acid thermal decomposition [11], the behavior depends on the pretreatment temperature. Higher pretreatment temperature favors the observation of peaks in CV. This is due to the sintering of the porous film or the rough metal-electrolyte contact, leading to an agglomerated, smoother, more compact microstructure [11] and to an extended Pt/YSZ surface [15]. In literature [4, 6, 15], this effect is usually obtained for treatment at temperatures equal to or above 900°C. Interestingly, as seen in this chapter, non-heat-treated sputtered electrodes feature a high Pt/YSZ behavior due to their non porous compact structure and intimate Pt/YSZ contact, typical for sputter deposition. However, the film tends to aggregate and become porous when treated at intermediate temperature (600 - 700°C), leading to the disappearance of the peaks in cyclic voltammetry.

3.5   Conclusion

In this chapter, electrodes prepared according to various procedures have been characterized by SEM and by cyclic voltammetry at 450°C in 20 kPa oxygen. It has been shown that the electrode preparation, consequently, the microstructure has a spectacular effect on cyclic voltammetry measurements. The major outcomes are summarized as follow:

-    Cyclic voltammetry appears a useful tool to identify the type of behavior and the nature of the Pt/YSZ contact. It gives precious in situ information on an interface, which is unavailable to surface analysis techniques.

–   Cyclic voltammetry characteristics such as cathodic peaks and the anodic wave are distinctly observed with electrodes treated at high temperature (> 1000°C) and non-porous sputtered electrodes (compact film).

–   The charge obtained by integration of the cathodic peak in the cyclic voltammogram of non-porous sputtered electrodes tends to the value of a Pt-O monolayer.

–   Heat treatment of the sputtered electrode at 700°C in 20 kPa O_2 resulted in a porous structure by the formation of aggregates. Cyclic voltammetry on the electrode features a non-pseudocapacitive behavior, suggesting that the oxygen exchange reaction is favored over charge-storing processes.

-      Promising results were obtained with the cermet electrode. Indeed, it made possible the observation of a second peak in cyclic voltammetry. Unlike for the first cathodic peak, which has been discussed in a few papers, little is known on the second peak because it has been rarely reported. In addition, literature on the electrochemistry of cermet electrodes is less abundant than on non-cermet platinum film. However, it takes more importance with the increasing interest in the field of gas sensing or fuel cells.

Due to these promising results, additional electrochemical techniques will be performed on the cermet electrode. These are presented in the following chapter.

3.6   References

1   J. Poppe, S. Völkening, A. Schaak, J. Janek, R. Imbihl, Phys. Chem. Chem. Phys. 1 (2000) 5241

2   L. Bultel, P. Vernoux, F. Gaillard, C. Roux, E. Siebert, Solid State Ionics 176 (2005) 793

3   A. Jaccoud, G. Foti, C. Comninellis, Electrochim. Acta 51 (2006) 1264

4   Tsaofang Chao, K. J. Walsh, P. S. Fedkiw, Solid State Ionics 47 (1991) 277

5   M. W. Breiter, K. Leeb, G. Fafilek, J. Electroanal. Chem. 434 (1997) 129

6   J. Yi, A. Kaloyannis, C. G. Vayenas, Electrochim. Acta 38 (1993) 2533

7   S. P. Yoon, S. W. Nam, S.-G. Kim, S.-A. Hong, S.-H. Hyun, J. Power Sources 115 (2003) 27

8   S. P. Yoon, S. W. Nam, J. Han, T.-H. Lim, S.-A. Hong, S.-H. Hyun, Solid State Ionics 166 (2004) 1

9   S. V. Karpachev, Y. M. Ovchinnikov, Russ. J. Electrochem. 5 (1969) 200

10   J. E. Bauerle, J. Phys. Chem. Solids 30 (1969) 2657

11   S. Pizzini, M. Bianchi, P. Colombo, S. Torchio, J. Appl. Electrochem. 3 (1973) 153

12   J. W. Jian, B. C. Yang, Y. K. Zhang, Wuji Cailiao Xuebao/Journal of Inorganic Materials 19 (2004) 93

13   S. P. S. Badwal, F. T. Ciacchi, Solid State Ionics 18-19 (1986) 1054

14   E. Varkaraki, Electrochemical promotion of an IrO2 catalyst for the gas phase oxidation of ethylene, Thesis Nr. 1455, EPFL, Lausanne (1995)

15   T. Kenjo, Y. Yamakoshi, K. Wada, J. Electrochem. Soc. 140 (1993) 2151

16   G. Foti, V. Stankovic, I. Bolzonella, C. Comninellis, J. Electroanal. Chem. 532 (2002) 191

17   B. E. Roustom, G. Foti, C. Comninellis, Electrochem. Comm. 7 (2005) 398

18   G. Fafilek, K. Leeb, M. W. Breiter, Solid State Ionics 86-88 (1996) 1415

19   C. G. Vayenas, A. Ioannides, S. Bebelis, J. Catal. 129 (1991) 67

20   H. Angerstein - Kozlowska, B. E. Conway, W. B. A. Sharp, J. Electroanal. Chem. 43 (1973) 9

21   L. D. Burke, M. B. C. Roche, J. Electroanal. Chem. 137 (1982) 175

CHAPTER 4

Electrochemical investigation of the $O_{2(g)}$,Pt/YSZ system in 20 kPa O_2

In this chapter, a series of electrochemical techniques are performed on the cell equipped with cermet electrodes, described in the previous chapter. These techniques are chronoamperometry, chronopotentiometry, cyclic voltammetry, steady state polarization and impedance spectroscopy. In order to simplify the discussion, the electrochemical responses are divided into transient and stationary contributions. It is shown that the transient behavior is caused by pseudocapacitive processes. Indeed, during the anodic polarization, charge is found to be stored in the form of Pt-O species. The kinetics of the charging/discharging processes is studied and discussed with emphasis being put on the slow processes occurring under extended anodic polarization. In particular, linear sweep voltammetry after prolonged anodic polarization allowed distinguishing three species responsible for the charge storage. Based on the effect of the polarization time on the amount of the stored charge, these three species were attributed to Pt-O species being stored at three different locations on the electrode: 1) at the Pt/YSZ interface, 2) along the Pt/gas interface 3) from the Pt/YSZ interface toward the bulk of the platinum electrode.
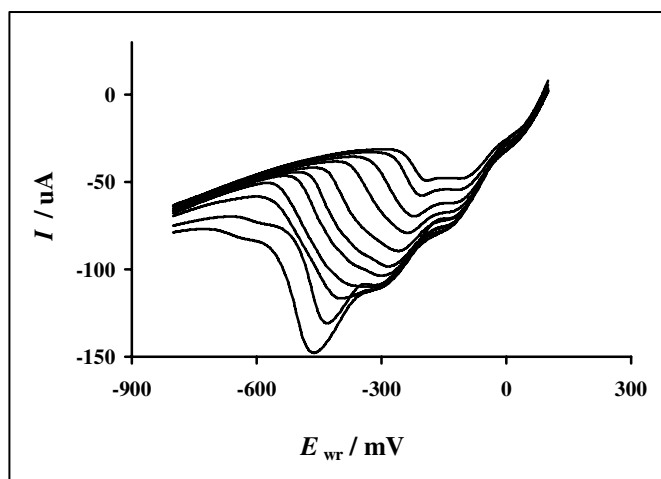
4.1   Introduction

Electrochemical systems are often investigated by applying a perturbation and observing the way in which the system responds. In these measurements, the electrochemical cell is considered as a "black box" to which a certain excitation function (e.g. a potential step) is applied, and a certain response function (e.g. the resulting variation of the current with time) is analyzed, with all other system variables held constant. The aim of the experiments is to obtain information from observations of the excitation and response functions and knowledge of appropriate models for the system.

4.2   Experimental

As proposed in the previous chapter (chapter 3 : preliminary studies), the cell equipped with cermet electrodes, prepared by screen printing of a paste containing Pt and YSZ particles, is studied. The preparation of the cell and the description of the set-up for electrochemical measurements are given in the previous chapter.

4.2.1   Investigation   of   the $O_{2(g)}$,Pt/YSZ   system   by   single   step chronoamperometry

The current transient expected for single step chronoamperometry at a blocking interface [1]

A blocking metal/electrolyte interface can be approximated by an electrical circuit with an arrangement in series of a resistor, R_S, representing the electrolyte resistance and a capacitor, C_d, representing the double layer capacity at the metal/electrolyte interface.
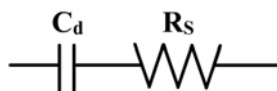
Fig. 1   Approximated equivalent circuit of a blocking metal/electrolyte interface. C_d : double layer capacity. R_S : electrolyte resistance

For the *RC* circuit (Fig. 1), the behaviour of the current *I*, with time *t*, when applying a potential step of magnitude E_{WR}, is

$$I = \frac{E_{WR}}{R_S} \cdot e^{-t/R_S C_d} = \frac{E_{WR}}{R_S} \cdot e^{-t/\tau} \qquad 4.1$$

where $\tau = R_S \cdot C_d$ is the time constant of the system.

Equation 4.1 is derived from the general equation for the charge, *Q*, on a capacitor as a function of the applied voltage E_C.

$$Q = C_d\, E_C \qquad 4.2$$

At any time, the sum of the voltages, E_R and E_C, across the resistor and the capacitor, respectively, must be equal to the applied voltage:

$$E_{WR} = E_R + E_C = IR_S + Q/C_d \qquad 4.3$$

$I = dQ/dt$, therefore,

$$\frac{dQ}{dt} = \frac{-Q}{R_S C_d} + \frac{E_{WR}}{R_S} \qquad 4.4$$

For an initially uncharged capacitor ($Q = 0$, $t = 0$), the solution is

$$Q = E_{WR}C_d \left[1 - e^{-t/\tau} \right] \qquad 4.5$$

Equation 4.1 is obtained by differentiating 4.5.

The expected current transient obtained at different E_{WR} for the $O_{2(g)}$,Pt/YSZ electrode, assumed to be totally blocking, is given by eq. 4.1. These transients have been calculated using the typical value for the double layer capacitance per unit area: 10 $\mu F/cm^2$ [1], but

also higher capacitance values (100 μF/cm^2 and 1mF/cm^2). They are shown in Fig. 2. As a first assumption, the capacitance C_d is calculated considering the geometric surface of the studied electrode (0.08 cm^2). The electrolyte ohmic resistance R_S used in the calculation has been measured by impedance spectroscopy: R_S = 980 Ω at 450°C.

Fig. 2 shows that all calculated current transients decay, originating at 100 μA (t = 0) and tending to zero at infinite time (steady state). The time constant characterizing the current decay $\tau = R_S C_d$ is the time at which the current drops to 36% of its initial value. This time constant is τ = 0.78 ms for 10 μF/cm^2, it is τ = 7.8 ms for 100 μF/cm^2 and τ = 78 ms for 1 mF/cm^2. These calculations show that increasing the capacity of the electrode is expected to cause an increase in the characteristic time constant and consequently, in the time required to reach steady state when polarization is applied.
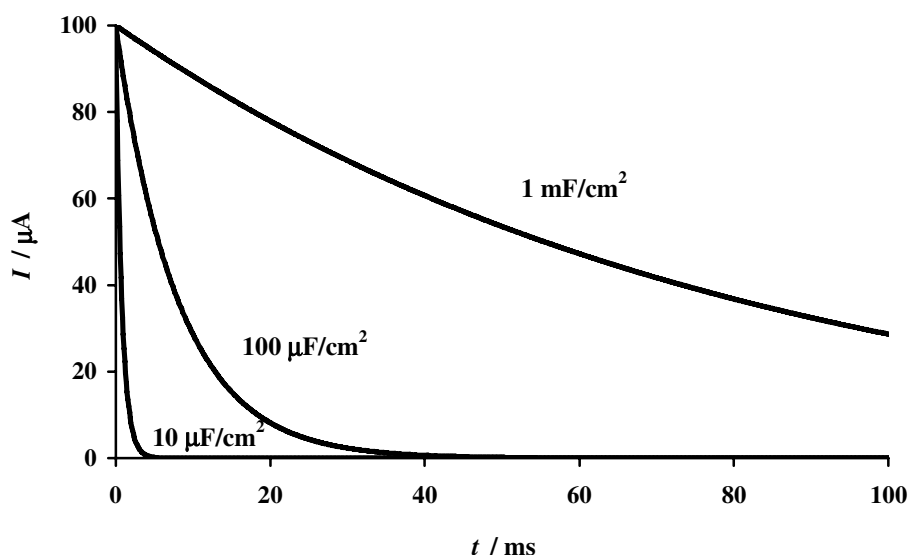
Fig. 2   Current transient resulting from a potential step experiment according to equation 4.1 with the assumption of a totally blocking interface. Three different values of double layer capacitance per area unit are considered. E_{WR} = 0.1 V, R_S = 1000 Ω, electrode geometric surface = 0.08 cm^2.

Results

To verify the expected current transient (Fig. 2) based on the assumption of a blocking interface, single-step chronoamperometry has been performed at 450°C in 20 kPa O_2. The potential program used is composed of a pretreatment step and the measurement step itself, as illustrated by Fig. 3.

Pretreatment step

The cathodic pretreatment step aims to reduce any residual oxidised species and guarantee identical reproducible initial state before each experiment. It consists of a polarization at a constant potential E_{pre} = -400 mV during t_{pre} = 60 s. E_{pre} and t_{pre} have been optimised based on preliminary chronoamperometry and cyclic voltammetry experiments. The t_{pre} value has been chosen long enough to guarantee a negligible amount of residual anodically formed species. The value of E_{pre} is an optimum. If it is too negative, it may cause alteration of the solid electrolyte [2, 3], leading to non-negligible unwanted effects on the subsequent measurement. Oppositely, if E_{pre} is too high, it might not reduce the residual oxidised species to negligible amounts.

Anodic potential holding step

This step is the chronoamperometric measurement itself. It consists of the application of a constant anodic holding potential E_h during t_h = 500 s. the polarisation time t_h has been chosen long enough for the current to reach a steady state.
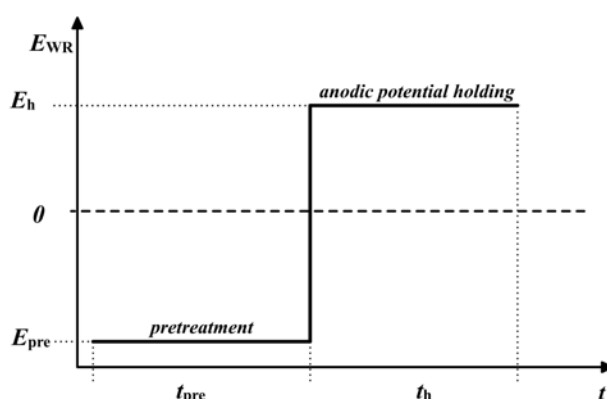
Fig. 3   Potential program used during single step chronoamperometry

Chronoamperometric curves obtained at various E_h

Fig. 4 shows the effect of the anodic holding potential E_h on the corresponding I-t curves. In the very early stage, near t = 0, the value of the current is very dependent on E_h. It increases with increasing E_h. In addition, a fast initial current drop is observed at very short times (t < 10 s), this drop is sharper as E_h increases.

At longer times (10 s < t < 100 s), a current peak appears, its intensity depends strongly on E_h. Indeed, for low E_h (< 0.1 V), the peak is invisible. However, increasing E_h causes the peak to grow, in the form of a shoulder (0.15 V < E_h < 0.4 V), then as a fully developed

peak ($E_h > 0.45$ V). One can notice that the time elapsed before the appearance of the peak decreases with increasing E_h.

At longer times ($t > 150$ s), the current reaches a steady state, which also depends on the applied E_h.
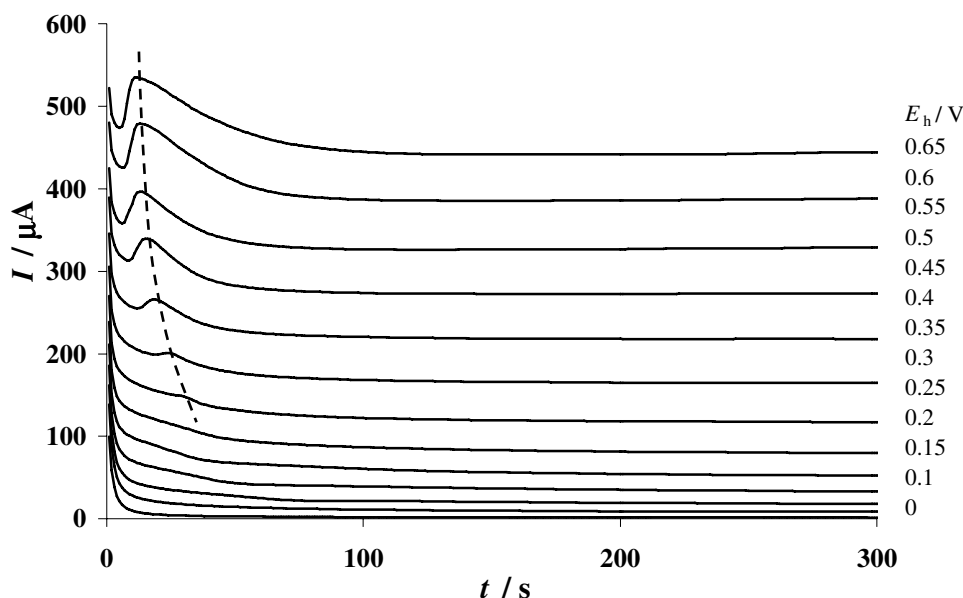
Fig. 4   Chronoamperometric curves at various anodic holding potentials E_h. $T = 450°C$; $pO_2 = 20$ kPa.

Discussion

The expected current transient according to equation 4.1, assuming a totally blocking electrode (Fig. 2), is compared to the experimental chronoamperometric curves obtained at various holding potentials (Fig. 4).

At $E_h = 0$ V, the measured anodic current decay indicates that species present at the Pt/YSZ interface or at the tpb are oxidized when the applied potential is switched from the pretreatment potential $E_{pre} = -0.4$ V to $E_h = 0$ V.

At non-zero E_h potentials, three main differences between the expected and the experimental current-time curves stand out quite clearly. These differences are discussed in the following paragraphs (A to C).

A) The steady state current, expected to be zero for a totally blocking electrode (see Fig. 2), is found experimentally to increase with E_h (Fig. 4). Consequently, the electrode is not totally blocking and can therefore not be assimilated to a simple *RC* circuit (Fig. 1). Therefore, there is an anodic Faradaic process occurring when positive polarization is applied, which persists at infinite time. This process is certainly the oxygen evolution reaction:

$$O^{2-}_{(YSZ)} \longrightarrow \frac{1}{2}O_{2(gas)} + 2e^- \qquad 4.6$$
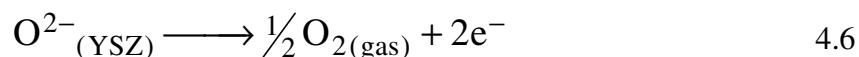
This reaction and the influence of E_h on its kinetics will be discussed more thoroughly later in this work.

B) Another disparity between the expected (Fig. 2) and the experimental current behavior (Fig. 4) is the huge difference of time scale (time constant τ). Indeed, in the expected *I-t* curve (Fig. 2), the time constant for a typical double layer capacity per unit area (10 $\mu F/cm^2$) is $\tau = 0.78$ ms, and $\tau = 78$ ms for a capacity hundred times greater. However, in the experimental measurement (Fig. 4), the time constant is in the order of a few seconds or a few tens of seconds. This indicates that the effective capacity of the electrode is orders of magnitude higher than the typical double layer capacity. Such huge capacitance values per geometric surface unit area can only be achieved in two cases:

1) The real surface area is orders of magnitude greater than the geometric area, giving rise to a dramatic increase in the double layer capacity value per unit area. This can be achieved with cermet electrodes, where the interfaces are extended into the whole volume of the electrode. In this work, the electrode being a cermet, this could explain the great apparent capacity values. It is worthwhile noting that the double layer capacity is of electrostatic type and its charging/discharging process takes place via a non-Faradaic process.

2) The charge is stored under the form of chemical species via Faradaic processes. In this type of charge storage, called "pseudocapacity", the stored charge is released when a potential change causes the inverse electrochemical reaction to take place. In order to store

charge by this mean, the species must accumulate near the electrochemical reaction site (ERS) and be easily available for the inverse reaction (discharging). The pseudocapacitance is usually orders of magnitude over that of the double-layer capacitance. In addition, since a chemical reaction needs to take place, pseudocapacitive processes are usually slower than the charging/discharging of the double layer, which is purely electrostatic. In the present case, pseudocapacity might explain the large time constants observed by chronoamperometry.

C) The variation of the anodic holding potential E_h (Fig. 4) reveals an unexpected intriguing feature; the current peak occurring in the time interval 10 s $< t <$ 100 s. The peak must be due to an additional anodic electrochemical process. The most questioning aspect is that this process does not start immediately after the potential application ($t = 0$), but appears only after a certain elapsed time. This time increases with decreasing E_h, as indicated by the dotted line in Fig. 4. One may however remark that, for every E_h, the peak appears during the first current decay, when the current approaches the value of the steady state current.

4.2.2 Investigation of the $O_{2(g)}$,Pt/YSZ system by double step chronoamperometry

In the previous section, it was shown that Faradaic processes occur during the anodic polarisation and may cause pseudocapacitive charge storage. The use of the double step chronoamperometry method is expected to give further information on the nature of these stored species. In this section, double step chronoamperometry is performed on the $O_{2(g)}$,Pt/YSZ system at 450°C in 20 kPa O_2. The aim is to store charges by an extended anodic polarization (as in single step chronoamperometry) and to reduce these stored charges during the subsequent cathodic polarisation.

Results

Fig. 5 shows the applied potential program. It is composed of a pretreatment step and two measurement steps. The pretreatment and the anodic potential holding are similar to those described in single step chronoamperometry (see Fig. 3). However, in this section (double step chronoamperometry), the duration of the anodic potential holding t_h was varied to study its influence on the discharging step and E_h was kept constant (100 mV).
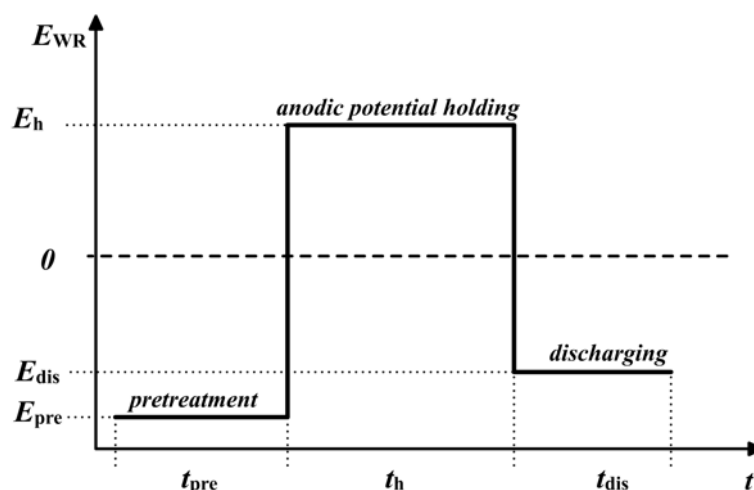
Fig. 5   Potential program used during the double step chronoamperometric measurements

The discharging step was carried out at a constant cathodic potential $E_{dis} = -300$ mV during $t_{dis} = 150$ s. This step aims to reduce the species formed during the preceding anodic potential holding step. t_{dis} has been chosen long enough for the current to reach steady state. The E_{dis} value was optimised based on preliminary chronoamperometry and cyclic voltammetry measurements.

Fig. 6 shows the current behaviour when the potential program described above (Fig. 5) is applied. During the pretreatment step, the cathodic current drops from about -300 µA to a steady state value (-50 µA) within 30 s. At $t = 60$ s, when the anodic step starts, the current jumps to 130 µA before decaying to 10 µA within a period of 250 s. During the remaining holding time t_h, the current is at steady state. The application of the discharging step ($t = 60$ s) causes the cathodic current to drop to -240 µA and then to reach a steady state value (-33 µA) within a period of 30 s.

The duration of the anodic potential holding t_h (Fig. 5) was varied from 5 to 80 minutes. Fig. 7 shows the effect of t_h on the current behaviour of the third chronoamperometry step (discharging). For $t_h = 5$ min, a relatively fast decay of the cathodic current is observed, approaching a steady state value (-30 µA) after about 10 s. The other curves also show a rapid decay in the initial stage of the cathodic current ($t < 10$ s), but as t_h increases, more time is needed to reach the steady state current. In particular, after a long polarisation time ($t_h = 80$ minutes), 80 seconds are necessary to reach the steady state.
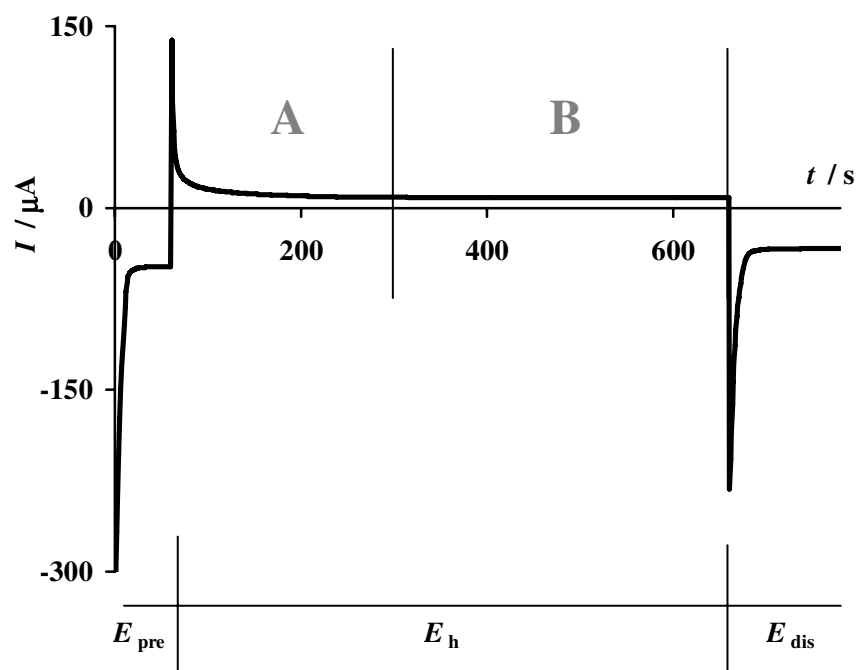
Fig. 6   Current behavior under the double step potential program, E_{pre} = -400 mV, t_{pre} = 60 s, E_h = 100 mV, t_h = 600 s, E_{dis} = -300 mV, t_{dis} = 150 s, T = 450 °C, pO_2 = 20 kPa.
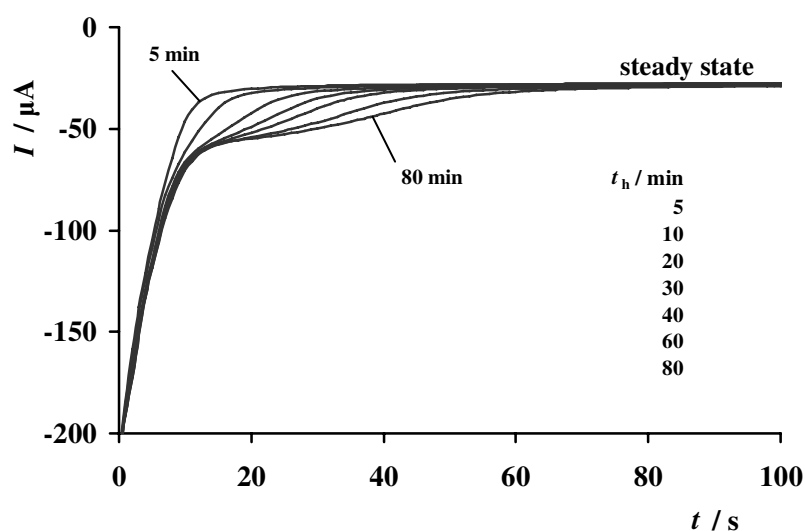
Fig. 7   Double step chronoamperometric measurements. *I-t* transients obtained during the discharging step. Influence of the holding time t_h at the anodic potential E_h = 100 mV. E_{dis} = -300 mV, T = 450°C, pO_2 = 20 kPa.

Discussion

As discussed in the previous section, the measured capacity during the anodic polarization is believed to be due, almost exclusively, to pseudocapacitive processes. In other words, during anodic polarization, charge is stored in the form of chemical species via a Faradaic process. The fact that we are dealing with pseudocapacitance and not electrostatic capacitance is consolidated by the double step chronoamperometric measurements. However, this technique has demonstrated that the charge storage in the anodic polarization step is not limited during the anodic current decay (domain A in Fig. 6) but is extended to the region of steady state (domain B), in parallel to the main reaction of O_2 evolution (eq. 4.6). This is clearly seen in Fig. 7, which shows that for $t_h > 5$ min (time at which steady state current is reached as shown in Fig. 6), the stored charge continues to increase.

4.2.3 Investigation of the $O_{2(g)}$,Pt/YSZ system by chronocoulometry

So far, our investigation has been based on *I-t* curves, stimulated by potentiostatic steps. The next stage is the integration of these *I-t* curves, to obtain the charges involved in the storage process. By varying the anodic holding time, we aim to determine the kinetic law that governs the anodic charge storage.

Charge integration

To determine the amount of charge stored on the electrode, the *I-t* chronoamperometric curves must be integrated using a proper baseline. It has been shown in section 4.2.1 that the *I-t* curves feature both a time-dependent and a steady state part. As a first approximation, the steady state current is chosen as baseline for the integration. Fig. 8 illustrates the different charges. Since the steady state current $I_{ss\ charging}$ is used as baseline, the stored charge $Q_{charging}$ is given by integration of the time dependent current fraction measured during the anodic potential holding step. In contrast, Q_{ss} is given by the integration of the steady state current over t_h.

Similarly, the time dependent fraction of the cathodic current during the discharging step can be integrated with the steady state current $I_{ss\ discharging}$ as baseline. The resulting charge, $Q_{discharging}$ is considered the charge, which had been effectively stored during the anodic step.
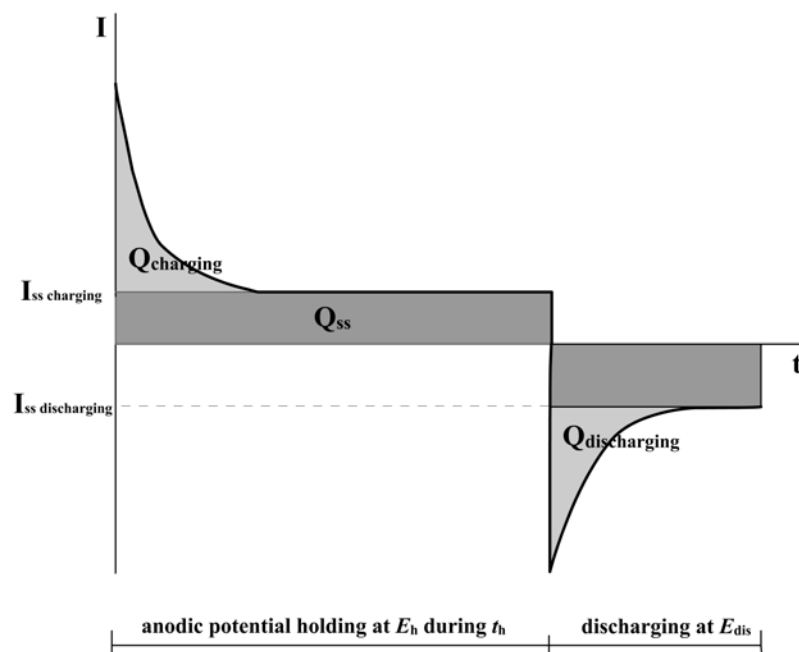
Fig. 8   Schematic representation of the *I-t* behavior during the anodic potential step (charging) and discharging step (Fig. 5). The gray areas represent the charges, determined by integration of the *I-t* plot. Q_{ss} is the charge determined by integration of the constant current at steady state $I_{ss\ charging}$ during the anodic potential step.

Results

Variation of the holding time t_h

Double step chronoamperometry measurements with varying anodic holding times t_h (from 5 to 80 minutes) have been presented in the previous section (see Fig. 6 and Fig. 7). Integration of the *I-t* curves as illustrated in Fig. 8 gives the values of $Q_{charging}$ and $Q_{discharging}$ for each t_h. The dependence of the holding time t_h on these charges is shown in Fig. 9. $Q_{charging}$ does not vary when t_h is increased from 5 to 80 minutes. This could be expected since, as shown in Fig. 4, the steady state current during the anodic step is already reached after 5 minutes.

In contrast, there is a positive effect of t_h on $Q_{discharging}$, the effectively stored charge. At low t_h (5 min), both charges are comparable (roughly 1 mC). This means that the totality of the charge apparently stored during the anodic charging step is released during the discharging step. However, as t_h increases, $Q_{discharging}$ exceeds $Q_{charging}$, meaning that the electrode has stored more charge than expected from the anodic *I-t* curve. The difference between these two charges is called "extra charge" and written Q_{extra}.

$$Q_{\text{extra}} = Q_{\text{discharging}} - Q_{\text{charging}} \qquad\qquad 4.7$$

The amount of the extra charge is not negligible. Indeed, at t_h = 80 min, the $Q_{\text{discharging}}$ is more than twice greater than Q_{charging}.
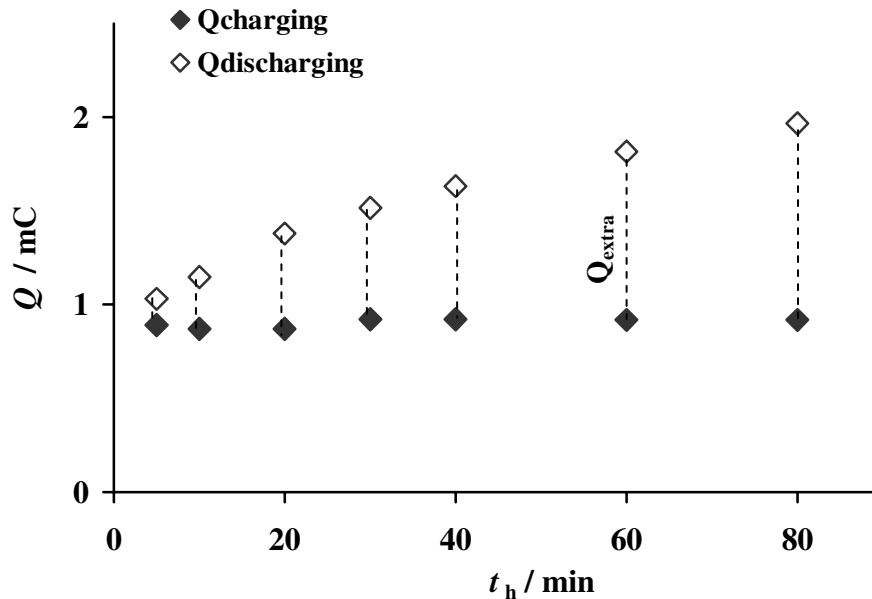
Fig. 9   Effect of the holding time t_h on Q_{charging}, and $Q_{\text{discharging}}$. T = 450°C, pO$_2$ = 20 kPa. E_h = 100 mV, E_{dis} = -300 mV.

In order to gain knowledge on the process leading to the storage of the extra charge, it is important to determine its kinetic law. It has been found that there is a linear relation between the amount of the extra charge Q_{extra} and the square root of the anodic holding time t_h. This is illustrated in Fig. 10, where the extra charge Q_{extra} is plotted as a function of $t_h^{1/2}$. Linear regression gives the following kinetic expression:

$$Q_{\text{extra}} = A\, t_h^{1/2} + B \qquad\qquad 4.8$$

with A = 1.7 10^{-5} C/s$^{1/2}$ and B = -1.4 10^{-4} C.

The non-zero B value indicates that Q_{extra} is not exactly proportional to $t_h^{1/2}$. Indeed, the linear extrapolation does not pass through the origin of the plot. The Q_{extra} = 0 is met at $t_h^{1/2}$ = 10 s$^{1/2}$. This means that there is a delay of roughly 100 s after the onset of the anodic polarization before extra charge starts being stored.
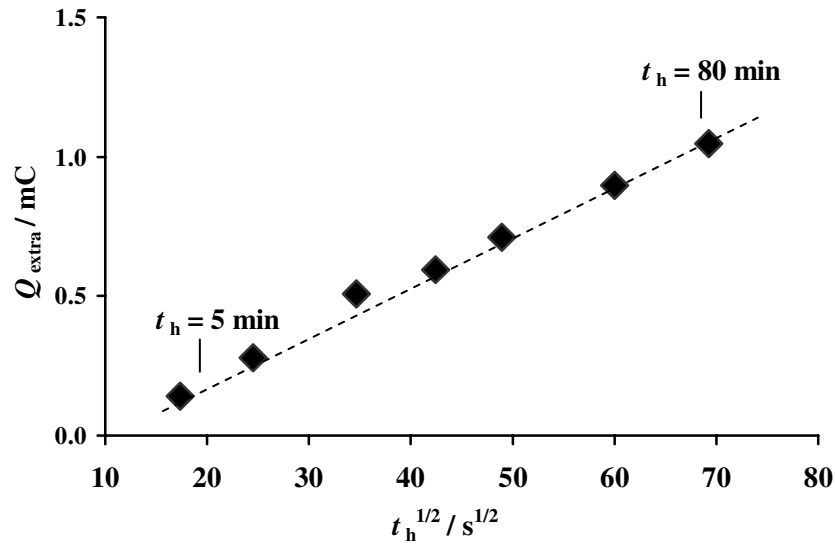
Fig. 10   Effect of t_h on the extra charge. $T = 450°C$, $pO_2 = 20$ kPa. $E_h = 100$ mV.

These results indicate that the extra charge Q_{extra} is stored from 100 s of anodic polarisation and that this storage process goes on during the totality of anodic polarisation step, including the steady state period. This means that a certain portion of the apparent steady state current ($I_{ss\ charging}$ in Fig. 8) is in fact stored as extra charge. We can define the charge storage yield (CSY) as the extra charge Q_{extra} divided by the total charge passing as steady state current Q_{ss}. (eq. 4.9)

$$CSY = Q_{extra} / Q_{ss} \qquad\qquad 4.9$$

The charge storage yield can be calculated for each holding time interval Δt_h. This gives the so-called instantaneous charge storage yield (ICSY). Fig. 11 represents the value of the instantaneous charge storage yield at various t_h. The yield lies between 1.5 and 6 % and tends to decrease with increasing t_h.
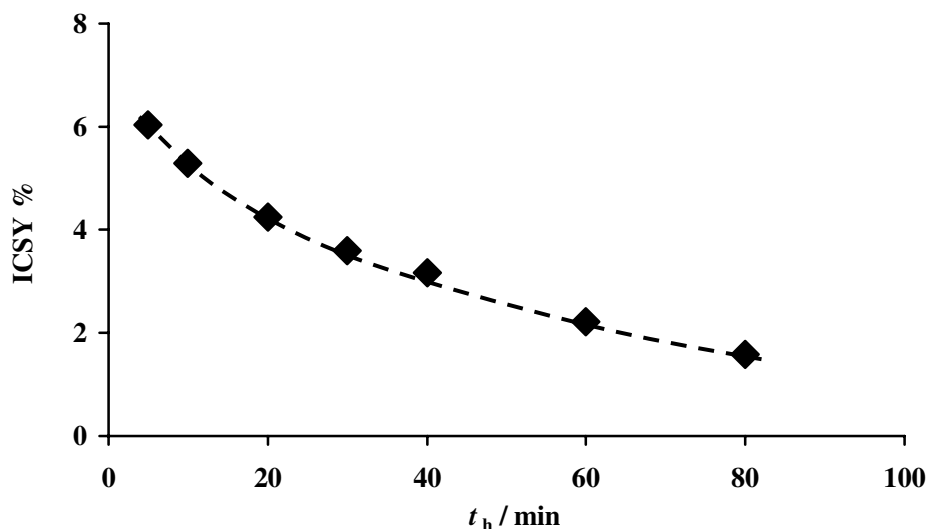
Fig. 11   Instantaneous charge storage yield (ICSY) for various anodic holding times t_h. $T = 450°C$, $pO_2 = 20$ kPa. $E_h = 100$ mV.

Discussion

By integrating the time dependent sections of the *I-t* curves, it has been shown in Fig. 9 that, for short t_h (5 min), the charge stored ($Q_{charging}$) is almost totally released during the subsequent cathodic step ($Q_{discharging}$). However, for prolonged anodic polarization ($t_h > 5$ min), $Q_{discharging}$ exceeds $Q_{charging}$, indicating that extra charge Q_{extra} is stored during the steady state period.

The kinetic law governing the extra charge storage has been determined. The amount of extra charge Q_{extra} has been found to increase linearly with the square root of the anodic holding time t_h and does not show sign of saturation. The slow process leading to extra charge storage may be limited by a diffusion step. Indeed, $t^{1/2}$ laws are commonly found for diffusion-limited processes.

At this point, the question of the nature of the species involved in the storage-release process remains open. However, basic ideas on the physicochemical interpretation of the experiments are expressed here and will be completed later in this chapter.

As mentioned above (section 4.2.1), Faradaic processes are thought to govern both the time dependent and the steady state current fractions of the chronoamperometric measurements. A sketch of a possible reaction path involving anodic Faradaic processes is

proposed. It is illustrated by reaction paths 4.10 and 4.11. The two anodic reaction paths share the same reactant O^{2-}, the charge carrier in the solid electrolyte YSZ. These two paths are electrochemical and they both release two electrons. The measured current is the sum of the currents corresponding to the two paths.

$$O^{2-} \xrightarrow{-2e^-} O \xrightarrow{+Pt} Pt-O \qquad\qquad 4.10$$

$$O^{2-} \xrightarrow{-2e^-} O \longrightarrow \tfrac{1}{2}O_{2\ (gas)} \qquad\qquad 4.11$$
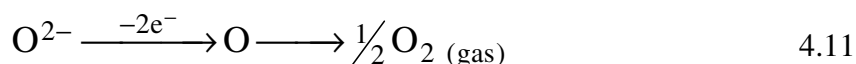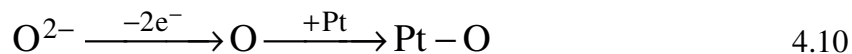
In the first path (eq. 4.10), O^{2-}, originating from the YSZ lattice, gets in contact with the Pt electrode. It releases two electrons to the electrode and reacts with platinum to form a platinum-oxygen compound. This compound remains at the electrode and accumulates (oxygen injection). The number of Pt atoms at the ERS being finite, the reaction rate decreases with time. However, due to a strong concentration gradient, the accumulating Pt-O species slowly diffuse away from the electron exchange site, following a $t^{1/2}$ kinetics. Later, when the discharging step is applied, the inverse reaction path takes place. The total amount of Pt-O is reduced (oxygen ejection) and the corresponding cathodic current decay is observed. This includes the Pt-O accumulated at the electron transfer site and the Pt-O which have diffused.

This charging/discharging scenario of oxygen injection/ejection may interpret the pseudocapacitive character of the electrode, for instance, the current decay observed immediately after the application of the anodic polarization. It may also interpret the slow extra charge storage process illustrated in Fig. 9.

The second path (eq. 4.11) is the electrochemical formation of molecular oxygen, also called "oxygen evolution". This reaction has been widely studied [4-28], nevertheless, there is still a controversy about the precise mechanism, in particular, the electron exchange sequence and the rate determining step (RDS). Basically, a O^{2-} atom reaches the triple phase boundary region (tpb) and releases two electrons to the electrode, forming a chemisorbed oxygen atom. It desorbs to the gas phase as molecular oxygen O_2. Since the latter does not accumulate at the electrode, the reaction may proceed indefinitely. This path may interpret the non-zero steady state current observed in chronoamperometry when overpotential is applied (Fig. 4 and Fig. 6).

4.2.4   Investigation of the $O_{2(g)}$,Pt/YSZ system by chronopotentiometry

In previous sections, steps of constant potential were applied to the system, while the current was measured as a function of time (chronoamperometry). In this present section, chronopotentiometry is used. It differs from chronoamperometry by the fact that stationary current steps are applied whereas the potential E_{WR} is the dependent variable and is recorded as a function of time. In chronopotentiometry, the applied current is forced to flow through the electrode and the corresponding potential adapts. This method is used to complement chronoamperometry measurements.

Chronopotentiometry has been developed and employed mainly in the field of liquid phase electrochemistry. However, by analogy, the method, its theoretical background and the interpretation of its results can be used in solid state electrochemistry.

In section 4.2.1, in chronoamperometric measurements, interesting features appearing at short times after the on-set of the positive potential have been reported. Indeed, a current peak, occurring at $10 < t < 100$ s, appears under the application of high holding potentials E_h (see Fig. 4). The peak was attributed to an additional anodic electrochemical process. Its most intriguing characteristic is that it does not starts immediately after the application of the positive potential step, but seems triggered after a few seconds. The current peak spans only over a few tens of seconds. After this period, the current reaches its steady state. This suggests that the presumed anodic reaction causing the current peak, once triggered, takes place only during a limited period, then slows down and stops.

Based on theory on chronopotentiometry [1], this time limited anodic reaction is expected to give rise to a plateau in the E_{WR}-t curve spanning over a limited amount of time before rising to higher values.

In this work, single-step chronopotentiometry has been performed at 450°C in 20 kPa O_2 in He on the $O_{2(g)}$,Pt/YSZ system. The current program used is composed of a pretreatment step and the measurement step itself as illustrated by Fig. 12.

Results

Pretreatment step

As for chronoamperometry, a pretreatment step is applied to reduce any residual species and guarantee an identical reproducible initial state before each experiment. It consists of a polarization at a constant current I_{pre} = -25 μA during t_{pre} = 60 s. I_{pre} and t_{pre} have been chosen to match the pretreatment step performed prior to the chronoamperometry measurements (section 4.2.1).

Anodic current holding step

This step is the chronopotentiometric measurement itself. It consists of the application of a constant anodic holding current I_h during t_h = 400 s. I_h has been varied to study its influence on the E_{WR}-t transients.
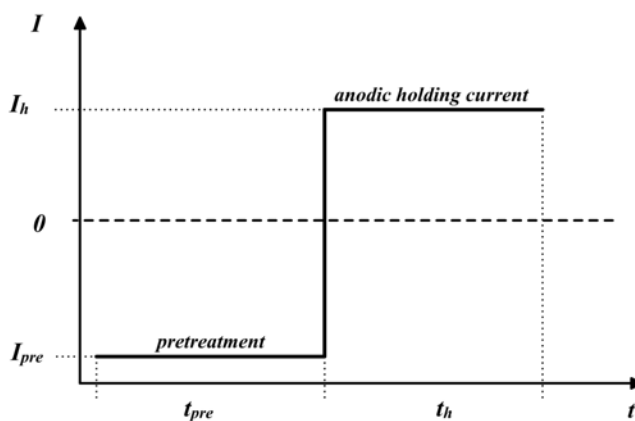
Fig. 12   Current program used during single step chronopotentiometry

Fig. 13 shows the effect of anodic holding current I_h on the E_{WR}-t curves. Initially ($t < 10$ s), the potential increases rapidly. This rapid increase in potential is related to the charging of the $O_{2(g)}$,Pt/YSZ system. At intermediate time (10 s < t < 100 s), under high anodic currents I_h, a plateau is observed. Then, at longer times (100 s < t), a steady state potential is reached.

The appearance of a plateau in the chronoamperometric curves at high anodic currents indicates the presence of an additional electrochemical reaction in parallel to the steady state main reaction of O_2 evolution. It must be related to the current peak observed at high E_h in chronoamperometry (Fig. 4). A model similar to that proposed in section 4.2.3 can be proposed (eq. 4.10 and eq. 4.11)
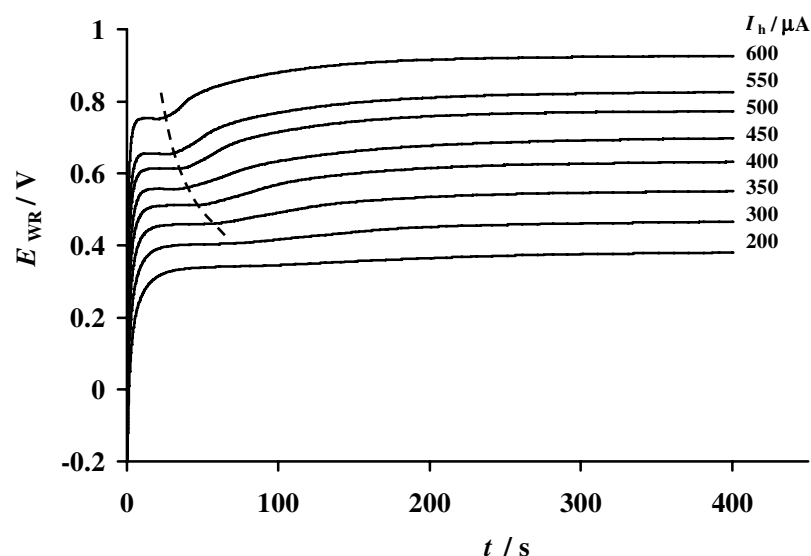
Fig. 13   Chronopotentiometric curves at various holding current I_h. $T = 450°C$; $pO_2 = 20$ kPa.

4.2.5   Investigation of the $O_{2(g)}$,Pt/YSZ system by programmed cyclic voltammetry

In the previous sections, the $O_{2(g)}$,Pt/YSZ system (electrode) has been studied by single step and double step chronoamperometry, by chronocoulometry and by chronopotentiometry. It has been demonstrated that application of an anodic potential results to charge storage (oxygen injection), possibly in the form of Pt-O species. A subsequent cathodic step reduces this charge (oxygen ejection). Both the chronoamperometric and chronopotentiometric measurements have shown some intriguing results, i.e. the appearance of a current peak in the chronoamperometric measurements (Fig. 4) and a potential plateau in the chronopotentiometric measurements (Fig. 13) in the (10 s < t < 100 s) time domain at high E_h and I_h values, respectively. In order to elucidate these intriguing results, we propose to use linear sweep voltammetry.

This technique is well suited to distinguish electrochemical processes on the basis of their kinetic and/or electrochemical characteristics. It has been developed initially for liquid electrochemistry, but has then been used also in the field of high temperature solid electrochemistry [4, 29-33].

Results

The potential program shown in Fig. 14 has been applied to the given $O_{2(g)}$,Pt/YSZ system. This program consists of a pretreatment step at E_{pre} and an anodic potential holding step at E_h. Both are identical to the ones described in section 4.2.1. The holding potential $E_h = 100$ mV is used in most experiments presented in this section because it has been found to give the best peak resolution.
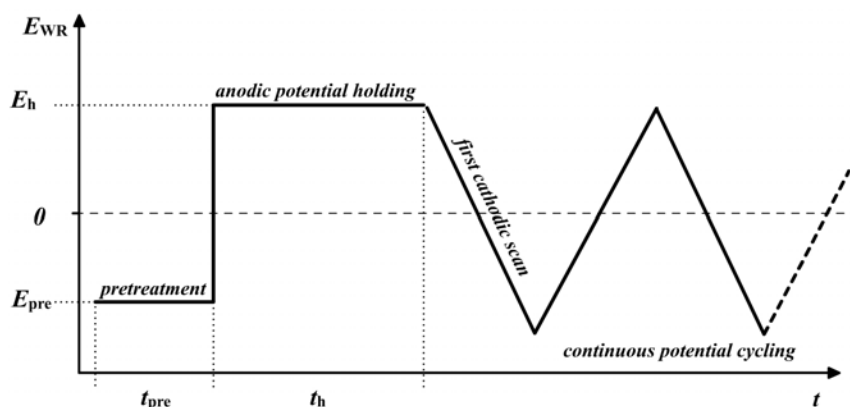
Fig. 14   Scheme of the applied potential program.

The anodic potential holding step is followed by a linear potential sweep down to a given cathodic potential (first cathodic scan). The scan rate $v = 10$ mV/s is used in most experiments presented in this work because it has also been found to give a good peak resolution.

After the first cathodic scan, cyclic voltammetry is performed under continuous potential cycling between these two potential limits with the same scan rate v.

The current behavior during the first cathodic scan and the continuous potential cycling

Fig. 15 shows the typical voltammetric response of the given $O_{2(g)}$,Pt/YSZ system obtained with a scan rate of 10 mV/s at $T = 450°C$ and $pO_2 = 20$ kPa. Two voltammograms recorded in the potential region between +100 and -500 mV are shown. One of them is recorded during the first cathodic potential sweep after an anodic potential holding ($E_h = 100$ mV, $t_h = 10$ min). It exhibits two distinct reduction peaks at about -150 and -250 mV, respectively. The second voltammogram shown in Fig. 15 has been measured by continuing the potential cycling after the first cathodic scan, as shown in Fig. 14. The subsequent cyclic voltammograms remain invariant during continuous potential cycling. They superimpose each other. It is important to note that only the first cathodic

scan has a different shape. This means that after the first cathodic scan, all the effects of the anodic potential holding is removed. The voltammogram under continuous cycling exhibits no distinct anodic peak during the positive scan. During the negative scan, a wide reduction peak is observed in the vicinity of -100 mV, and a second smaller peak appears near -200 mV. At more negative potentials ($E_{WR} < $ -300 mV), no peak is observed.

Note, that after prolonged anodic polarization the first cathodic scan begins at $E_h = 100$ mV with a very small current, however, in the subsequent scan the current at this potential is in the vicinity of 35 μA. This means that during the 10 minute holding at 100 mV, the current drops from around 35 μA to a few μA. This current drop, during the anodic potential holding step, already reported in some papers [30, 31], corresponds to the decay observed in chronoamperometry (see Fig. 4).
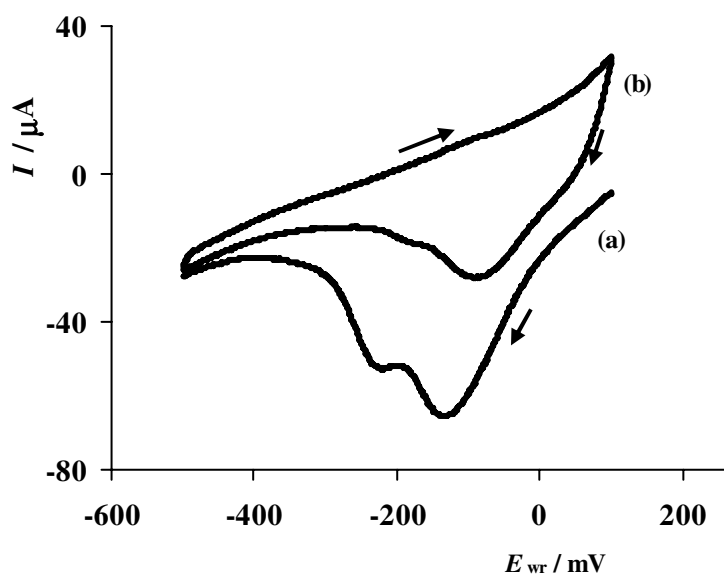
Fig. 15   Cyclic voltammogram of the $O_{2(g)}$,Pt/YSZ system at $T = 450°C$, $pO_2 = 20$ kPa, $v = 10$ mV/s. a) First cathodic scan after $t_h = 10$ min holding at $E_h = 100$ mV. b) Voltammogram under continuous cycling.

Effect of oxygen partial pressure pO_2 on the first cathodic scan

In order to study the effect of pO_2 on the intensity and position of the reduction peaks obtained in the voltammograms, it was varied from 20 kPa to 0.2 kPa. In these measurements, the reference electrode was exposed to a variable oxygen partial pressure

in the reactor; therefore, in order to keep the same reference electrode and to compare the results, a correction is necessary. This correction is made using Nernst equation 4.12.

$$E_{\mathrm{WR}}(20\,\mathrm{kPa}) = E_{\mathrm{WR}}(p_{O_2}) + \frac{RT}{4F}\ln\left(\frac{p_{O_2}}{20\,\mathrm{kPa}}\right) \qquad 4.12$$

where $E_{\mathrm{WR}}(pO_2)$ is the potential difference between the working and the reference electrodes exposed to the varying experimental pO_2. $E_{\mathrm{WR}}(20\ \mathrm{kPa})$ is the potential difference between the working and the reference electrode, where the effect of the O_2 pressure difference on the reference electrode potential is corrected.
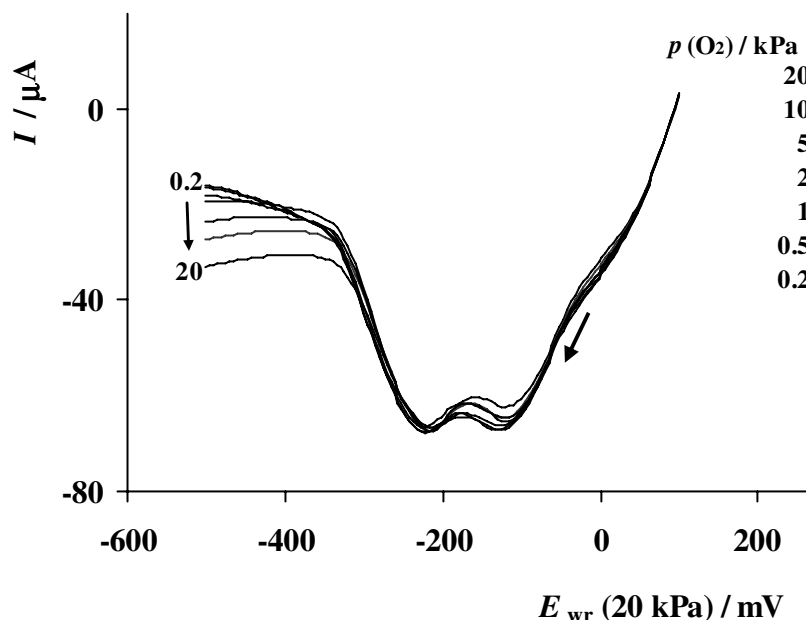
Fig. 16   Voltammogram of the $O_{2(g)}$,Pt/YSZ system. Effect of oxygen partial pressure on the cathodic scan. $T = 450°C$, $v = 10\ \mathrm{mV\ s^{-1}}$, holding time $t_h = 15$ min at $E_h\ (20\ \mathrm{kPa}) = 100$ mV. The reference electrode potential is corrected with respect to $pO_2 = 20$ kPa using equation 4.12.

Fig. 16 shows the effect of oxygen partial pressure on the first cathodic scan ($t_h = 15$ minutes, $E_h(20\ \mathrm{kPa}) = 100$ mV). The reported potentials given in Fig. 16 are corrected with respect to 20 kPa O_2. Both the position and intensity of the two cathodic peaks are independent of the oxygen partial pressure. However, the current in the low potential domain ($E_{\mathrm{wr}} < -300$ mV), after the second peak, depends strongly on the oxygen

partial pressure in this domain. Low oxygen partial pressures ($pO_2 < 1$ kPa) leads to low cathodic currents (< 20 μA).

Effect of the holding potential E_h

Fig. 17 shows the first cathodic scans recorded after holding at various potentials, E_h, during $t_h = 10$ minute. Increasing E_h results in an increase in peak intensities and causes a shift of the peak potentials E_p to more negative values. This is valid for both the first and the second cathodic peak. However, their size ratio remains fairly constant.
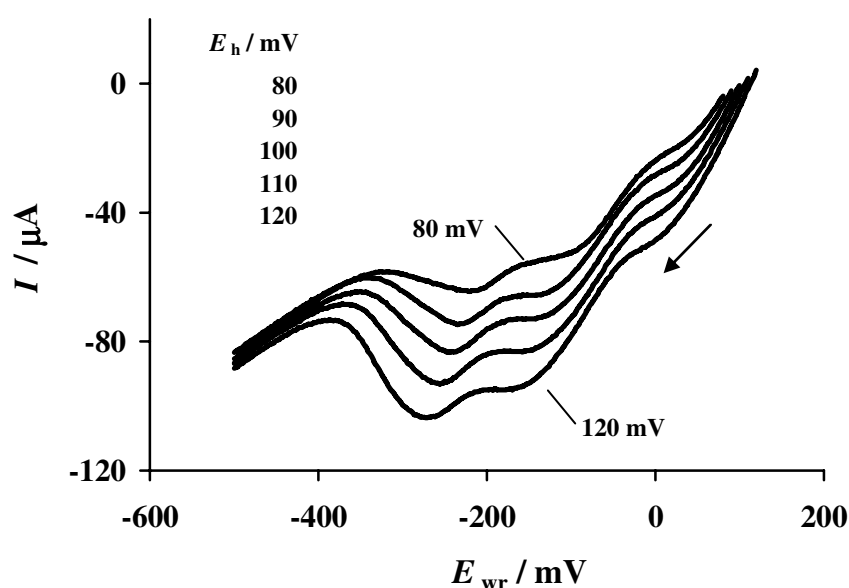
Fig. 17   Voltammogram of the $O_{2(g)}$,Pt/YSZ system. Effect of the holding potential, E_h, on the cathodic scan. $T = 450°C$, $pO_2 = 20$ kPa, $v = 10$ mV s^{-1}, $t_h = 10$ min.

Effect of reversal potential E_r

Fig. 18 shows the effect of the anodic reversal potential, E_r, on the intensity and the position of the cathodic peaks during continuous cycling. When $E_r < 25$ mV, no significant cathodic peak appears. However, at higher potentials, one first cathodic peak and a second poorly defined peak are observed. Fig. 18 also shows that increasing E_r results in a strong increase in the peak current I_p and also a slight negative shift of the peak potential E_p.
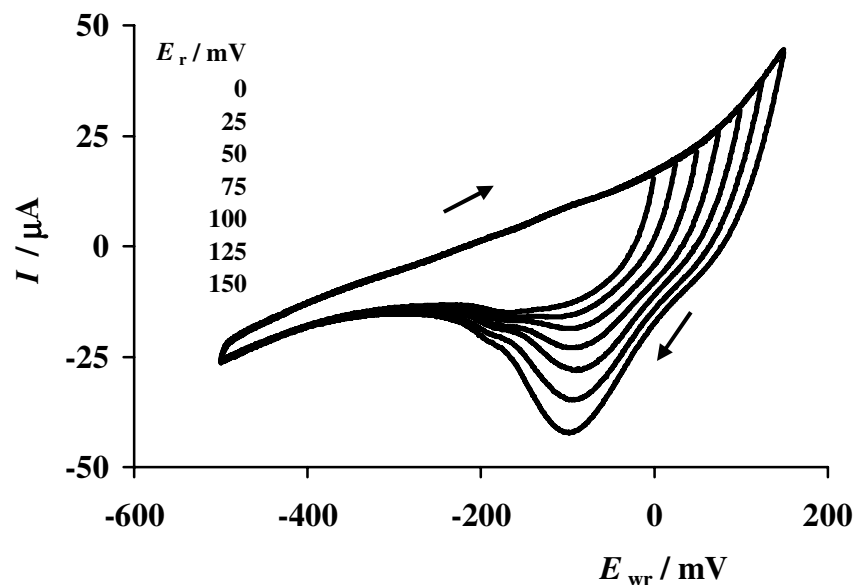
Fig. 18   Cyclic voltammogram of the $O_{2(g)}$,Pt/YSZ system. Effect of the reversal potential, E_r, on the cyclic voltammogram. $T = 450°C$, $pO_2 = 20$ kPa, $v = 10$ mV s^{-1}.

Effect of the scan rate v
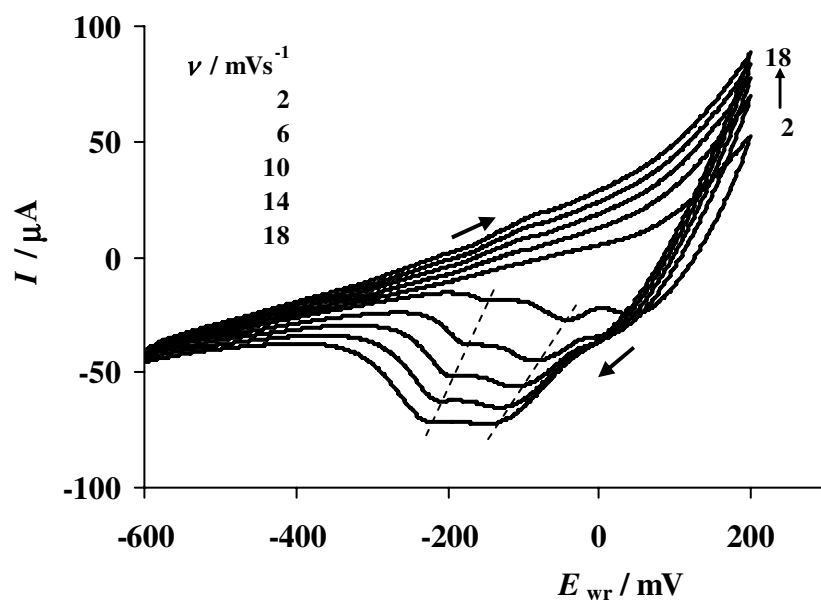
Fig. 19   Cyclic voltammogram of the $O_{2(g)}$,Pt/YSZ system. Effect of the scan rate on the continuous cyclic voltammogram at $T = 450°C$ and $pO_2 = 20$ kPa.

Fig. 19 shows the effect of the scan rate v on the cyclic voltammogram recorded between +200 and -600 mV. Increasing the scan rate causes an increase in the peak current, I_p, and a shift into more cathodic peak potentials E_p. It also increases the anodic current, especially in the higher E_{WR} domain ($E_{WR} > -300$ mV). However, at low E_{WR} (< -400 mV), the scan rate has very little influence on the measured current.

Effect of holding time t_h

The holding time, t_h, at $E_h = 100$ mV was varied from 1 to 200 minutes and the potential was then swept from $E_{WR} = 100$ to $E_{WR} = -800$ mV (first cathodic scan) (Fig. 20a). At a very low holding time (1 min), the first and second peaks already appear with comparable sizes. However, by increasing t_h, the second peak increases more rapidly than the first peak. By further increasing the holding time, a third peak appears. At this point, it is important to note that the third peak was not present at very low t_h, but it is developed progressively. In fact, one can discern the third peak already at $t_h = 20$ min.
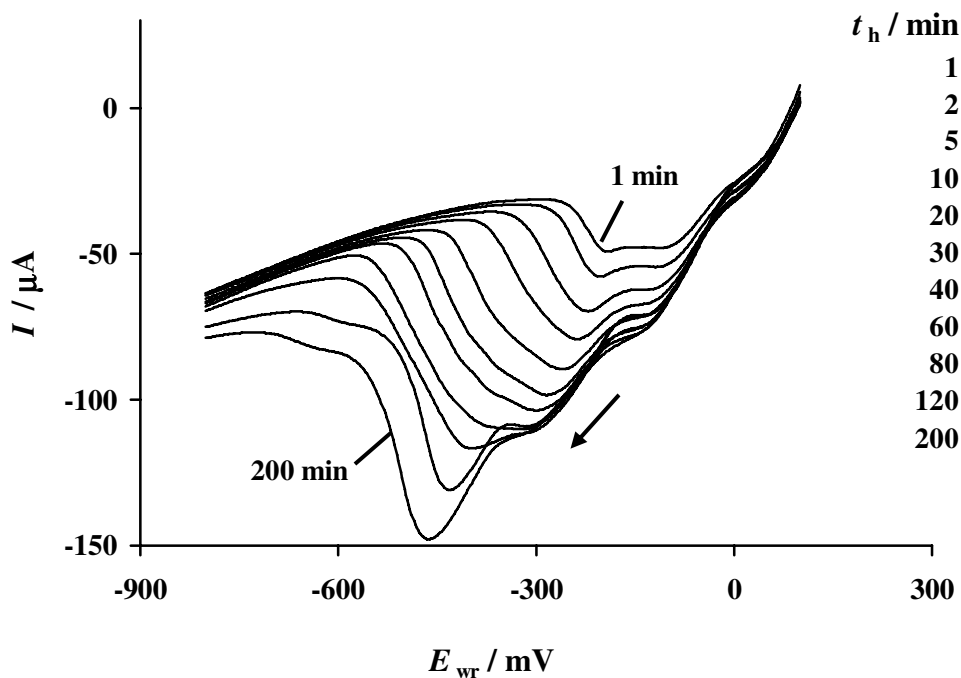
Fig. 20a   Voltammogram of the $O_{2(g)}$,Pt/YSZ system. Effect of the holding time, t_h, at $E_h = 100$ mV on the first cathodic scan. $T = 450°C$, $pO_2 = 20$ kPa, $v = 10$ mV/s.

At higher holding times ($t_h > 60$ min), the first and second peaks have stopped growing. However, even at very long holding time (up to 2000 min), the third peak shows no sign of saturation (Fig. 20b).
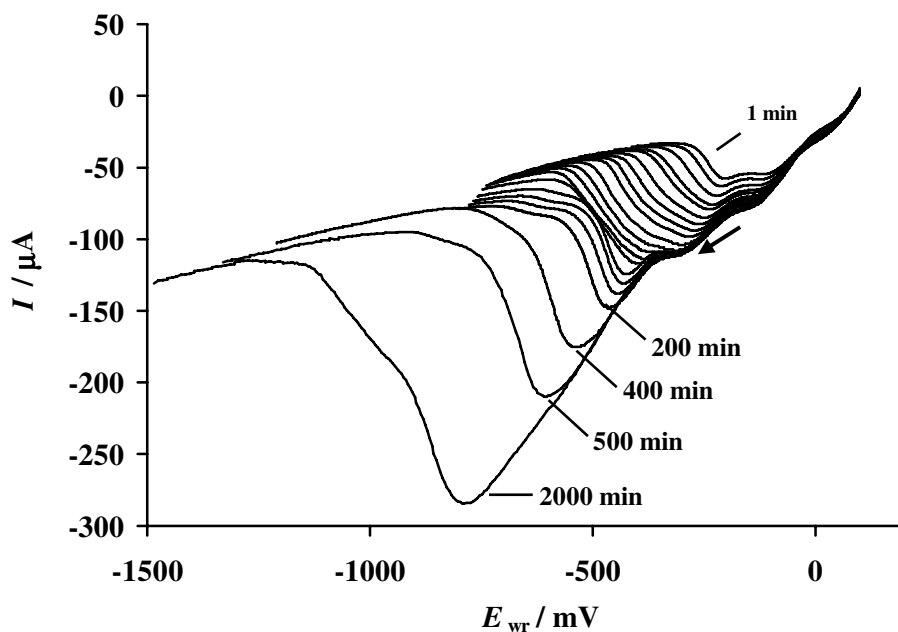
Fig. 20b   Voltammogram of the $O_{2(g)}$,Pt/YSZ system. As Fig. 20a with longer holding time t_h (up to 2000 min.)
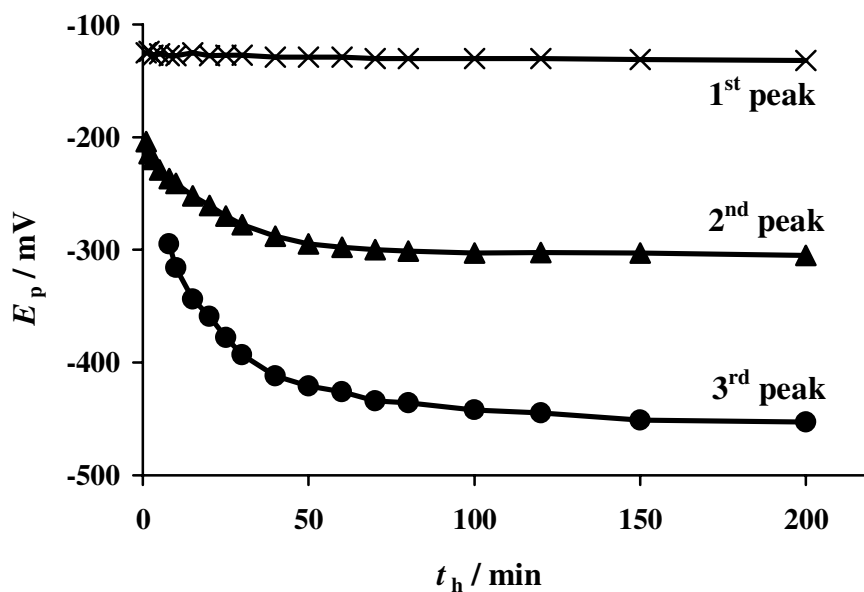
Fig. 21a   Effect of holding time, t_h, at $E_h = 100$ mV on the three peaks obtained in the voltammograms of Fig. 20a.
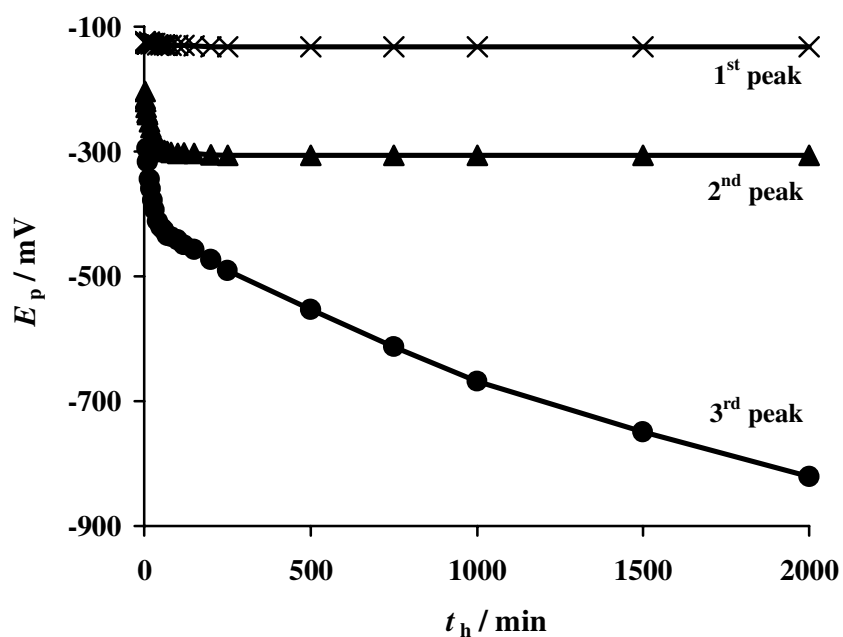
Fig. 21b   Effect of holding time, t_h, at $E_h = 100$ mV on the three peaks obtained in the voltammograms of Fig. 20. As Fig. 21a with longer holding time t_h (up to 2000 min.).

Fig. 21 show the effect of the holding time on the peak potentials E_p for the series of measurements shown in Fig. 20. The potential of the first peak is fairly independent of the holding time ($E_p = -100$ mV). The potential of the second peak decreases with increasing t_h up to its saturation point ($t_h = 60$ min). Its final reduction peak value E_p is about -300 mV. The potential of the third peak seems to follow a similar behavior up to $t_h = 200$ min. However, as clearly seen in Fig. 20b and Fig. 21b, the peak potential decreases with increasing t_h and does not reach a constant level at holding times as long as 2000 min.

Discussion

Application of the potential program illustrated in Fig. 14 to the cermet electrode lead to very interesting current features. The common features as well as the effects of the experimental conditions are discussed.

The shape of the voltammograms (Fig. 15 - Fig. 20)

The shapes of the voltammograms demonstrate that during the positive scan, charge is being stored (oxygen injection). During the subsequent negative scan, the charge is released (oxygen ejection), giving rise to up to three cathodic peaks (Fig. 20). This

indicates that the injected oxygen species (Pt-O), formed during the anodic polarization, are present in three different states.

Variation of the oxygen partial pressure pO_2 (Fig. 16)

Fig. 16 shows that the size and position of the first two cathodic peaks are not modified in a significant manner by varying the oxygen partial pressure. This confirms the hypothesis of the electrochemical origin of these peaks. In other words, it confirms that the injected oxygen species, responsible for the charge storage (pseudocapacity) are produced during the anodic polarization.

Fig. 16 also shows that in the low potential domain ($E_{WR} < -300$ mV), the cathodic current decreases with decreasing oxygen partial pressure. This confirms that in this domain, the measured current is certainly limited by the electrochemical O_2 reduction (eq. 4.13).

$$\frac{1}{2}O_{2 \ (gas)} \longrightarrow O \xrightarrow{\ +2e^- \ } O^{2-} \qquad\qquad 4.13$$
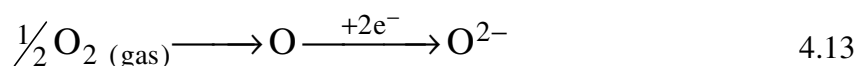
Variation of the holding potential E_h (Fig. 17)

The variation of the holding potential was also used to confirm the electrochemical origin of the cathodic peaks. Indeed, as E_h increases, the peaks increase, their size ratio remaining constant. Furthermore, as the peaks grow, their peak potentials E_p shift to more negative values.

Variation of the holding time t_h (Fig. 20)

One of the most relevant observations made in these measurements is the electrochemical ejection of the oxygen species (injected during long anodic polarization) giving rise to three peaks, indicating three different states.

Two of them are observed already at small holding times (t_h = 1 min) whereas longer t_h (> 20 min) are needed to observe the third state. As shown in Fig. 20, increasing the holding time t_h causes the second state to grow and exceed the first state. A similar behavior has been reported in the literature [31]. The third peak appears initially (at t_h > 20 min) as a widening of the second peak to lower potentials, then as a fully grown peak (at t_h > 60 min). This result confirms that the pseudocapacitive charge stored at the electrode

during an anodic polarization does not consist of one unique injected oxygen species (see equation 4.10).

These three oxygen states seem to be linked one to another. In fact, the first peak saturates at an early stage, followed by the saturation of the second peak. However, the third peak does not seem to saturate, even at very long polarization times (t_h = 2000 min). Apparently, the holding time is the only experimental parameter capable of modifying the peak size ratio in a significant manner (Fig. 20).

Pseudocapacity is charge storage in the form of chemical species (oxygen injection). The results given in this section suggest that the injected oxygen species are present in at least three different states involved in the pseudocapacitive charge storage. Each state has its own electrochemical characteristic and storage capacity. The process corresponding to the third peak seems to have an infinite capacity.

4.2.6 Investigation of the $O_{2(g)}$,Pt/YSZ system

Charges involved in cyclic voltammetry

It has been seen in section 4.2.3. that the integration of the chronoamperometric curves gave some very valuable pieces of information on the charge storage mechanism. For instance, charge integration permitted to determine the $t_h^{1/2}$ kinetic law for the extra charge storage process. By analogy, it may be of great interest to integrate the pseudocapacitive charge stored and released during the experiments of cyclic voltammetry.

Results

Integration of the cathodic peaks obtained at various holding times t_h

From the series of voltammetric scans shown in Fig. 20, obtained at different holding times t_h, the amount of charges released (ejected) for each peak are plotted as a function of the holding time t_h (Fig. 22). These charges are expressed for each peak (1st, 2nd and 3rd) in terms of equivalent amount of injected oxygen atoms (N_1, N_2, N_3 respectively), calculated assuming the exchange of two electrons.

It is clearly seen in Fig. 22, that the amount of injected oxygen related to the first and second peaks (N_1 and N_2) increases, reaching saturation after t_h = 10 min and t_h = 80 min

respectively. In contrast, the third peak grows continuously and, even for holding times as long as 2000 min, there is no sign of saturation.

Discussion

Saturation is reached for oxygen coverages of N_1 = 8.2·10^{15} atom/cm^2 and $N_2 = 6·10^{16}$ atom/cm^2 (electrode geometric area of 0.08 cm^2). These values indicates that we are dealing with monolayer oxygen coverages (≈ 10 ^{15} atom/cm^2). We can speculate that N_1 corresponds to the formation of an oxygen monolayer at the Pt/YSZ interface (solid/solid) according to reaction 4.14

$$Pt_{(Pt/YSZ)} + O^{2-} \rightleftharpoons Pt - O_{(Pt/YSZ)} + 2e^- \qquad 4.14$$
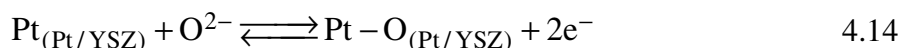
As the anodic potential is applied, Pt-O compounds accumulate at the interface up to an equilibrium state. For increasing applied potentials E_{WR}, the fraction of the interfacial Pt atoms, which are occupied by oxygen, tends to one (complete oxygen monolayer). In literature, all papers agree that the first peak corresponds to the reduction of a Pt-O compound. It is attributed either to the reduction of oxygen atoms adsorbed at the tpb [31] or, as speculated here, to the reduction of oxygen formed at the Pt/YSZ interface [4, 29-31, 33]. In particular, a paper by Kenjo et al. proposes to use the charge calculated by integration of the first cathodic peak to determine the Pt/YSZ interface area [30].

In the present case, due to the electrode preparation (cermet), we expect the real Pt/YSZ surface to be greater than the geometric electrode surface. Therefore, by using the geometric surface, we surely underestimated the Pt/YSZ surface, explaining that the rather high calculated N_1 value (8.2·10^{15} atom/cm^2).

We can also speculate that N_2 corresponds to the formation of oxygen at the triple phase boundary (tpb) sites, which spread over the gas exposed platinum surface (Pt/gas interface).
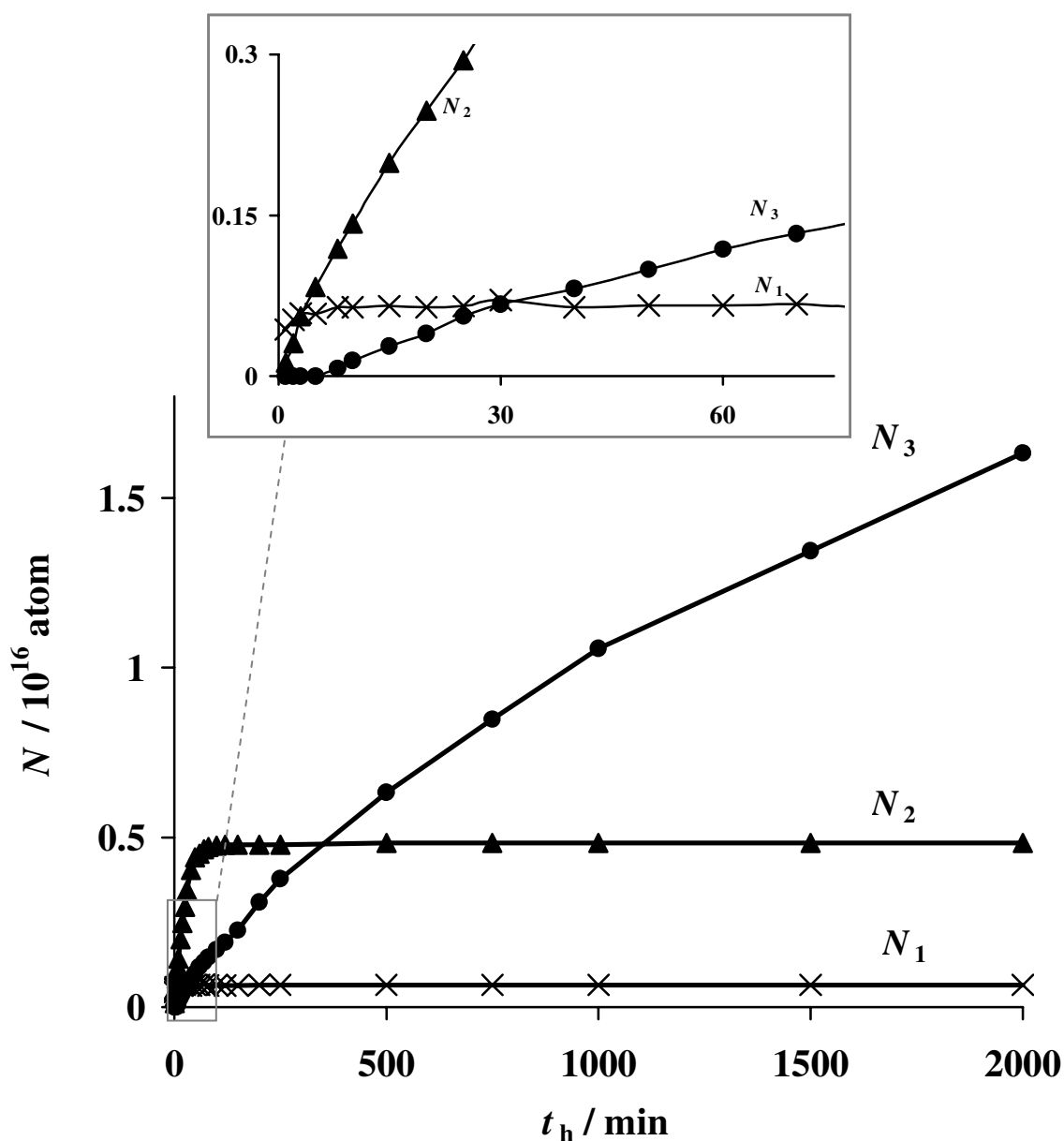
Fig. 22 Effect of holding time, t_h, at $E_h = 100$ mV on the amount of injected oxygen related to the 1st, 2nd and 3rd peaks. The amount of oxygen atoms, N, is calculated assuming the exchange of two electrons. $T = 450°C$, $pO_2 = 20$ kPa, $v = 10$ mV s^{-1}.

In literature, the second, often poorly defined, cathodic peak has also been reported a few times. It has been interpreted as the formation of oxygen atoms spreading over the Pt/gas interface [31, 33] or as the growth of a distinct type of platinum oxide [4, 31].

Assuming that the cathodic peak corresponds to the reduction of oxygen atoms formed anodically at the tpb and spreading over the gas exposed electrode surface, Vayenas et al.

propose a method based on cyclic voltammetry measurements to determine the number of sites at the tpb [34]. This method is applicable in solid state electrochemistry, but it is analogous to the determination of the number of reaction sites in aqueous electrochemistry. It assumes that oxygen atoms, once anodically formed at the tpb sites, diffuse on the Pt/gas interface up to a certain distance L_t, depending on the diffusion coefficient D_S of oxygen on the platinum surface and the potential scan rate ν:

$$L_t = (D_S \, RT/F\nu)^{1/2} \qquad\qquad 4.15$$

The third peak has been observed for the first time in our laboratories. Such an observation is certainly due to the specific electrode preparation procedure and to the fact that the measurements were carried out at very long holding times t_h. The continuous increase of this peak with holding time indicates that we are dealing with the formation of an oxygen multilayer film, probably from the Pt/YSZ interface toward the platinum bulk. In addition, the fact that N_3 increases with $t_h^{1/2}$ (Fig. 23) indicates that the growth of this film is controlled by diffusion.
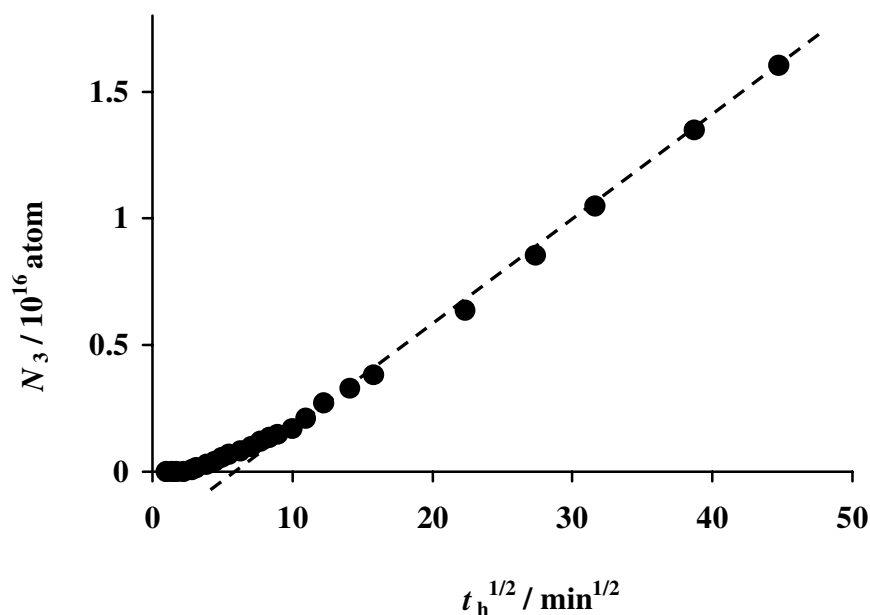
Fig. 23   Plot of the amount of injected oxygen related to the third peak expressed in terms of equivalent amount of oxygen atoms, N_3, as a function of the square root of holding time, t_h, at $E_h = 100$ mV.

In order to confirm this hypothesis, we will try to estimate the diffusion coefficient D using relation 4.16 [1]

$$D = \frac{L_t^2}{2 \cdot t} \qquad\qquad 4.16$$

where L_t is the diffusion length at a certain diffusion time t. Considering that N_1 corresponds to the formation of an oxygen monolayer at the Pt/YSZ interface and N_3 to the formation of multilayer, we can estimate from Fig. 22 and Fig. 23 the diffusion length L_t at a given time:

$$L_t = \frac{N_3(t)}{N_1} \cdot d \qquad\qquad 4.17$$

where $N_3(t)$ is the amount of oxygen atoms in the multilayer at time t. N_1 is the amount of oxygen atom in the monolayer at the Pt/YSZ interface ($6.6 \cdot 10^{14}$ atom) and d is the average thickness of an oxide layer (estimated by the Pt-Pt atomic distance $2.7 \cdot 10^{-10}$ m [35]). The calculated diffusion coefficient at 450°C is

$$D = 3 \cdot 10^{-22} \text{ m}^2/\text{s}$$

This low diffusion coefficient value is typical for a diffusion process inside a solid phase. In particular, it is in agreement with the diffusion coefficient predicted by Velho et al. [36] for the diffusion of oxygen inside platinum at the experimental $T = 450°C$.

Fig. 23 shows that the production of the species corresponding to the third peak does not occur immediately as soon as the anodic holding potential is applied, $t_h = 0$. Indeed, it is found to take place only after a few minutes of polarization. An identical feature has already been observed in section 4.2.3 (see Fig. 10) for the case of the so-called extra charges, experienced with double step chronoamperometry. In addition, it had been found that these extra charges were also produced following a $t_h^{1/2}$ law, indicating that they are certainly linked to the third peak discussed here.

4.2.7 Investigation of the $O_{2(g)}$,Pt/YSZ system by steady state polarization

In chronoamperometry and chronopotentiometry, it has been seen that the measured current and the measured potential, respectively, tend to steady state values (see Fig. 4 and Fig. 13). The aim of this section is to study the $O_{2(g)}$,Pt/YSZ system by steady state polarization measurements and to investigate the kinetic features of the redox reaction (4.18) in both the anodic and the cathodic domain.

$$O^{2-}_{(YSZ)} \rightleftarrows \tfrac{1}{2}O_{2\,(g)} + 2e^{-}_{(Pt)} \qquad\qquad 4.18$$
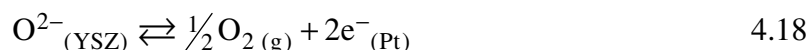
Theoretical background on multistep electrochemical processes

Electrochemical kinetic theories are often restricted to one-step, one-electron transfer reactions. However, most studied electrochemical processes involve multiple steps and the transfer of multiple electrons. For instance, the (O^{2-}/O_2) redox reaction (eq. 4.18) consists of the exchange of two electrons per oxygen atom and the charge transfer steps are preceded and followed by various non-electrochemical steps. Any of the steps (electrochemical or non-electrochemical) can be either limiting, non-limiting or partially limiting. In order to simplify the treatment of multiple-step multiple-electron systems, a method has been devolved by Bockris and Reddy [37]. Used in numerous papers [24, 38-40], this method is based on the assumption that the overall reaction rate is limited by only one step, the slowest, called rate determining step (RDS). Quasi-equilibrium is considered for all the other steps.

One considers a multi-step electrochemical reaction A + n e⁻ → Z, where the rate determining step R + r e⁻ → S is repeated ν times (see reaction scheme 4.19). The RDS is preceded by $\vec{\gamma}$ single-electron steps and followed by $\overleftarrow{\gamma}$ single-electron steps. These preceding and following steps are considered in quasi-equilibrium.

$$
\begin{aligned}
&\text{A} + \text{e}^- \rightleftharpoons \text{B} && \left[\text{Step 1}\right] \\
&\text{B} + \text{e}^- \rightleftharpoons \text{C} && \left[\text{Step 2}\right] \\
&\qquad \vdots \qquad\qquad \vdots \\
&\text{P} + \text{e}^- \rightleftharpoons \text{R} && \left[\text{Step } \vec{\gamma}\right] \\
&\nu\left(\text{R} + r\,\text{e}^- \longrightarrow \text{S}\right) && \left[\text{rds repeated } \nu \text{ times}\right]
\end{aligned}
$$

$$
\begin{aligned}
&\nu\text{S} + \text{e}^- \rightleftharpoons \text{T} && \left[\text{Step n} - \vec{\gamma} - r\nu \equiv \overleftarrow{\gamma}\right] \\
&\qquad \vdots \qquad\qquad \vdots \\
&\text{Y} + \text{e}^- \rightleftharpoons \text{Z} && \left[\text{Step n}\right]
\end{aligned}
$$

4.19
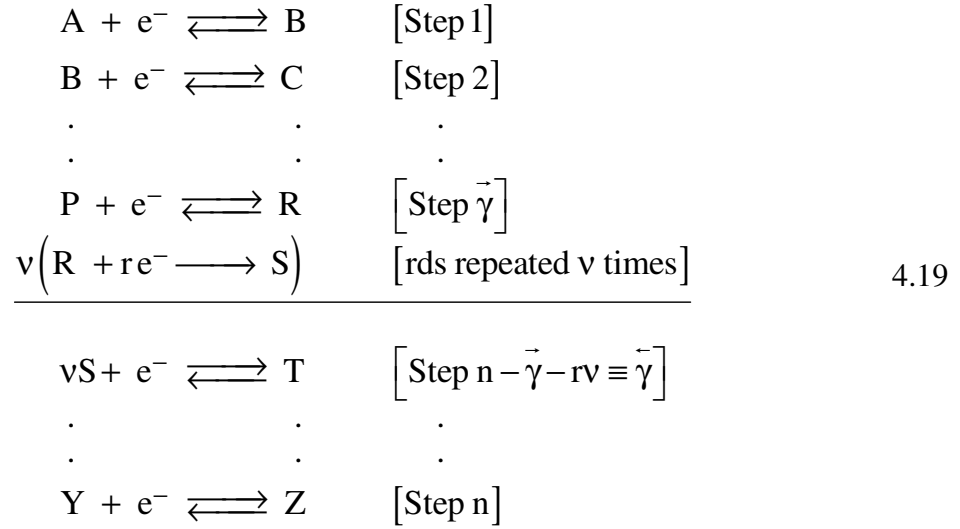
The current $\vec{I}_R$ of the rate-determining step is given by

$$
\vec{I}_R = FA\vec{k}_R c_R\, \text{e}^{-r\beta F\Delta\varphi/RT}
\qquad\qquad 4.20
$$

where A is the electrode geometric surface, k_R is the cathodic rate constant for the RDS reaction, c_R the concentration of R, $\Delta\varphi$ is the applied potential relative to a reference electrode, β the symmetry factor.

Since all the other steps are at equilibrium, the concentration of A and R are related by

$$
c_R = \left[\prod_{i=1}^{\vec{\gamma}} K_i\right] c_A\, e^{-\vec{\gamma} F\Delta\varphi/RT}
\qquad\qquad 4.21
$$

where K_i is the ratio between the cathodic and anodic rate constant of step i.

$$
K_i = \frac{\vec{k}_i}{\overleftarrow{k}_i}
\qquad\qquad 4.22
$$

By analogy, similar equations can be written for the current of the rate-determining step and the concentration of the reactants and products of the steps at equilibrium.

The net current flowing through the electrode is given by

$$I = n\left(\overleftarrow{I}_R - \overrightarrow{I}_R\right)$$
4.23

which is developed under the form of the Butler-Volmer equation for global multistep reactions

$$I = I_0 \left(e^{\alpha_a \frac{\eta F}{RT}} - e^{-\alpha_c \frac{\eta F}{RT}} \right)$$
4.24

where I_0 is the exchange current, η, the overpotential and α_a and α_c are the charge transfer coefficient given by the relations

$$\alpha_a = \frac{\overleftarrow{\gamma}}{\nu} + r - r\beta$$

$$\alpha_c = \frac{\overrightarrow{\gamma}}{\nu} + r\beta$$
4.25

$$\alpha_a + \alpha_c = \frac{n}{\nu}$$

Considering the symmetry coefficient $\beta = 0.5$ and using relations 4.25, one can evaluate the transfer coefficient values for any given set of elementary steps 4.19. Some sets of coefficient are presented in Table 1.

Table 1   transfer coefficients predicted from relations 4.25

$\vec{\gamma}$	r	v	$\overleftarrow{\gamma}$	n	α_c	α_a
0	0	1	1	1	0	1
1	0	1	1	2	1	1
0	2	1	0	2	1	1
2	0	2	2	4	1	1
0	1	1	1	2	0.5	1.5
1	1	1	2	4	1.5	2.5
1	1	2	1	4	1	1
2	1	2	2	6	1.5	1.5

Low field approximation

At low overpotentials, both exponential terms in the Butler–Volmer equation (4.24) can be linearised and the equation reduces to

$$I = I_0 \left(\alpha_a + \alpha_c \right) \frac{F\eta}{RT} \qquad\qquad 4.26$$

The low field version of Butler-Volmer equation can be used assuming a $\leq 2\%$ error when the following condition is met for both the anodic and the cathodic cases ($\alpha = \alpha_a$ and $\alpha = \alpha_c$) [41].

$$\eta \leq \frac{0.2\left(RT \right)}{\alpha F} \qquad\qquad 4.27$$

One may note that this potential domain depends on temperature and on the transfer coefficient.

High field approximation

At high overpotentials, one of the two exponential terms of Butler-Volmer equation (4.24) becomes negligible with respect to the other and can be dropped. The resulting expression gives the current I exponentially dependent of the overpotential η. Therefore, linearization of the expression is achieved by plotting $\ln|I|$ versus η.

$$\ln|I| = \ln I_0 + \frac{\alpha\,F}{RT}\cdot\eta \qquad\qquad 4.28$$

where α is the transfer coefficient α_a in the anodic case and α_c in the cathodic case.

Plotting $\ln|I|$ versus η is known as Tafel plot and is used to determine the transfer coefficients α_a and α_c from the slope of its linear part.

The overpotential beyond which the high field approximation is valid assuming a <1% error, is given by

$$|\eta| \geq \ln(99)\frac{RT\nu}{Fn} \qquad\qquad 4.29$$

Results

The steady state I-E_{WR} polarization in the high field domain

Fig. 24 represents the Tafel plot of the steady state curve in the positive potential region. The linear relation predicted by the high field approximation (4.28) is confirmed in the whole domain of applied positive potential (0.05 V > E_{WR} > 0.27 V).

Fig. 24   Tafel plot of the positive potential region of the steady state curve (ohmic drop corrected). $T = 450°C$, $pO_2 = 20$ kPa.

From the slope, the anodic transfer coefficient α_a appearing in Butler-Volmer's equation 4.24 can be calculated. In the given experimental conditions, a value of $\alpha_a = 1.1$ has been found. With $n/\nu = 2$, the validity domain of the high field approximation (4.29) is $|E_{WR}| \geq 0.14$ V. However, Fig. 24 shows that the linear relation is even respected down to $E_{WR} = 0.05$ V.

Fig. 25 represents the Tafel plot of the negative potential region of the steady state curve. The linear relation is only confirmed in the upper potential region (-0.15 V $> E_{WR} > -0.05$ V), where a $\alpha_c = 1.2$ value can be drawn from the slope. At more negative potentials, the apparent slope decreases indicating a negative deviation from the Butler-Volmer kinetic law. An identical behavior (the $\alpha_c = 1$ coefficient and the negative deviation at lower E_{WR}) has been reported by Wang et al. [39]. As in the anodic case, the calculated validity domain for the high field approximation is $|E_{WR}| \geq 0.14$ V. However, the linear relation is found to be valid up to $E_{WR} = -0.05$ V.
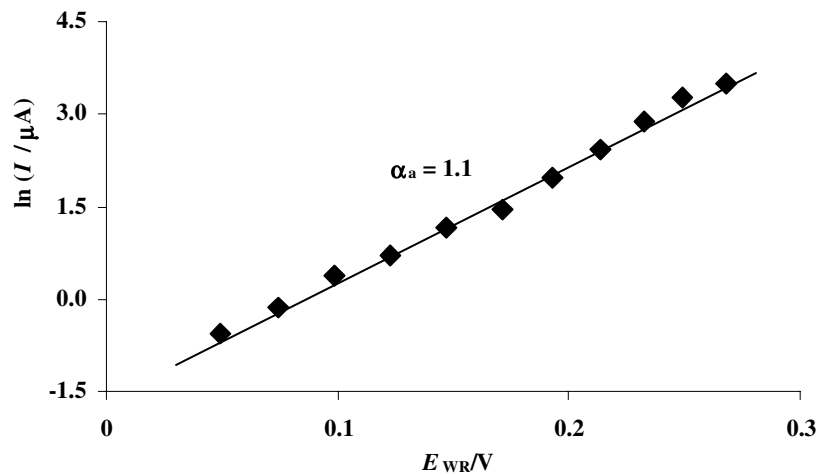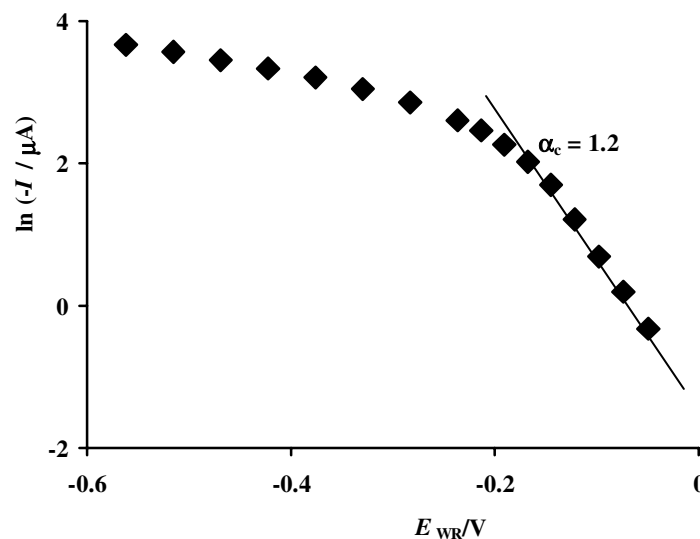

Fig. 25   Tafel plot of the negative potential region of the steady state curve (ohmic drop corrected). $T = 450°C$, $pO_2 = 20$ kPa.

The steady state I-E_{WR} polarization in the low field domain
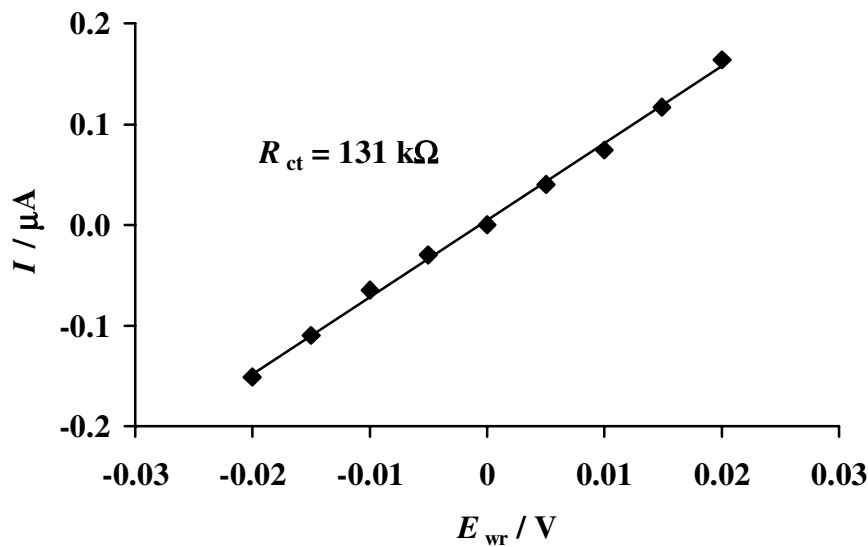
Fig. 26   Steady state I-E_{WR} plot of the $O_{2(g)}$,Pt/YSZ system in the low field domain. Ohmic drop corrected. $T = 450°C$; $pO_2 = 20$ kPa.

Fig. 26 shows the experimental steady state I-E_{WR} relation in the domain ($+0.02$ V $> E_{WR} > -0.02$ V). As expected, at low potentials, the I-E_{WR} shape is linear. Since the plot crosses the origin, the open circuit potential is $E_{WR} = 0$ V, as expected given that the reference and the working electrodes are identically prepared (see Chapter 3). The resistance of the charge transfer R_{ct} and the corresponding exchange current under these conditions can be drawn from the slope ($\alpha_a = \alpha_c = 1$ used for the calculation of I_0):

$R_{ct} = 131$ kΩ

$I_0 = 0.23$ µA

Using $\alpha = 1$, the validity domain of the low field approximation (4.26) is $|E_{WR}| \leq 12$ mV. However, Fig. 26 shows that the linear relation is respected up to $|E_{WR}| = 20$ mV.

The effect of the oxygen partial pressure pO_2 on the steady state current

In order to gain more knowledge on the nature of the limiting step of the overall reaction at negative potentials, steady state polarization has been performed at various oxygen partial pressures. These were varied from 20 kPa to 0.2 kPa. In order to keep the same

potential scale despite the varying oxygen partial pressure at the reference electrode, the applied potentials were corrected according to equation 4.12, and all potentials in Fig. 27 are given with respect to 20 kPa.

Fig. 27 shows that decreasing pO_2 causes a decrease in the measured cathodic current in the E_{WR} < -0.2 V region. As more negative potentials are applied, the current difference between high and low oxygen pressure is more pronounced. At low potential values (E_{WR} < -0.5 V), the 0.2 kPa curve tends to a limiting current.
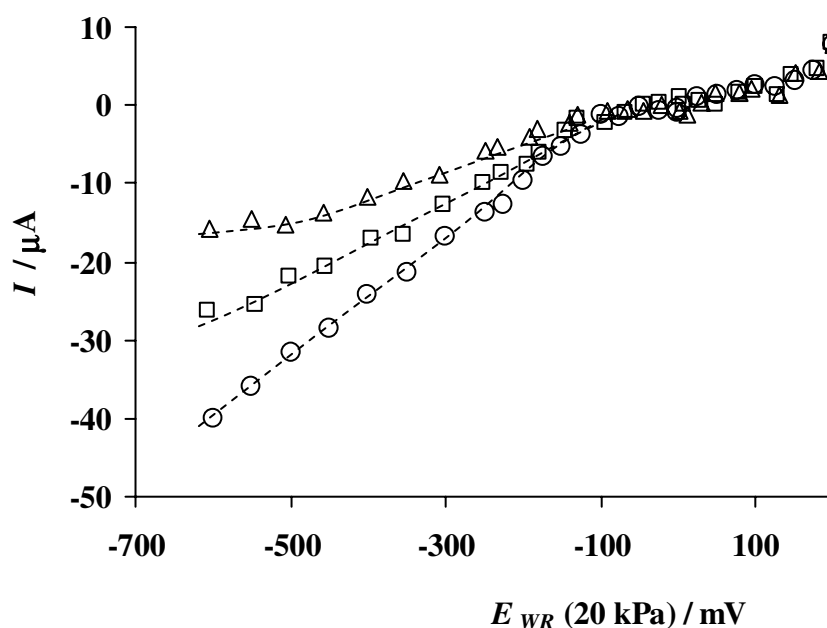
Fig. 27   Steady state I-E_{WR} curve at various oxygen partial pressures. ($\bigcirc$) pO_2 = 20 kPa, ($\square$) 2 kPa, ($\triangle$) 0.2 kPa. E_{WR} is corrected using equation 4.12. T = 450°C.

Discussion

Positive polarization

The Tafel plot for positive potentials (Fig. 24) confirms that the limiting step of the global reaction occurring at steady state is electrochemical. The linear plot is characterized by $\alpha_a = 1$, approximately. On the given electrode, in the anodic case, the step preceding the charge transfer is the migration of O^{2-} in the solid electrolyte toward the electrochemical reaction site (ERS). The fact that the overall rate follows Butler-Volmer's kinetics suggests that this step preceding the limiting charge transfer is in quasi-equilibrium, i.e. infinitely fast in comparison.

Negative polarization

The Tafel plot for negative potentials (Fig. 25) confirms that the global rate is limited by an electrochemical step in the domain $E_{WR} >$ -0.2 V. The linearization is characterized by a $\alpha_c = 1$ value, approximately. Most papers report $\alpha_a = \alpha_c = 1$ values for the oxygen exchange reaction on the platinum electrode [31, 39].

However, for $E_{WR} <$ -0.2, the negative deviation from the high field approximation indicates that the global reaction rate occurring at steady state is no longer limited by an electrochemical step. Fig. 27 shows that for a given applied negative potential $E_{WR} <$ -0.2V, the cathodic reaction rate decreases with decreasing oxygen partial pressure. This suggests that in the given experimental conditions, the delivery of the reactant (i.e. oxygen) to the ERS might be rate limiting.

In a given series of chemical and physical steps of an electrode process, only the charge transfer steps can be enhanced by increasing $|\eta|$. This means that the electrochemical step can be rate limiting at low $|\eta|$ (slow charge transfer) but may become non-limiting at high $|\eta|$ (fast charge transfer) if another non-electroactivated process becomes the slowest. If both the non-electroactivated and the electroactivated rates are comparable, a case of mixed kinetics is observed [1].

In the cathodic domain, deviation from the Butler-Volmer kinetics under high currents and/or low oxygen partial pressures is reported in various papers [31, 39]. It has been attributed to the limitation by the oxygen dissociation step or the diffusion of adsorbed oxygen on platinum. In addition, unexpected features in the steady state polarization curves of the $O_{2(g)}$,Pt/YSZ system such as bumps or hysteresis have been attributed to an effect of surface platinum oxide [31, 39]. Indeed, the presence of strongly bounded oxygen atoms or oxides at key sites of the cathodic reaction, i.e. in the vicinity of the triple phase boundary, may constitute a barrier and cause an increase of the overall resistance, impeding the delivery of oxygen to the ERS [12].

Possible reaction mechanisms for $\alpha_a = \alpha_c = 1$

As shown in the Tafel plots (Fig. 24 and Fig. 25), $\alpha_a = \alpha_c = 1$ values are found for the oxygen exchange reaction in the potential domain where the rate follows Butler-Volmer's kinetics ($E_{WR} >$ -0.15 V). Based on the model developed by Bockris and Reddy [37], this set of transfer coefficients leads to two mechanism patterns.

The first possible pattern for the given set of transfer coefficient is ($n = 2$, $\vec{\gamma} = \overleftarrow{\gamma} = 1$, $r = 0$, $\nu = 1$). It corresponds to a non-electrochemical limiting step preceded and followed by non-limiting single-electron steps:

$$O \underset{-e^-}{\overset{+e^-}{\rightleftarrows}} O^- \xrightarrow{\text{rate limiting step}} O^- \underset{-e^-}{\overset{+e^-}{\rightleftarrows}} O^{2-} \qquad 4.30$$
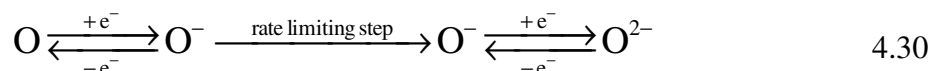
The charge transfer steps are considered to occur at the tpb, where all three reactants (O, O^{2-} and the electrons) are available. Consequently, the non-electrochemical rate limiting step must also occur at the tpb. It could be a rearrangement step or the penetration/extraction of O^- into/from the electrolyte via reaction with an oxygen vacancy.

The second possible pattern ($n = 2$, $\vec{\gamma} = \overleftarrow{\gamma} = 0$, $r = 2$, $\nu = 1$ and $\beta = 0.5$) corresponds to the rate limitation by a two-electron charge transfer step preceded and followed by non-electrochemical steps at quasi-equilibrium.

$$O \xrightarrow[\text{rate limiting step}]{+2e^-} O^{2-} \qquad 4.31$$

However, in terms of probability, a 2-electron transfer step is unfavorable. Indeed, it is a widely held concept in electrochemistry that truly elementary electron transfer reactions always involve the exchange of one electron [1].

The mechanism patterns presented here are to be taken as assumptions. They are based on the model developed by Bockris and Reddy. However, this model assumes that there is only one rate limiting step and all other steps are at quasi-equilibrium. This drastic assumption might not always be verified in real electrochemical systems. Indeed, mixed kinetics is often found when two or more steps occur at comparable rates [23, 25]. Therefore, it does not consider the case where the two electrons are exchanged via two 1-electron transfer steps of comparable rate. The real mechanism could be an intermediate between the two limit cases 4.30 and 4.31.

4.2.8 Investigation of the $O_{2(g)}$,Pt/YSZ system by impedance spectroscopy

In steady state polarization measurements, the measured current is dictated by the overall electrode resistance. In this section, impedance spectroscopy is used to determine whether this overall resistance can be divided into various resistive components, attributed to distinct steps of the global oxygen exchange reaction.

In impedance spectroscopy, the potential signal applied to the electrode is the sum of a stationary potential E_{WR} and a sinusoidal wave of small amplitude ΔE_{WR} and of frequency f. The resulting measured sinusoidal current is the sum of a stationary current and a sinusoidal wave of amplitude ΔI and frequency f with a phase shift ϕ. The real (Z') and imaginary (Z'') part of the impedance Z are obtained as a function of f. Upon crossplotting the two parts for different values of frequency, a Nyquist plot is obtained.

Impedance spectroscopy on the $O_{2(g)}$,Pt/YSZ system has been widely described in literature and semicircles in the Nyquist plane are often reported for measurements performed on similar electrodes in comparable experimental conditions [5, 22-25, 39]. The interpretation of the semicircle shape is often based on the analogy with a R_S (R_p C) circuit (in Boukamp's notation [42]), for which, the first intersection of the semicircle with the abscissa (at high frequencies) gives the electrolyte resistance R_S and the second intersection (at low frequencies) gives the total resistance $R_{tot} = R_p + R_S$.

The resistance of the electrolyte is due to the intrinsic ohmic resistance of the electrolytic material whereas the polarization resistance R_p involves the other processes, electrochemical and chemical, which participate in the overall resistance [5, 23-25]. The polarization resistance can be further divided into two components: $R_p = R_{ct} + R_{chem}$. The term R_{ct} is the resistance due to the electron transfer steps (charge transfer) whereas the term R_{chem} is the resistance due to non-electrochemical processes. These processes include the diffusion of gaseous O_2 between the electrode surface and the gas phase via the pores, the diffusion of adsorbed oxygen atom on the surface of the electrode and the oxygen adsorption and desorption process at the platinum surface; i.e. any step other than the migration of O^{2-} in the electrolyte or the charge transfer steps.

According to the Butler-Volmer equation, the charge transfer resistance is expected to decrease when the applied overpotential in absolute values $|\eta|$ is increased. In the high

field domain, the expected charge transfer resistance can be obtained by deriving equation 4.28, giving

$$R_{ct} = \frac{RT}{\alpha F} \cdot \frac{1}{|I|} \qquad\qquad 4.32$$

where the current I is given by Butler Volmer's equation 4.24.

Results

Impedance spectroscopy under positive potentials

Fig. 28 represents the Nyquist plot of the $O_{2(g)}$,Pt/YSZ system at open circuit and at various positive potentials. At all potentials, the shape of the spectrum keeps its depleted semicircle form, however, as E_{WR} increases, the polarization resistance R_p decreases dramatically (from 131 kΩ at $E_{WR} = 0$ V to 7 kΩ at $E_{WR} = 0.4$ V).
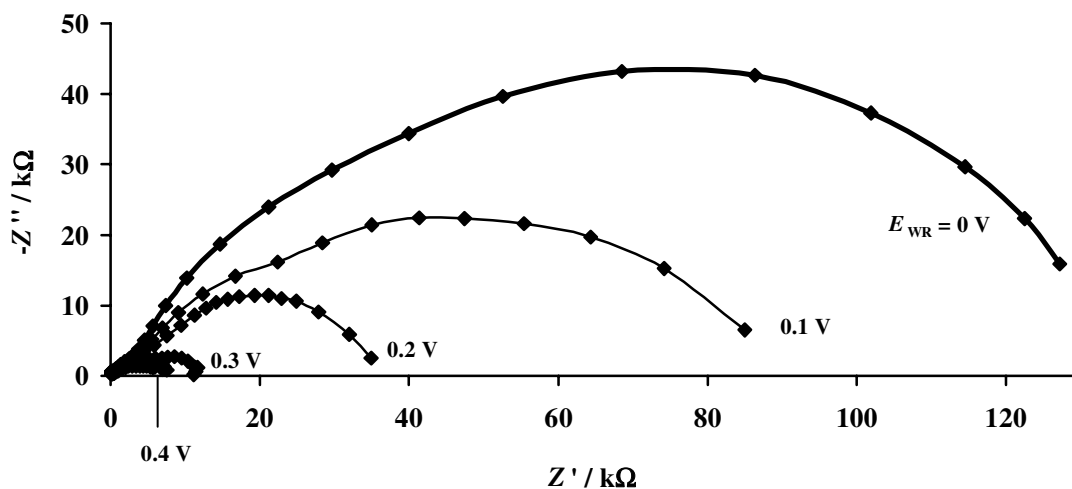
Fig. 28   Nyquist plot of the $O_{2(g)}$,Pt/YSZ system measured at various E_{WR} ranging from 0 V to 0.4 V. $pO_2 = 20$ kPa, $T = 450°C$, 30 points, frequencies f comprised in the domain 10 kHz $> f >$ 5 mHz, $\Delta E_{WR} = 10$ mV.

In order to determine whether the system follows a Butler-Volmer type kinetics, the polarization resistance drawn from Fig. 28 is compared to the expected charge transfer resistance calculated using 4.32. This is shown in Fig. 29. One notices that the experimental R_p values and the charge transfer resistance R_{ct} are very similar in the domain $E_{WR} \geq 0.1$ V. This indicates that the polarization resistance measured by

impedance spectroscopy in the positive potential domain corresponds to the charge transfer resistance expected from Butler-Volmer's kinetics. Consequently, this confirms that the global reaction rate in this domain is limited by a charge transfer step.

Fig. 29   Comparison of the experimental polarization resistance in the positive potential domain with the expected charge transfer resistance. Black squares: R_p extracted from Fig. 28. Dashed line: R_{ct} calculated using eq. 4.32 using parameters $I_0 = 0.23$ µA, $\alpha_a = 1$, $T = 450$°C.

Impedance spectroscopy under negative potentials

Fig. 30 represents the Nyquist plot of the $O_{2(g)}$,Pt/YSZ system at various negative potentials. It shows that at $E_{WR} = -0.1$ V, the polarization resistance R_p decreases compared to the open circuit condition (131 kΩ at $E_{WR} = 0$ V and 39 kΩ at $E_{WR} = -0.1$ V). However, the tendency is reversed when the applied potential is set to even lower values ($R_p = 93$ kΩ at $E_{WR} = -0.2$ V).

The behavior of the polarization resistance at various negative potentials is represented in Fig. 31. For comparison, the expected charge transfer resistance from the Butler-Volmer equation is plotted (dashed line). From 0V to -0.1V, the polarization resistance decreases, suggesting that the rate is limited by a charge transfer step, as in the anodic case. But at lower potentials, the measured polarization resistance R_p is much higher than the expected R_{ct}. This indicates that the resistance R_{chem} corresponding to a non-electrochemical step start to govern the overall rate at these low potentials. One observes that the polarization

resistance does not tend to infinity, as it is expected when a limit current occurs, but it tends to a constant value, approaching an ohmic behavior.
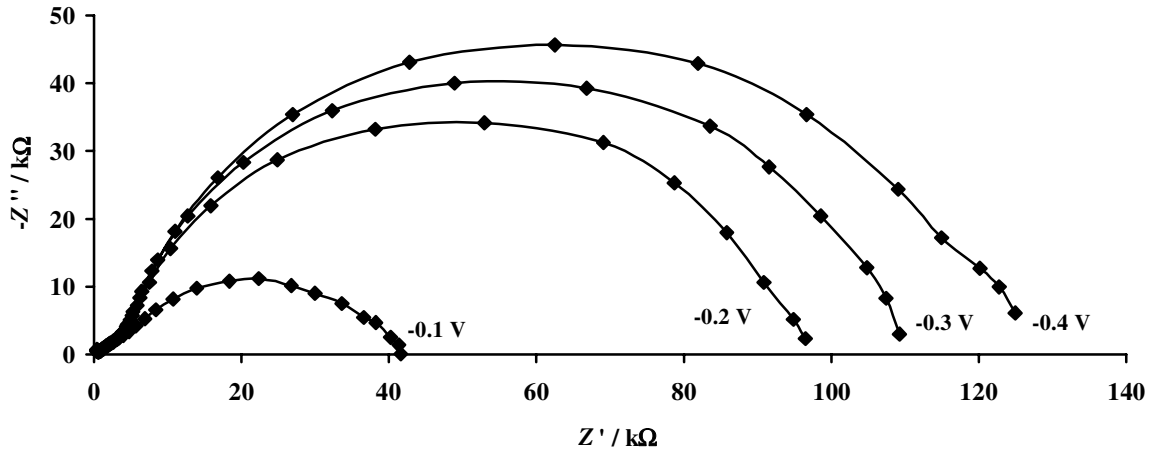
Fig. 30   Impedance spectra (Nyquist plot) of the O$_{2(g)}$,Pt/YSZ electrode measured at various E_{WR} ranging from -0.1 V to -0.4 V. Same experimental conditions as in Fig. 28.
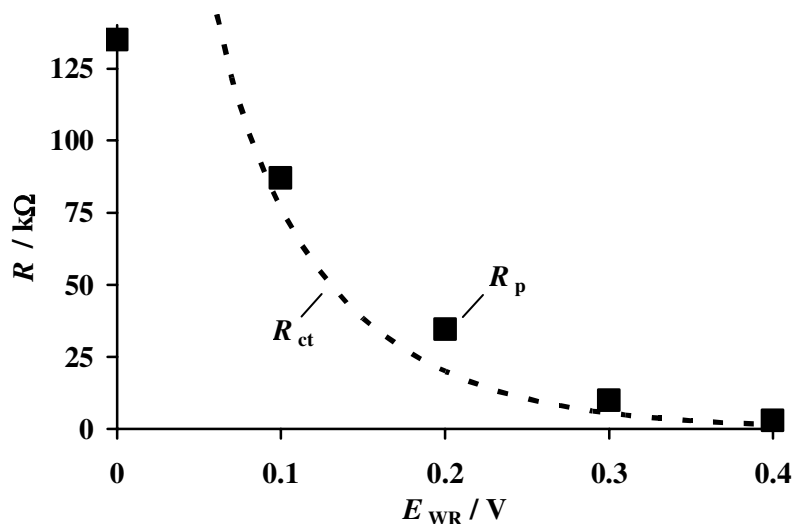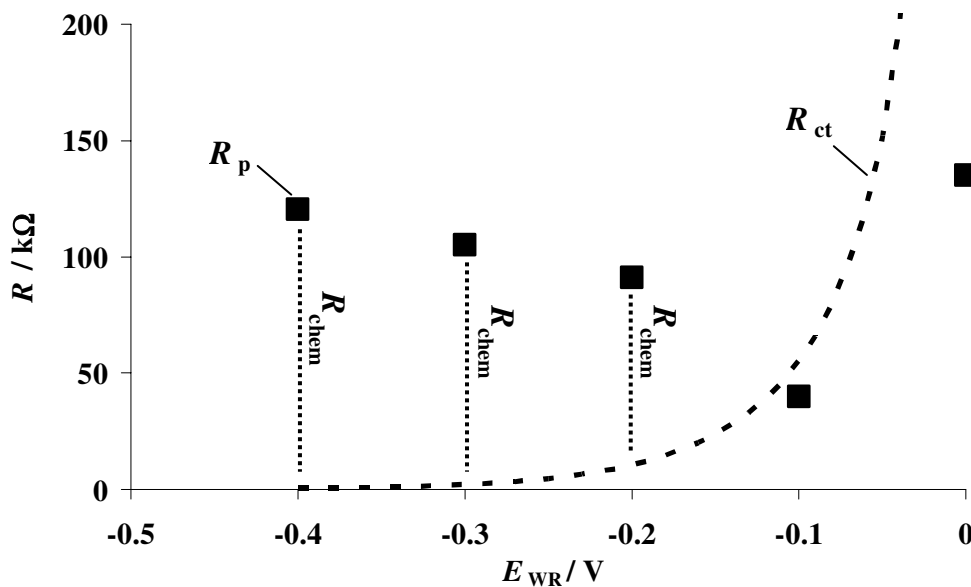

Fig. 31   Comparison of the experimental polarization resistance in the negative potential domain with the expected charge transfer resistance. Black squares : R_p extracted from Fig. 30. Dashed line: R_{ct} expected by equation 4.32 derived from the Butler-Volmer equation 4.24 using parameters $I_0 = 0.23$ µA, $\alpha_c = 1$, $T = 450$°C.

Discussion

In the given conditions, only one semicircle was clearly observed. This enabled us to discern two types of resistance, i.e. the resistance of the electrolyte and the polarization resistance.

Under a positive potential, the global reaction rate is found to be governed by the charge transfer step. This confirms the steady state polarization results presented above in section 4.2.7.

Under negative polarization, the global rate has been found to follow a Butler-Volmer behavior at $E_{WR} \geq$ -0.1 V. This indicates, as for the anodic case discussed above, that in this potential domain, the rate is limited by the charge transfer process, indicating that adsorbed oxygen atoms are provided to the electrochemical reaction site ERS at a sufficient rate. The divergence from the Butler-Volmer kinetics observed at lower applied potentials $E_{WR} <$ -0.1 V indicates that non-electrochemical processes become limiting in this domain. These processes are:1) The diffusion of gaseous O_2 from the gas phase within the pores of the electrode to the metal/gas interface. 2) The dissociative adsorption of oxygen at the metal/gas interface. 3) The diffusion of adsorbed oxygen atom toward the ERS. This question has been treated many times in literature [5, 20, 21, 24, 25, 27, 39, 43-45] and the limiting step for the reduction of oxygen has been found to depend on the experimental conditions and the electrode microstructure. In the present case, the diffusion of adsorbed oxygen atoms is thought to be limiting.

4.3 General Discussion

In this work, the $O_{2(g)}$,Pt/YSZ system has been investigated using several electrochemical methods such as single and double step chronoamperometry, chronopotentiometry, cyclic voltammetry, chronocoulometry, steady state polarization and impedance spectroscopy.

The results of all these techniques support the same conclusion. They demonstrate that under anodic polarization, two parallel reactions take place. One is the oxygen evolution reaction and the other is oxygen storage (oxygen injection). The oxygen storage occurs via complex multistep processes, characterized by distinct kinetic behaviors (e.g. fast or slow process, time delay, $t^{1/2}$ law). The processes of oxygen release (ejection) also occur following distinct kinetics. This gives rise to the three distinct peaks in cyclic voltammetry. In order to explain these results, two approaches will be considered.

a) **Distinct oxide stoichiometries**

In the field of solid electrochemistry, multipeaks in cyclic voltammetry were attributed to the step-wise consecutive oxidation and reduction of the working electrode made of various metals : Fe, Ni, Cu and Co and their oxides [32].

By analogy, a similar behavior can be imagined on the platinum electrode, where each cathodic peak corresponds to the reduction of an oxide of distinct stoichiometry. In literature, despite extended studies on the Pt-O interactions, the issue of surface platinum oxide is still ambiguous [46-52]. Many studies mention the coexistence of various types of Pt-O or oxide species [49, 53-55]. In terms of electrochemistry, each species corresponds to a certain oxide/Pt couple. If such distinct platinum oxides are produced on the electrode, they may be distinguishable based on the redox potentials E^0 of the couple.

Based on this idea, the presence of three reduction peaks in the voltammetric measurements can be explained by the successive formation of three platinum oxides according to:

1) $Pt + \frac{1}{2} O^{2-} \rightarrow \frac{1}{2} Pt_2O + e^-$ first peak E_1^0

2) $\frac{1}{2} Pt_2O + \frac{1}{2} O^{2-} \rightarrow PtO + e^-$ second peak E_2^0

3) $PtO + O^{2-} \rightarrow PtO_2 + 2e^-$ third peak E_3^0
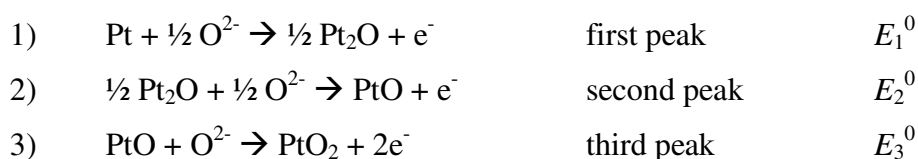
Since these oxides are formed via consecutive reactions, they are expected to be situated at the same geometrical location.

However, even if this model can explain the peaks observed in linear sweep voltammetry, it does not explain all the results. For instance, it does not make clear why the species corresponding to the first and second peaks reach saturation, while the species corresponding to the third peak grows indefinitely. In addition, it does not explain why the first and the second peak are found to grow in parallel while the third peak seems to be consecutive to the first one. If it is true that the species remain on the Pt/YSZ interface, how to explain the $t_h^{1/2}$ kinetic law obtained for the growth of the second and the third peaks? This $t_h^{1/2}$ law suggests the occurrence of a diffusion process. It could indicate that the corresponding Pt-O species diffuses toward another location on the electrode. For instance, it could diffuse toward the bulk of the electrode as discussed by van Manen et al.

[32]. This suggests that the assumption of the species being confined to a sole location and distinguished based on their stoichiometry is not satisfying. In order to complete the model, the possibility of storing Pt-O species on various sites must therefore be considered.

b)   Distinct storage locations

In this case, as a first assumption, we consider that the Pt-O species can be stored at various locations on the electrode, at interfaces or inside phases. Since the oxygen originates from the YSZ, the species must be formed at an interface directly in contact with the electrolyte; i.e. the tpb or the Pt/YSZ interface, but it may then diffuse on other interfaces and inside phases. The $O_{2(g)}$,Pt/YSZ system is composed of three phases and four interfaces, each featuring its own local chemistry. Consequently, the chemical environment of the stored Pt-O species will depend much on the storage location. The Pt-O species will behave differently and the corresponding redox potential E^0 of the Pt-O/O^{2-} couple will also depend on the storage location. In particular, the more stable the Pt-O in its environment, the more negative the E^0 value.

The first cathodic peak

As seen in Fig. 21, the first reduction peak appears at a fairly constant potential (E_p = -120 mV). This potential is not very far from the holding potential (E_h = 100 mV), indicating that the process is more reversible than the subsequent peaks. This means that, once anodically formed, the corresponding Pt-O species undergoes no strong stabilization. It also means that the species does not diffuse far away from the electron transfer site, but stays available for the subsequent reduction reaction. As mentioned in section 4.2.6, this peak is attributed to the build-up of an oxygen monolayer at the Pt/YSZ interface (see eq. 4.14).

The second cathodic peak

Fig. 22 shows that the first peak reaches a saturation value at low holding times. Saturation of the peak, indicates that the equilibrium condition has been reached and that no more Pt-O species can be stored at the Pt/YSZ interface. However, after extended polarization at the holding potential E_h, second and a third cathodic peaks appear, implying that the Pt-O species are stored on other geometrical location. Since the mobility

of platinum is limited at the given temperature and due to the lack of electronic conductivity in YSZ, the YSZ/gas interface and the YSZ phase are not considered as possible charge storage sites. Consequently, the Pt-O species can only be stored on the Pt/gas interface or in the platinum bulk phase.

In this model, the Pt-O species corresponding to the second peak is considered to be stored at the Pt/gas interface after being formed at the tpb site (eq. 4.33 and eq. 4.34).

$$Pt_{(tpb)} + O^{2-} \rightleftharpoons Pt - O_{(tpb)} + 2e^- \qquad\qquad 4.33$$

$$Pt - O_{(tpb)} \xleftrightarrow{\text{diffusion}} Pt - O_{(M/g)} \qquad\qquad 4.34$$
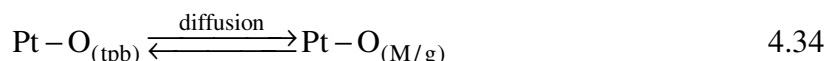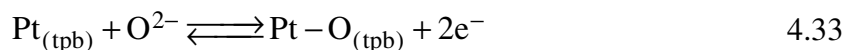
In this path, O^{2-} from the YSZ lattice is oxidized at the tpb releasing two electrons into the electrode forming a Pt-O compound, which may diffuse on the electrode/gas interface (eq. 4.34).

It is worthwhile to mention that the two paths (4.14 and 4.33) are parallel electrochemical reactions. They can occur simultaneously, explaining the simultaneous growth of the first two peaks at low holding times (see Fig. 22).

The Pt-O species produced by this path (4.33 and 4.34) diffusing over the gas exposed platinum surface might correspond to the oxygen back-spillover species $O^{\delta-}$ presented in Chapter 2 (Bibliography). These species consists of oxygen atoms, originating from the solid electrolyte via the tpb, which modifies the work function of the metal and often causes dramatic alteration of its catalytic activity via modification of the binding energy of chemisorbed reactants (EPOC). In Fig. 22, it is seen that the second peak reaches saturation after a few tens of minutes. This is in good agreement with the time constant of the transient activity curves commonly observed in EPOC experiments.

In literature, the second, often poorly defined, cathodic peak has also been reported a few times [4, 29, 31]. Various interpretations are proposed involving back-spillover oxygen spreading over the Pt/gas interface [31, 33] or a distinct type of platinum oxide [4, 31].

The third cathodic peak

As seen in Fig. 22, the third reduction peak is related to an even slower process exhibiting no tendency to saturate even after anodic polarization as long as 2000 minutes. So far in the discussion, only interfaces have been considered for the storage of charges. But since the YSZ phase and the YSZ/gas interface are not suited to store anodic charges, the only geometric location available for the charge storage is the platinum itself. Due to its 3-dimension geometry, the phase offers an extended storage capacity in comparison to the rather limited storage capacity at interfaces.

Based on these considerations, the species stored under anodic polarization and released under the form of the third peak in linear sweep voltammetry is attributed to the storage of Pt-O into the bulk of platinum; i.e. the growth of a platinum oxide layer. This layer grows from the Pt/YSZ interface. The transformation of chemisorbed oxygen into subsurface oxygen is believed to occur spontaneously at $T > 400°C$ [54] and oxygen diffusion is driven by the concentration gradient between the oxygen containing Pt/YSZ interface and the initially oxygen-free metal. In section 4.2.6, the diffusion coefficient D of oxygen in platinum has been calculated from the slope in Fig. 23 and has been found to be in the order of the values found in literature.

In literature, the oxide growth from the electrolyte/electrode interface toward the bulk of the electrode has been thoroughly studied in aqueous liquid electrochemistry of platinum [56-58]. In addition, in high temperature solid state electrochemistry, an identical oxide layer growth from the metal/YSZ interface toward the bulk phase of the electrode has been observed for various metals (Fe, Ni, Cu, Co) by cyclic voltammetry [32].

It is thought that in order to initiate the diffusion of oxygen inside the platinum phase, a certain oxygen coverage must be reached, through reaction 4.14. This means that path 3 does not take place immediately after the onset of the anodic polarization, but is delayed. This may explain that the third peak starts growing only at $t_h > 10$ min, when the first peak has stopped growing (see Fig. 22).

It is found in literature that subsurface oxygen is more stable than chemisorbed oxygen [49, 59]. By entering the platinum lattice, the oxygen atom reaches a lower (more stable)
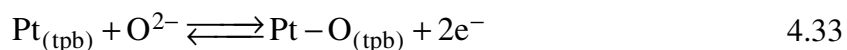
energy state. Consequently, more electrical activation energy is needed to reduce this stabilized species. Reduction of the stabilized oxygen appears at a lower potential value. This may explain why in the present system, the reduction peak of the third species is always lower than the reduction peaks of the two other species (Fig. 21).

4.3.1　The global model

In this section, the paths described throughout the chapter are brought together and presented as a global model. Based on this global picture, the key results presented in this chapter are interpreted. For clarity, the anodic and the cathodic cases are discussed separately.

The anodic case

When E_{WR} is switched from any given value to a higher value, the oxidation of O^{2-} into a Pt-O compound occurs simultaneously at both interfaces in contact with the electrolyte (Pt/YSZ and tpb). This corresponds to reactions 4.14 and 4.33.

$$Pt_{(Pt/YSZ)} + O^{2-} \rightleftharpoons Pt-O_{(Pt/YSZ)} + 2e^- \qquad 4.14$$

$$Pt_{(tpb)} + O^{2-} \rightleftharpoons Pt-O_{(tpb)} + 2e^- \qquad 4.33$$
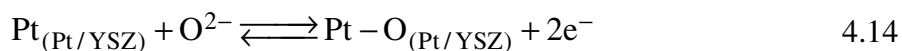
The corresponding anodic current is measured. As Pt-O accumulates at both the Pt/YSZ and the Pt/gas interfaces via paths 1 and 2 (see Fig. 32), the rate decreases with time. It is due to the decreasing amount of non-occupied Pt atoms at the ERS (the oxygen coverage θ_O increases). Consequently, the measured anodic current also decreases with time. This effect is seen in chronoamperometry (section 4.2.1) but also in the anodic region of the cyclic voltammograms (section 4.2.5).

The adsorbed oxygen species Pt-O formed according to path 2 may desorb into molecular oxygen O_2 and liberate Pt sites (path B). If the desorption step is not infinitely fast compared to the electrochemical step, the Pt-O species has a certain life span and may diffuse along the Pt/gas interface to a certain extent. Diffusion of chemisorbed oxygen originating from the YSZ due to totally or partially limiting desorption step has been

discussed in recent papers dealing with the electrochemical promotion of catalysis on the $O_{2(g)}$,Pt/YSZ system [60, 61].
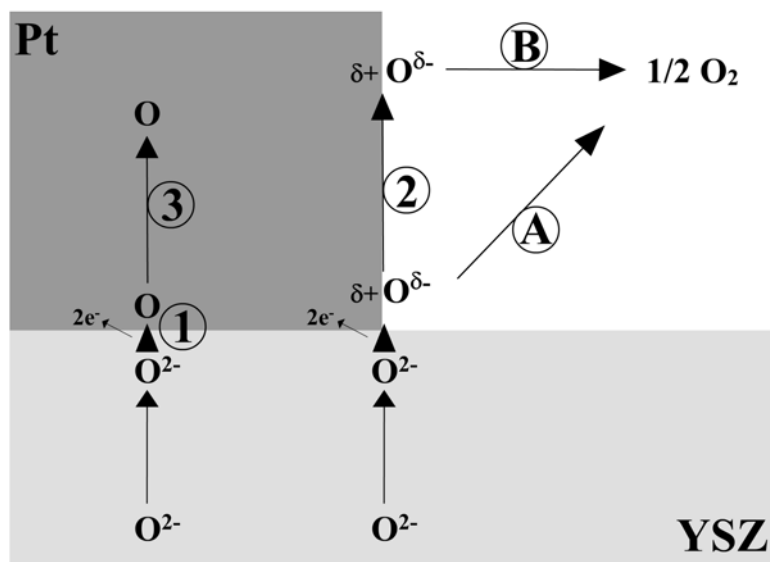
Fig. 32   Representation of the reaction paths during the application of an anodic polarization

Each desorbed Pt-O must be replaced. This is done through the process of electrochemical oxidation of O^{2-}, liberating two electrons (equation 4.33) and the corresponding anodic current is measured. After a certain anodic polarization time, when the Pt/gas interface near the tpb is already populated by a large amount of Pt-O species, the newly produced oxygen may have no other alternative than to desorb directly to the gas phase without diffusing on the Pt/gas interface (path A). In the field of electrochemical promotion of catalysis, this mechanism has been presented to interpret the catalytic rate transients appearing in the minutes after the onset of an anodic polarization [62].

Eventually, after a sufficient period under anodic potential, the amount of reactants and products at the electrochemical reaction sites reach stationary values. The rates of electrochemical formation and desorption of Pt-O species also become constant with time. Theoretically, an infinite amount of time would be necessary, but in fact, as shown in Fig. 6, five minutes are sufficient for the system to reach the apparent steady state. At this

point, the measured current corresponds mainly to path A and B, i.e. the oxygen evolution reaction.

However, under prolonged anodic polarization, due to the high oxygen coverage at the Pt/YSZ interface produced by path 1, oxygen atoms may enter the platinum lattice and diffuse in the metal sublayers (slow oxide growth). This corresponds to path 3. This process causes the extra charge Q_{extra} that are stored during the anodic holding time, including the steady state period (see section 4.2.3).

The penetration of oxygen into the metal is also believed to give rise to the peak current observed in chronoamperometry under high potential E_h application (Fig. 4). It is thought that the trigger for the penetration step is a critical amount of oxygen coverage on the platinum surface. This would explain why the peak is delayed to a few tens of seconds. The rate of this process may also depend on the amount of Pt-O species at the Pt/YSZ interface. This would explain the fact that the peak is only distinctly observed when high potentials E_h are applied.

The cathodic case

When the applied potential is switched to a lower value, the system aims to reach the new equilibrium conditions. Consequently, the reaction scheme (Fig. 33) is exactly opposite to the anodic case described above.

The measured cathodic current is the sum of the current contribution of all paths 1, 2, 3, A and B. In chronoamperometry, since the negative potential is applied at once, all processes occur simultaneously. It is therefore hard to distinguish the response of each process. However, if the negative potential is applied progressively, sweeping linearly with time, under certain experimental conditions, one may observe distinct cathodic peaks. This is due to differences in the reduction kinetics and the reduction potentials of the different reducible species.

Eventually, after a sufficient period under cathodic potential, a stationary current is measured. At this point, a vast majority of Pt-O species has been reduced and the measured current corresponds mainly to path A and B, i.e. the oxygen reduction reaction.
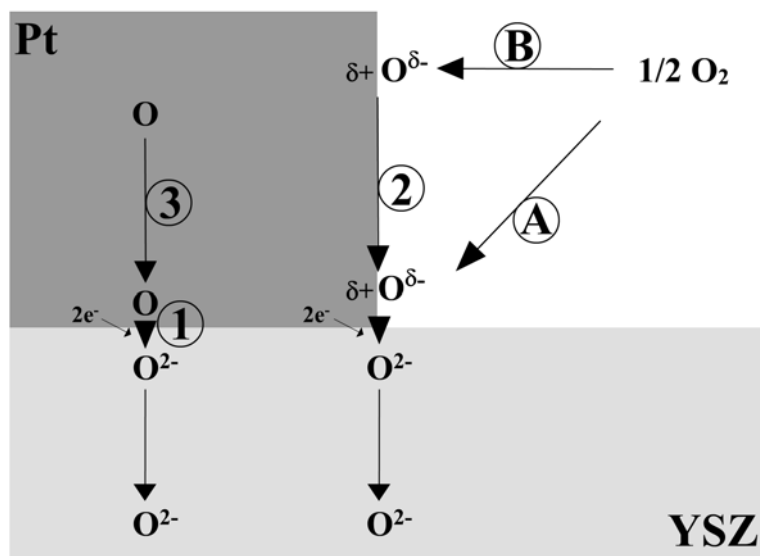
Fig. 33 Representation of the global reaction paths during the application of a cathodic polarization

The interaction between paths

The paths represented in Fig. 32 and Fig. 33 can be separated in two groups. The first group comprises the paths occurring without need to have access to the gas phase (path 1 and 3). The electron transfer occurs at the Pt/YSZ interface, and diffusion of oxygen proceeds into the platinum sublayers. The second group comprises the paths occurring with the need to have access to the gas phase (paths 2, A and B). The electron transfer occurs at the tpb. It is followed by diffusion along the Pt/gas interface and /or desorption into the gas phase under the form of molecular oxygen.

One may note that these two path groups may be dependent of each other. They may interfere. For instance, since the tpb is also part of the Pt/YSZ interface, the presence of an oxide layer at the Pt/YSZ interface may affect the mechanism and kinetics of the processes occurring at the tpb by changing the electronic properties of the metal surface and by imposing a barrier to charge transfer [12].

As shown in this chapter, the measured electrochemical response is almost always a superposition of the contribution of both groups. In order to measure the current of one specific group of path in particular, it is possible to prevent the other group from occurring. The two path groups are defined by the geometry of their electrochemical

reaction site (tpb or Pt/YSZ). Therefore, one way to favor one group over the other would be to prepare electrodes featuring very different ratios of ternary/binary interface sites. For instance, a non-porous compact electrode may tend to favor path 1 and 3, whereas an electrode featuring very tiny pores may favor path 2, A and B. In literature, the sintering temperature in the electrode preparation has been shown as a decisive factor to modify, at a small degree, the ternary/binary interface site ratio [30]. The great influence of the microstructure of the electrode on the electrochemical response has also been shown in chapter 3 of this work (Preliminary studies).

An alternative way to block some path is simply to limit the amount of reactant. In literature, decrease of the oxygen partial pressure in the reactor is often used to eliminate partially the background current due to the oxygen reduction reaction (A and B in Fig. 33). By doing so, one allows a better distinction of the cathodic peaks in cyclic voltammetry [30, 32, 63].

4.4   Conclusions

In this chapter, electrochemical measurements have been performed on a cermet O$_{2(g)}$,Pt/YSZ electrode prepared by screen printing. These measurements consist of chronoamperometry, chronocoulometry, chronopotentiometry, cyclic voltammetry, steady state polarization and impedance spectroscopy. The electrical response to these experiments could be separated into a time dependent and a steady state contribution. The results showed that the time dependent behavior of the electrode is dominated by pseudocapacitive processes. The charge storage occurs only under anodic conditions and is attributed to the production of various Pt-O species. Linear sweep voltammetry after prolonged anodic polarization allowed distinguishing three species responsible for the charge storage. Based on the effect of the polarization time on the stored charge, these three species were attributed to Pt-O species being stored at three different locations on the electrode:

1) the build-up of an oxygen monolayer layer at the Pt/YSZ interface,

2) the production of a Pt-O species at the tpb and its diffusion along the Pt/gas interface

3) the diffusion of oxygen from the Pt/YSZ interface toward the bulk of the platinum electrode.

4.5 References

1 A. J. Bard, L. R. Faulkner, Electrochemical Methods: Fundamentals and Applications (Wiley, New York, 1980)

2 H. D. Wiemhofer, Solid State Ionics 75 (1995) 167

3 W. Gopel, H. D. Wiemhofer, Ber. Bunsenges. Phys. Chem. 94 (1990) 981

4 Tsaofang Chao, K. J. Walsh, P. S. Fedkiw, Solid State Ionics 47 (1991) 277

5 S. P. Yoon, S. W. Nam, S.-G. Kim, S.-A. Hong, S.-H. Hyun, J. Power Sources 115 (2003) 27

6 A. Barbucci, R. Bozzo, G. Cerisola, P. Costamagna, Electrochim. Acta 47 (2002) 2183

7 L. Bay, T. Jacobsen, Solid State Ionics 93 (1997) 201

8 W.-F. Zhang, P. Schmidt-Zhang, U. Guth, Solid State Ionics 169 (2004) 121

9 S. N. Shkerin, Russ. J. Electrochem. 39 (2003) 863

10 M. G. H. M. Hendriks, B. A. Boukamp, J. E. ten Elshof, W. E. van Zyl, H. Verweij, Solid State Ionics 146 (2002) 123

11 T. Jacobsen, L. Bay, Electrochim. Acta 47 (2002) 2177

12 S. Sridhar, V. Stancovski, U. Pal, Solid State Ionics 100 (1997) 17

13 J. Nowotny, T. Bak, C. C. Sorrell, Adv. Appl. Ceram. 104 (2005) 214

14 R. Radhakrishnan, A. V. Virkar, S. C. Singhal, J. Electrochem. Soc. 152 (2005)

15 D. T. Dimitrov, C. D. Dushkin, Central European Journal of Chemistry 3 (2005) 605

16 J. W. Jian, B. C. Yang, Y. K. Zhang, Wuji Cailiao Xuebao/Journal of Inorganic Materials 19 (2004) 93

17 J. Poppe, A. Schaak, J. Janek, R. Imbihl, Berichte der Bunsen-Gesellschaft 102 (1998) 1019

18 E. J. L. Schouler, M. Kleitz, J. Electrochem. Soc. 134 (1987) 1045

19 T. H. Etsell, S. N. Flengas, J. Electrochem. Soc. 118 (1971) 1890

20 J. Mizusaki, K. Amano, S. Yamauchi, K. Fueki, Solid State Ionics 22 (1987) 313

21 J. Mizusaki, K. Amano, S. Yamauchi, K. Fueki, Solid State Ionics 22 (1987) 323

22 J. Sasaki, J. Mizusaki, S. Yamauchi, K. Fueki, Solid State Ionics 3-4 (1981) 531

23 A. Mitterdorfer, L. J. Gauckler, Solid State Ionics 120 (1999) 211

24 A. Mitterdorfer, L. J. Gauckler, Solid State Ionics 117 (1999) 187

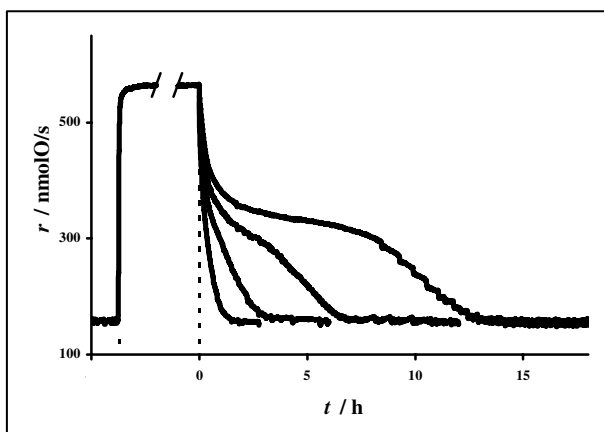25 A. Mitterdorfer, L. J. Gauckler, Solid State Ionics 117 (1999) 203

26   M. J. Verkerk, M. W. J. Hammink, A. J. Burggraaf, J. Electrochem. Soc. 130 (1983) 70

27   S. P. Yoon, S. W. Nam, J. Han, T.-H. Lim, S.-A. Hong, S.-H. Hyun, Solid State Ionics 166 (2004) 1

28   T. M. Gur, I. D. Raistrick, R. A. Huggins, J. Electrochem. Soc. 127 (1980) 2620

29   M. W. Breiter, K. Leeb, G. Fafilek, J. Electroanal. Chem. 434 (1997) 129

30   T. Kenjo, Y. Yamakoshi, K. Wada, J. Electrochem. Soc. 140 (1993) 2151

31   J. Yi, A. Kaloyannis, C. G. Vayenas, Electrochim. Acta 38 (1993) 2533

32   P. A. van Manen, R. Weewer, H. W. de Wit, J. Electrochem. Soc. 139 (1992) 1130

33   A. Jaccoud, G. Foti, C. Comninellis, Electrochim. Acta 51 (2006) 1264

34   C. G. Vayenas, S. Bebelis, C. Pliangos, S. Brosda, D. Tsiplakides, Electrochemical Activation of Catalysis: Promotion, Electrochemical Promotion, and Metal-Support Interactions (Kluwer Academic / Plenum Publishers, New York, 2001)

35   A. P. Markusse, B. F. M. Kuster, D. C. Koningsberger, G. B. Marin, Catal. Lett. 55 (1998) 141

36   L. R. Velho, R. W. Bartlett, Metallurgical Transactions 3 (1972) 65

37   J. Bockris, A. Reddy, Modern Electrochemistry (Plenum Press, New York, 1970)

38   C. Athanasiou, G. Karagiannakis, S. Zisekas, M. Stoukides, Solid State Ionics 136-137 (2000) 873

39   D. Y. Wang, A. S. Nowick, J. Electrochem. Soc. 126 (1979) 1155

40   B. A. van Hassel, B. A. Boukamp, A. J. Burggraaf, Solid State Ionics 48 (1991) 139

41   A. C. Co, S. J. Xia, V. I. Birss, J. Electrochem. Soc. 152 (2005) A570

42   B. A. Boukamp, Solid State Ionics 20 (1986) 31

43   N. L. Robertson, J. N. Michaels, J. Electrochem. Soc. 137 (1990) 129

44   D. Y. Wang, A. S. Nowick, J. Electrochem. Soc. 128 (1981) 55

45   O. J. Velle, T. Norby, P. Kofstad, Solid State Ionics 47 (1991) 161

46   C. R. Parkinson, M. Walker, C. F. McConville, Surf. Sci. 545 (2003) 19

47   R. Ducros, R. P. Merrill, Surf. Sci. 55 (1976) 227

48   C.-B. Wang, C.-T. Yeh, J. Catal. 178 (1998) 450

49   H. Niehus, G. Comsa, Surf. Sci. 93 (1980) L147

50   J. L. Gland, B. A. Sexton, G. B. Fisher, Surf. Sci. 95 (1980) 587

51   C.-B. Wang, H.-K. Lin, S.-N. Hsu, T.-H. Huang, H.-C. Chiu, J. Molec. Catal. A 188 (2002) 201

52   T. Matsushima, D. B. Almy, J. M. White, Surf. Sci. 67 (1977) 89

53   C.-P. Hwang, C.-T. Yeh, J. Catal. 182 (1999) 48

54   R. J. Berry, Surf. Sci. 76 (1978) 415

55   Y. K. Peng, P. T. Dawson, Can. J. Chem. 52 (1974) 3507

56   H. Angerstein - Kozlowska, B. E. Conway, W. B. A. Sharp, J. Electroanal. Chem. 43 (1973) 9

57   L. D. Burke, M. B. C. Roche, J. Electroanal. Chem. 137 (1982) 175

58   G. Jerkiewicz, G. Vatankhah, J. Lessard, M. P. Soriaga, Y.-S. Park, Electrochim. Acta 49 (2004) 1451

59   J. Lauterbach, K. Asakura, H. H. Rotermund, Surf. Sci. 313 (1994) 52

60   I. Riess, Solid State Ionics 176 (2005) 1667

61   J. Fleig, J. Jamnik, J. Electrochem. Soc. 152 (2005) E138

62   G. Foti, V. Stankovic, I. Bolzonella, C. Comninellis, J. Electroanal. Chem. 532 (2002) 191

63   G. Fafilek, K. Leeb, M. W. Breiter, Solid State Ionics 86-88 (1996) 1415

CHAPTER 5

The behavior of the $O_{2(g)}$,Pt/YSZ system in the presence of C_2H_4

This chapter concerns the catalytic activity of YSZ supported Pt films toward the oxidation of ethylene. In particular, the emphasis is put on the variation of the catalytic activity caused by the presence of various oxygen species at the Pt surface, in a constant gas composition. The presence of surface oxides is found to cause deactivation whereas anodically produced $O^{\delta-}$ species cause the destabilization the oxide and triggers the electrochemical promotion of catalysis (EPOC). In addition, original results present the very fascinating effect of long polarization times (up to 11 h) on the catalytic rate relaxation transients. Based on these results, on the literature on the EPOC and on the results presented in chapter 4 of this work, a model is proposed to interpret this effect. According to this model, anodic polarization produces $O^{\delta-}$ back-spillover species, promoting the catalytic activity, in agreement with the mechanism of EPOC. In parallel, the anodic polarization produces oxygen species, stored in the Pt phase via the Pt/YSZ interface. Hidden from the gas phase, this species do not directly alter the catalytic properties of the gas-exposed surface during polarization. However, when the polarization is switched off, this hidden oxygen species diffuses to the gas-exposed surface and promotes the catalyst, as back-spillover $O^{\delta-}$ does. The large amount of stored charge and its slow diffusion-controlled appearance causes the rate enhancement to last for hours.

5.1   Introduction

In preceding chapters, we discussed the electrochemical behavior of the $O_{2(g)}$,Pt/YSZ system in an atmosphere composed of O_2 and He. It has been shown that the application of an anodic potential E_h during a time period t_h caused a charge storage of pseudocapacitive type. The charge was suggested to be stored in the form of Pt-O species at various interfaces of the system. Then by sweeping the potential linearly toward negative values, these species were reduced, giving rise to cathodic current peaks. It was shown that the storage of great amounts of charge was characterized by long time (hours) and followed a $t_h^{1/2}$ kinetic law, suggesting a diffusion controlled process.

In this chapter, we will discuss the influence of adding ethylene to the supplied gas mixture. Platinum is known to be a very good catalyst for the oxidation of hydrocarbons in presence of oxygen.

In presence of a $O_2 + C_2H_4$ gas mixture, the $O_{2(g)}$,Pt/YSZ system is expected to present a significant catalytic activity, leading to the production of CO_2 and H_2O.

$$C_2H_4 + 3O_2 \longrightarrow 2CO_2 + 2H_2O \qquad\qquad 5.1$$

Since the Pt film is deposited on YSZ solid electrolyte, it acts as a catalyst, but also as an electrode for the reaction involving the O_2/O^{2-} couple. On the $O_{2(g)}$,Pt/YSZ system, due to this dual catalyst-electrode function of the Pt film, the chemical (catalytic hydrocarbon oxidation) and electrochemical (O_2/O^{2-} couple) reactions are known to depend of each other. In particular, it is known that the catalytic activity of the catalyst film can be greatly altered by applying an electrical polarization with respect to the reference electrode. The phenomenon is known as the electrochemical promotion of catalysis (EPOC). Its phenomenology and mechanism have been presented in chapter 2.

This chapter focuses on the phenomenon of EPOC on the $O_{2(g)}$,Pt/YSZ system and, in general terms, on the influence of polarization application on its catalytic activity.

5.2   Experimental

A 1μm thick Pt film was deposited onto a 10 x 15 x 1 mm YSZ 8%mol pellet (Technox 802, Dynamic Ceramic Ltd) by magnetron sputtering in inert atmosphere at room temperature using the same technique as described in chapter 3. The film size was

7 x 5 mm giving a geometric surface of 0.35 cm^2. Gold counter and reference electrodes have been deposited on the reverse side of the pellet by thermal decomposition of a low-temperature electronic gold paste (Gwent Electronic Materials Ltd. C70219R4) at 550°C. The working and counter electrodes were located in a symmetrical face-to-face arrangement on the opposite sides of the YSZ pellet (Fig. 1). The electrochemical cell was heat treated at 700°C in air environment for 2 days, in to order to avoid sintering effects during the experiments.

The reactor used for catalytic rate measurements is described in chapter 3. The whole reactor assembly was put in a furnace (Horst, XVA271) equipped with a heat control system (Horst, RD4456) enabled temperature programmed experiments carried out with a heating/cooling rate of 35°C/h. The temperature was measured with a K-type (NiCr-Ni) thermocouple placed in proximity of the center of the catalyst surface. Reactants were Carbagas certified standards of C_2H_4 and O_2, both of 99.95% purity, supplied as 1 and 20% mixtures in He (99.996%), respectively.

Kinetic experiments were carried out in the temperature range of 350-600°C under a constant continuous gas flow rate of 200 ml min^{-1} STP. Feed composition and flow rate were adjusted and controlled by a mass control system (Bronkhorst, F/201C and E-5514-FA) while the reactor was operated at atmospheric pressure. The CO_2 production of the catalytic oxidation of ethylene at the outlet of the reactor was on-line monitored using an IR analyzer (Horiba PIR 2000). Electrochemical promotion experiments were realized in potentiostatic mode of operation of a galvanostat-potentiostat (EG&G PAR Model 362).
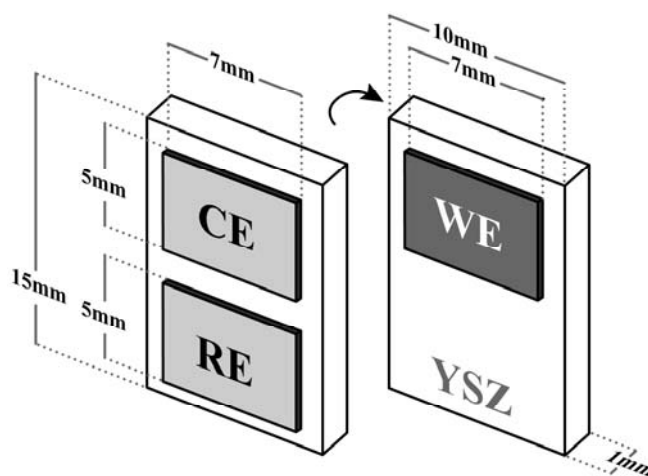

Fig. 1   Location and dimensions of the electrodes on the YSZ pellet. The working electrode is made of sputtered platinum. Counter and reference electrodes are made of gold.

Linear potential scan voltammetry measurements were made using a scanning potentiostat (*Autolab, Model PGSTAT30, Eco Chemie*).

The XPS (X-ray photoelectron spectroscopy) spectra presented in this work have been performed at room temperature in UHV after various treatments. The CasaXPS software was used to deconvolute the spectra. The binding energy scales of the graphs were fixed at 285 eV with respect to the C 1s carbon peak. The Pt 4f 7/2 and Pt 4f 5/2 binding energies of the surface oxidation states of platinum were drawn from Bancroft et al. [1].

5.3 Results

5.3.1 Catalytic activity measurements

Temperature cycling

Fig. 2 shows the temperature dependence of the open circuit catalytic rate of ethylene oxidation in a fixed gas composition ($pO_2 = 1$ kPa, $pC_2H_4 = 0.25$ kPa), a volumetric flow rate of 200ml/min STP and a temperature scan rate of 35°C/h. The catalytic activity r is given in terms of moles of oxygen atoms involved in the catalytic oxidation of ethylene (eq. 5.1). The initial state, prior to temperature cycling, is the open circuit steady state activity of the catalyst at 350°C. One observes that during cycling, the variation of the ethylene oxidation rate with temperature following the forward run (from 350°C to 600°C) is different in nature from that corresponding to the reverse scan (from 600°C to 350°C) and thus many distinguishing features can be derived from this figure.

During the forward scan, increasing the temperature from 350 to 470°C, the reaction rate increases slightly to a maximum value ($r = 275$ nmolO/s at 470°C). Then, an abrupt decrease begins resulting in a 35% loss of activity up to 540°C where a plateau extending to 560°C is reached. In the domain between 490 and 560°C rate oscillatory behavior is observed while above 560°C the reaction rate decreases again without exhibiting oscillations. Finally, the temperature reaches 600°C where the reaction rate is at the 53% of the initial value measured at 350°C.

The reverse scan starts as soon as the upper temperature limit is reached (600°C). From 600 to 580°C the reaction rate continues to decrease approximately down to one third of the initial value, while in the domain between 580 and 520°C it remains fairly constant. It then starts increasing slowly to reach a local maximum value at 410°C. It is worth pointing out the oscillatory behavior occurring in the same temperature range as during the

forward scan (580 - 470°C). When cooling down the reactor below 410°C the reaction rate decreases again and reaches its final value at 350°C, which is equal to 45% of the initial reaction rate at the same temperature.

The described heating cycle exhibits a strong hysteresis of the reaction rate and causes the deactivation of the Pt catalyst. Two states are distinguished, one "active" and another "deactivated". The former exhibits an activity roughly twice as high as that of the latter up to about 500°C.
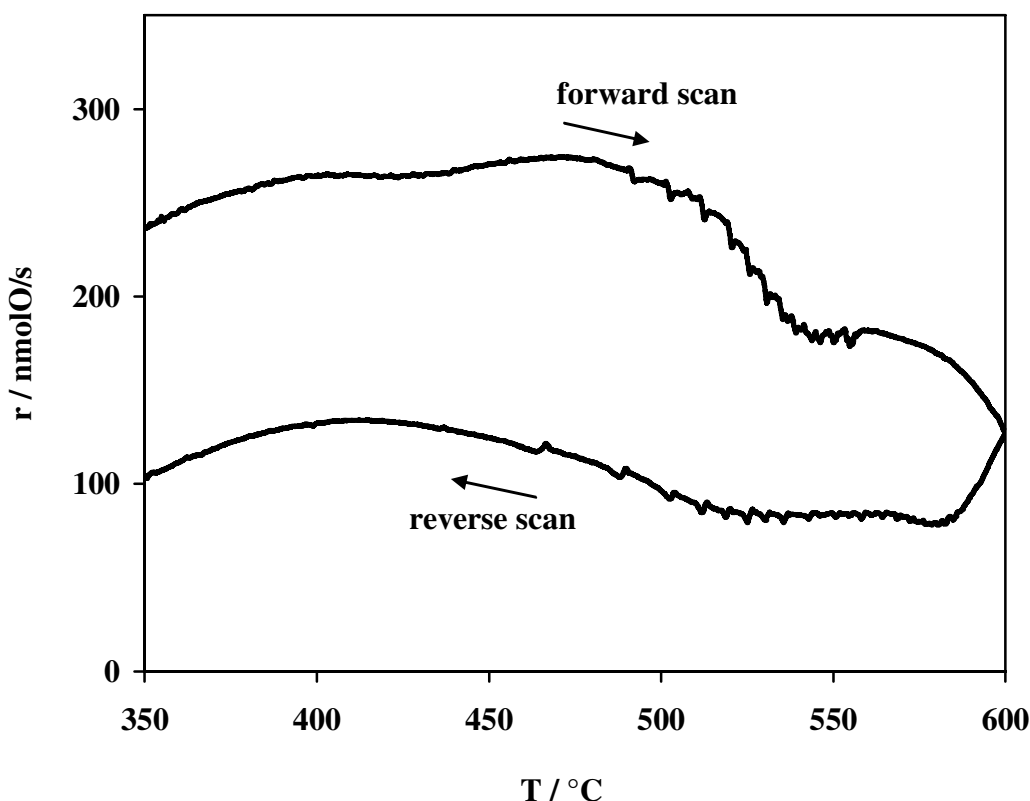
Fig. 2   Catalyst deactivation by transient heating cycle in open circuit conditions. Temperature scan rate = 35°C/h. $pC_2H_4 = 0.25$ kPa, $pO_2 = 1$ kPa.

Deactivation and activation procedures

Based on the curves shown in Fig. 2, protocols were established to obtain two well-defined reproducible limiting cases of platinum catalyst activity at the temperature of the following experiments (525°C). The deactivated state is obtained by a two-hour 600°C treatment in the same oxidizing gas mixture as in Fig. 2. The catalytic activity behavior during the deactivation procedure is shown in Fig. 3. By increasing the temperature from 525°C up to 600°C the rate marginally increases (+10 nmolO/s) before decreasing

dramatically to 8.3 nmolO/s. When the temperature is set back to 525°C the rate further decreases to 1 nmolO/s and a rather stable deactivated state is considered. However, in the given conditions of temperature and feed gas composition, the catalytic activity returns to its initial value following a very slow transient. This is depicted in Fig. 4 where catalytic rate is shown as a function of time. One observes an apparent incubation period of roughly 15 hours before the reactivation truly begins (catalyst self-activation). The symbol $r_0 (\infty)$ is used to represent the open circuit reaction rate in terms of consumed oxygen atoms under open circuit conditions at infinite time (steady state activity) and corresponds to the self-activated catalytic activity.
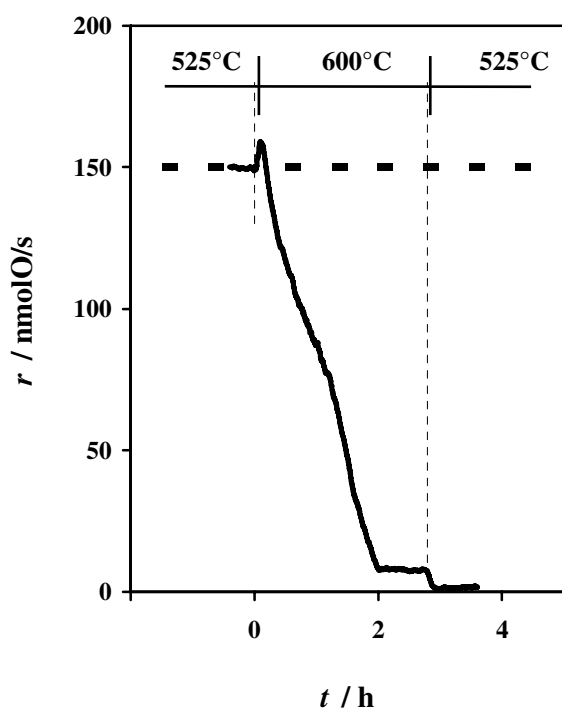

Fig. 3   Catalytic rate behavior during the deactivation procedure. $pC_2H_4 = 0.25$ kPa, $pO_2 = 1$ kPa at open circuit.
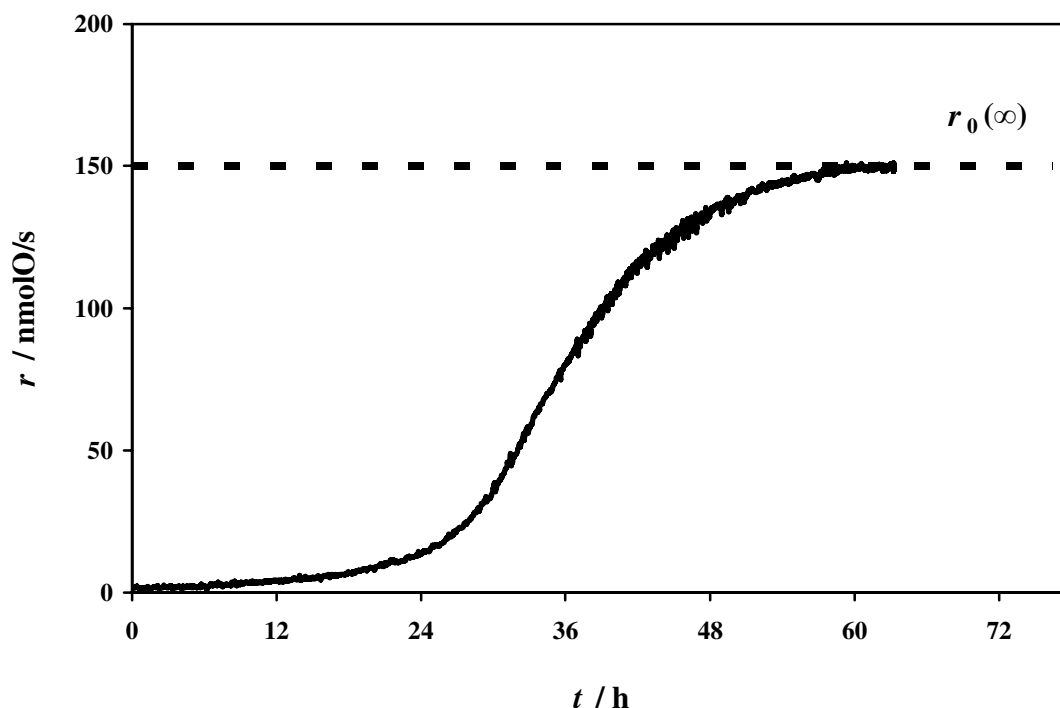
Fig. 4   Catalytic rate behavior during the spontaneous reactivation at $T = 525°C$. $pC_2H_4 = 0.25$ kPa, $pO_2 = 1$ kPa at open circuit.

Electrochemically induced reactivation

Starting from the metastable deactivated state reached following the protocol described above (Fig. 3), a series of polarization pulses are applied. Every polarization pulse lasts 30 minutes ($t_{pol} = 30$ min) at an applied potential of $E_{WR} = 400$ mV with respect to the gold reference electrode. The resulting current passing through the cell during the polarization periods is $I = 0.5$ mA. Fig. 5 shows the measured ethylene oxidation rate in function of time when polarization pulses are applied. Application of the first polarization pulse to the catalyst in its deactivated state provokes a dramatic activity increase, tending to a plateau after a few tens of minutes. When the polarization is switched off, the rate drops rapidly and tends to an intermediate activity between the deactivated (< 10 nmolO/s) and activated (150 nmolO/s) states. There is a four-fold permanent enhancement due to the first polarization pulse ($\gamma = 4$). Application of a subsequent 30 minute polarization has a similar effect on the catalytic rate and a yet higher permanent open circuit activity is reached ($\gamma = 2$). Application of a third pulse increases the open circuit activity further and the latter tends to the rate after spontaneous reactivation ($r_0 (\infty) = 150$ nmolO/s) as seen above in Fig. 4. Λ, ρ and γ values for each polarization pulse are shown in Fig. 5. The apparent Faradaic efficiency Λ decreases only slightly with increasing pulse number. This is due to

rather similar Δr values and a constant current (I = 0.5 mA) during the pulses. The rate enhancement factor ρ is rather important (ρ = 35) during the first pulse but drops to much lower values in the subsequent pulses. The very low catalytic rate r_0 in the deactivated state prior to the first pulse explains such values. This also explains the variation of the γ value with increasing pulse number.
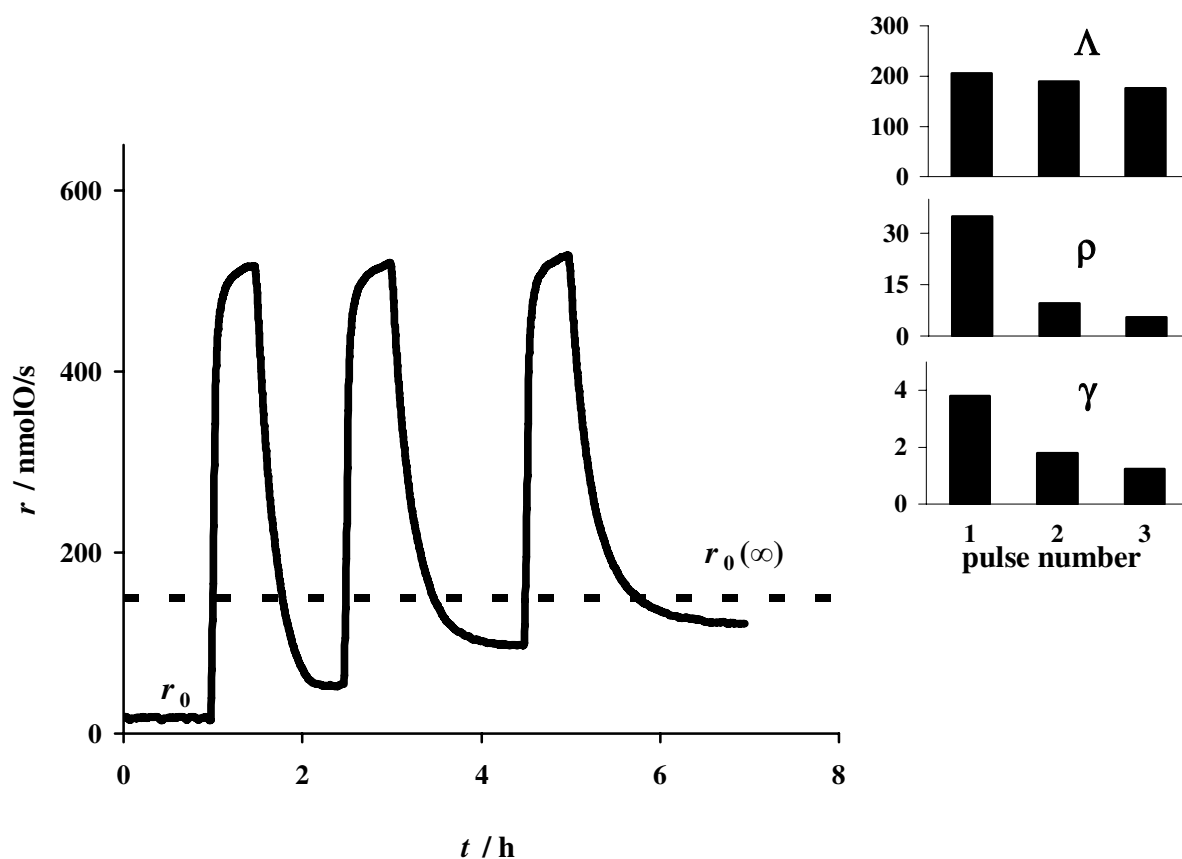
Fig. 5   Electrochemically assisted reactivation by successive 30 min polarization pulses (E_{WR} = 400 mV). Variation of EPOC Λ, ρ and γ with the pulse number. T = 525°C, pC_2H_4 = 0.25 kPa, pO_2 = 1 kPa.

Effect of the polarization time t_{pol}

The effect of the polarization time t_{pol} on the transient promotion experiments of the Pt catalyst in its open-circuit reactivated state ($r_0(\infty)$) by imposing an anodic potential at 525°C is depicted in Fig. 6. Initially the catalyst is under open circuit conditions and the unpromoted rate is $r_0 = r_0(\infty)$ = 150 nmolO/s. Once a catalyst potential E_{WR}=+400 mV is applied, the rate immediately starts increasing. The time needed for the catalytic rate to reach its new electropromoted steady state value (r = 560 nmolO/s) is approximately

1 hour. The rate enhancement ratio is $\rho = 3.5$ and the Faradaic efficiency is $\Lambda = 160$. Once the steady state rate is reached, it remains constant during the entire polarization period. The remarkable effect of the polarization time t_{pol} is only observed when the circuit is opened ($t = 0$ in Fig. 6). Indeed, the shape of the relaxation transient depends greatly on t_{pol}. For short polarization time, $t_{pol} = 1$ h, the rate drops abruptly and reaches the initial value $r_0 = 150$ nmolO/s) already 1.8 h after current interruption. In contrast, by increasing the polarization time, a longer time period is required to attain the initial rate, i.e. for $t_{pol} = 11$ h the rate transient is much longer and a relaxation time of 13 h is necessary for the catalytic rate to return to its initial value.
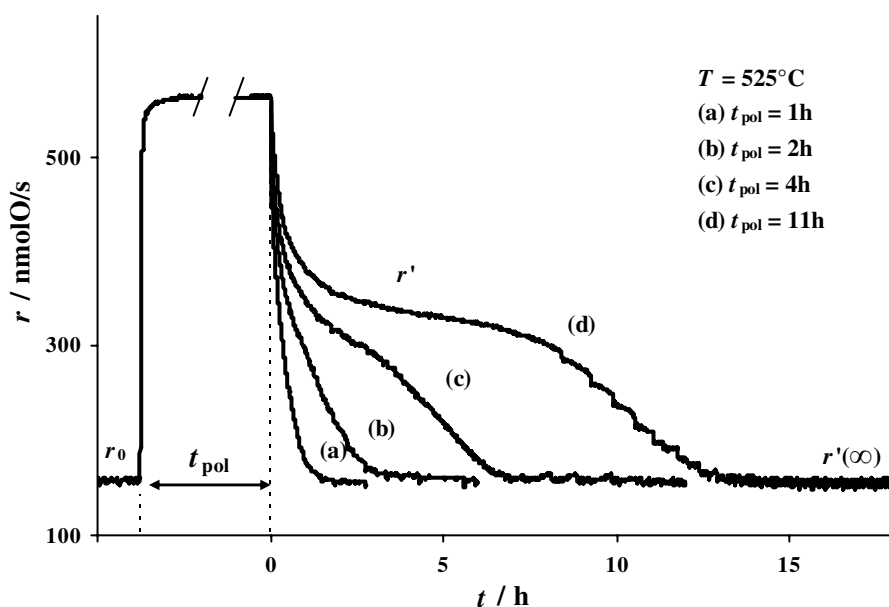
Fig. 6   Effect of the polarization time t_{pol} on the rate transient of EPOC. $E_{WR} = +400$ mV, $T = 525°C$, $pC_2H_4 = 0.25$ kPa, $pO_2 = 1$ kPa.

The effect of t_{pol} on the EPOC transient experiments at 600°C in the same feed gas composition ($O_2/C_2H_4 = 4$) is shown in Fig. 7. Increasing the temperature from 525°C to 600°C has a great impact on the reaction kinetics. Initially, the unpromoted rate r_0 at 600°C is much lower (10 nmolO/s) than at 525°C (150 nmolO/s) due to the deactivation process presented in Fig. 3. Application of catalyst potential $E_{WR} = +400$ mV causes the catalytic rate to increase dramatically and reach rapidly its steady state value ($r = 360$ nmolO/s). The rate enhancement ratio is $\rho = 24$ while the Faradaic efficiency is $\Lambda = 40$. During the entire polarization time, the rate remains practically constant. At low

polarization time (t_{pol} = 1 h), by current interruption, the rate drops very rapidly and the catalytic rate returns to its initial value r_0, indicating a totally reversible promotion as in the experiment at 525°C. Increasing the polarization time causes temporary increases in the apparent catalytic activity. Consequently, longer times are required to attain the initial rate r_0 and for t_{pol} = 11 h a relaxation time of 6.5 h is required for the rate to return to its initial value. Thus, similarly to the case of 525°C, t_{pol} does not affect the electro-promoted steady state rate, but it has a great influence on the relaxation transient once the circuit is opened. This is an intriguing element to comprehend the effects of long anodic polarization.

It is interesting to note that after very long polarization times ($t_{pol} \geq 4$ h), shortly after the current interruption ($t = 0$), the rate drops very rapidly to about $r = 50$ nmolO/s before increasing back up to a maximum value $r = 128$ nmolO/s (for $t_{pol} = 11$ h) (see arrow in Fig. 7). Later, it goes back to its final rate r' (∞), similar to the initial rate r_0.
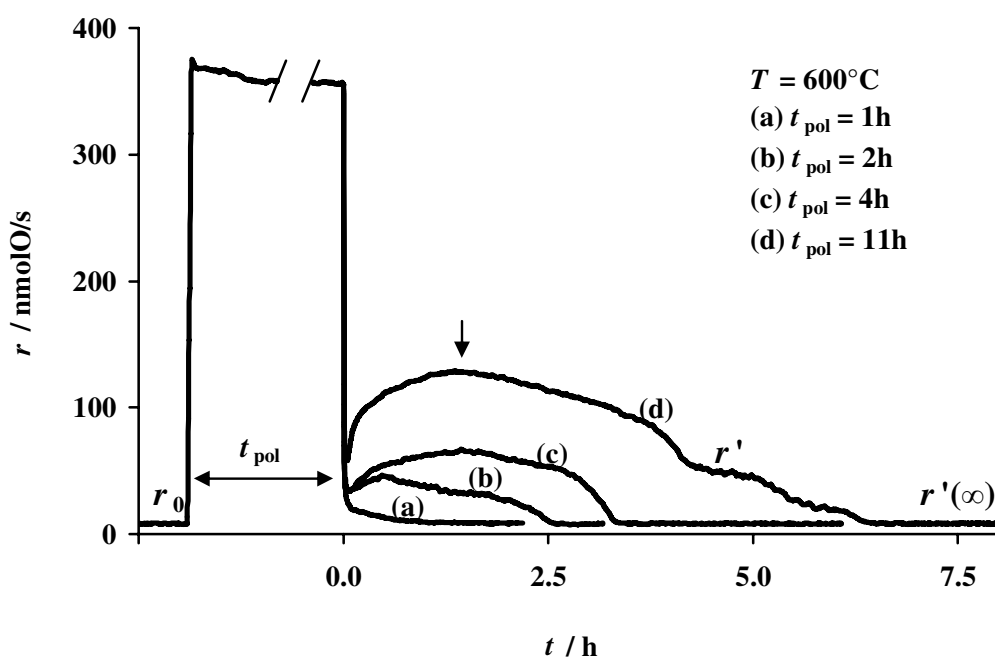
Fig. 7   Effect of the polarization time t_{pol} on the EPOC. E_{WR} = +400 mV, T = 600°C, pC_2H_4 = 0.25 kPa, $pO2$ = 1 kPa. The arrow represents the maximum open circuit activity in the given conditions.

5.3.2 Linear sweep voltammetry measurements

The linear sweep voltammetry method, described in chapter 4 and used to evidence the storage of Pt-O species, has been performed in the same ethylene containing gas mixture as the catalytic activity measurements presented above ($O_2/C_2H_4 = 4$). Fig. 8 shows the influence of the anodic potential holding time t_h on the shape of the first cathodic potential scan. The main feature of these curves is the cathodic peak, growing with increasing t_h values. It is not possible to observe distinctly separated peaks. However, a first wave is seen around $E_{WR} = -0,2$ V whereas the potential of the main peak shifts from -0,4 V to -0,6 V as t_h increases.
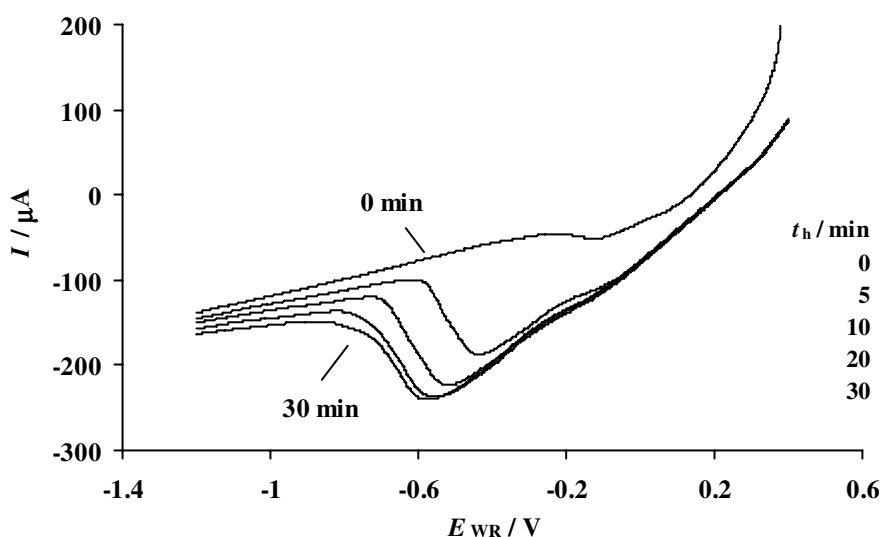
Fig. 8 Voltammogram of the $O_{2\ (g)}$,Pt/YSZ system in presence of ethylene. Effect of the anodic holding time, t_h, at the holding potential $E_h = 400$ mV, on the first cathodic scan. $T = 450°C$, $pO_2 = 1$ kPa, $pC_2H_4 = 250$ Pa, $v = 10$ mV/s.

By integrating the charge contained in the cathodic peak, one can deduce the corresponding amount of oxygen atoms involved in the charge storage (assuming two electrons per oxygen atom). Fig. 9 represents the amount of oxygen atoms per electrode geometric surface unit N_O for increasing $t_h^{1/2}$ values. One notices that there is a linear relation between the amount of stored oxygen and the square root of the holding time $t_h^{1/2}$.
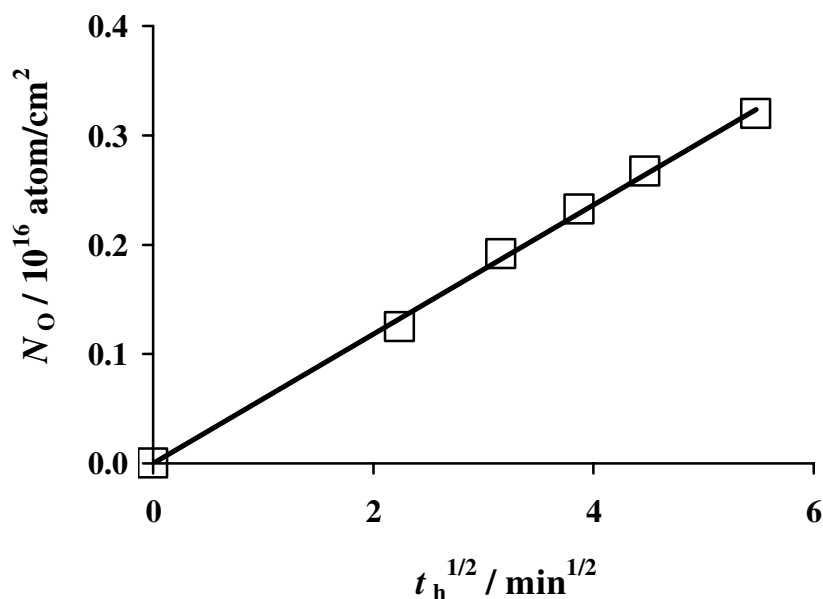
Fig. 9   Plot of the charge involved in the cathodic peak in Fig. 8, expressed in terms of equivalent amount of oxygen atoms, N_O, as a function of the square root of holding time, $t_h^{1/2}$, at $E_h = 400$ mV.

5.3.3   XPS measurements

X-ray photoelectron spectroscopy measurements have been performed on the Pt film in its as-sputtered state and after various treatments (sample 1 to 7 in Table 1). Fig. 10 shows the survey spectrum of the as-sputtered platinum film on the YSZ pellet. The highest peak, found around 70-80 eV corresponds to platinum 4f. The platinum 4d peaks are found around 330 eV. The peak of carbon is fixed at 285 eV and the peak of oxygen is found around 530 eV. The deconvolution of the Pt 4f spectrum, using binding energy values given by Bancroft et al.[1], allows determining of the relative percentage of each Pt oxidation state at the film surface and in the first layers. As an example, the specific 4f spectrum of sample 4 and its deconvolution is shown in Fig. 11. In Fig. 12, the deconvolution of all 7 samples are shown. The sample numbers, treatments, and corresponding relative oxidation states are summarized in Table 1. As expected, mainly metallic platinum (88 %) is found on the as-sputtered Pt film (sample 1). When heating the as-sputtered platinum film at 600 °C for 8 hours in air without polarization (open circuit), the 4f peaks appear at higher energies (sample 2). Spectrum deconvolution indicates that after such a treatment, the surface is totally oxidized, mainly in the PtO state (79 %). Applying a $E_{WR} = -1$ V polarization (with respect to the gold reference electrode

in air) during the 600°C treatment in air also leads to an oxidized surface, mainly in the PtO state (sample 3). However, the application of a $E_{WR} = +1$ V polarization during the 600 °C treatment in air (sample 4) seems to destabilize the surface oxide and leads to a surface composed of 66 % metallic Pt (see Fig. 11). However, this treatment does not eliminate all oxides and there is still a significant amount of PtO (24%) and even PtO_2 (10%).
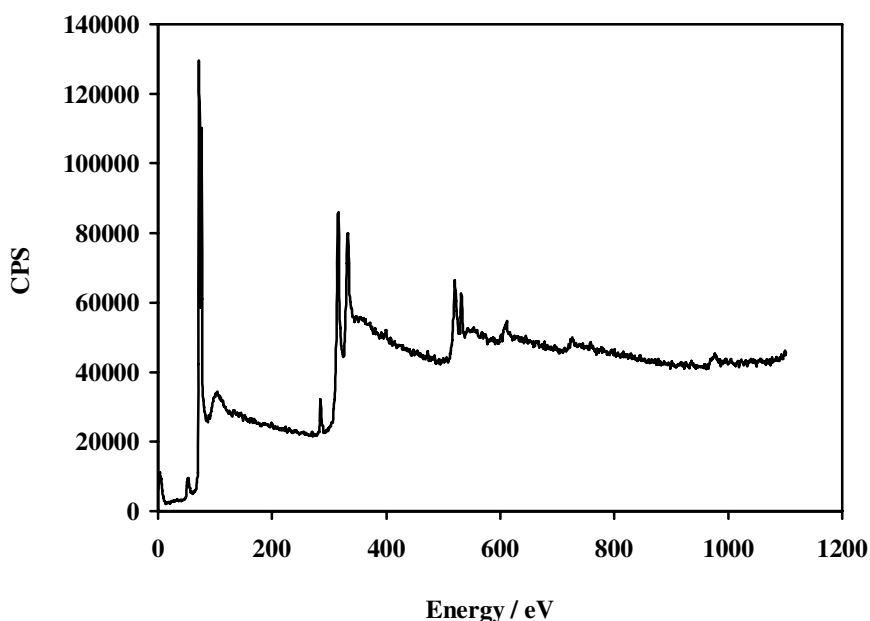
Fig. 10   XPS spectrum of sample 1 : as-sputtered platinum (thickness : 1 μm) on YSZ

XPS analysis has also been performed on the Pt film after a 72-hour deactivation treatment at 600°C in the same reactive gas mixture as the catalytic activity measurements shown above (250 Pa C_2H_4 + 1 kPa O_2 in He). This treatment (sample 5) corresponds to the deactivating procedure shown in Fig. 3, carried on during 72 hours. Deconvolution indicates that the surface is totally oxidized, mainly in the PtO state (91%). By letting this sample at 525°C in the same reactive gas mixture, spontaneous activity recovery is observed (as shown in Fig. 4). Prolonging this treatment for another 72 hours leads to a surface composed of 89% metallic and 11% oxidized Pt (sample 6). It has been shown in Fig. 5 that a $E_{WR} = 0,4$ V polarization could enhance the reactivation at 525°C. If this polarization is kept for 12 hours (sample 7), the resulting Pt surface is found to be mostly metallic (93%).
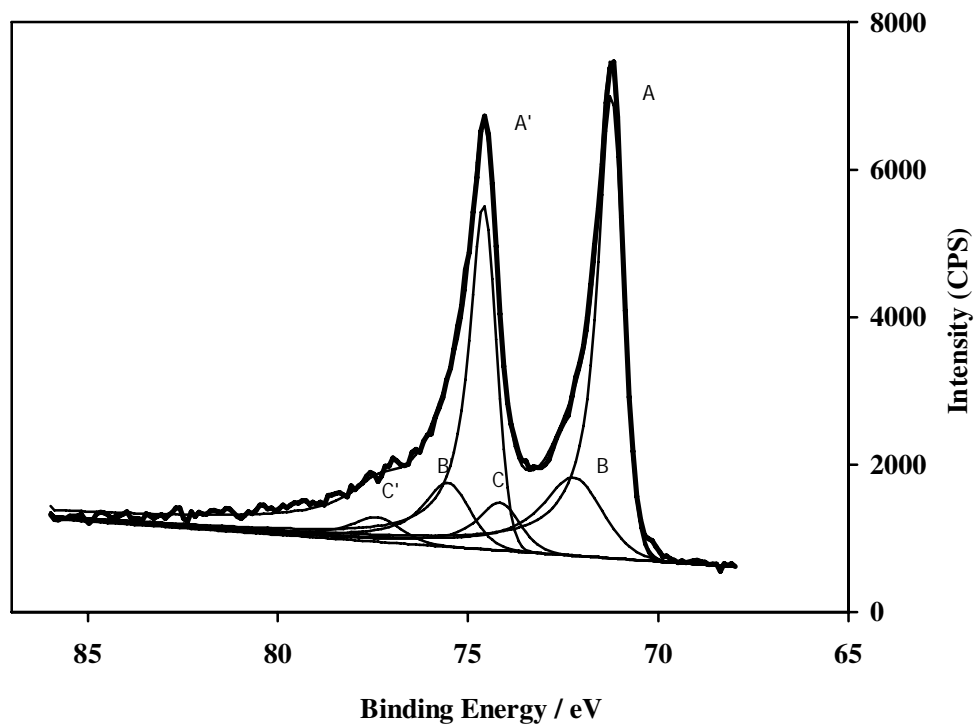
Fig. 11   XPS spectrum of sample 4. Treatment: 8 hours at 600°C in air under a $E_{WR} = +1V$ polarization. The (A A') doublet corresponds to metallic Pt, (B B') corresponds to PtO and (C C') corresponds to PtO_2.

Table 1   Surface oxidation state determined by deconvolution of the XPS spectra for different treatment. "reactive mixture" refers to 250 Pa C_2H_4 + 1 kPa O_2 in He.

Sample Nr. and treatment	Pt	PtO	PtO$_2$	Summary
1. As-sputtered Pt (1 μm thick)	88 %	12%	0%	Mainly metallic
2. 8 hours at 600 °C in air. Open circuit	0%	79%	21%	Totally oxidized, mainly PtO
3. 8 hours at 600 °C in air. E_{WR} = -1 V	0%	92%	8%	Totally oxidized, mainly PtO
4. 8 hours at 600 °C in air. E_{WR} = +1 V	66%	24%	10%	Mainly metallic, but also highly oxidized species
5. 72 hours at 600 °C in reactive mixture (deactivation)	0%	91%	9%	Totally oxidized, mainly PtO
6. 72 hours at 525 °C in reactive mixture (spontaneous activity recovery)	89%	11%	0%	Mainly metallic
7. 12 hours at 525 °C in reactive mixture under polarization at E_{WR} = +0.4 V (assisted activity recovery)	93%	7%	0%	Mainly metallic
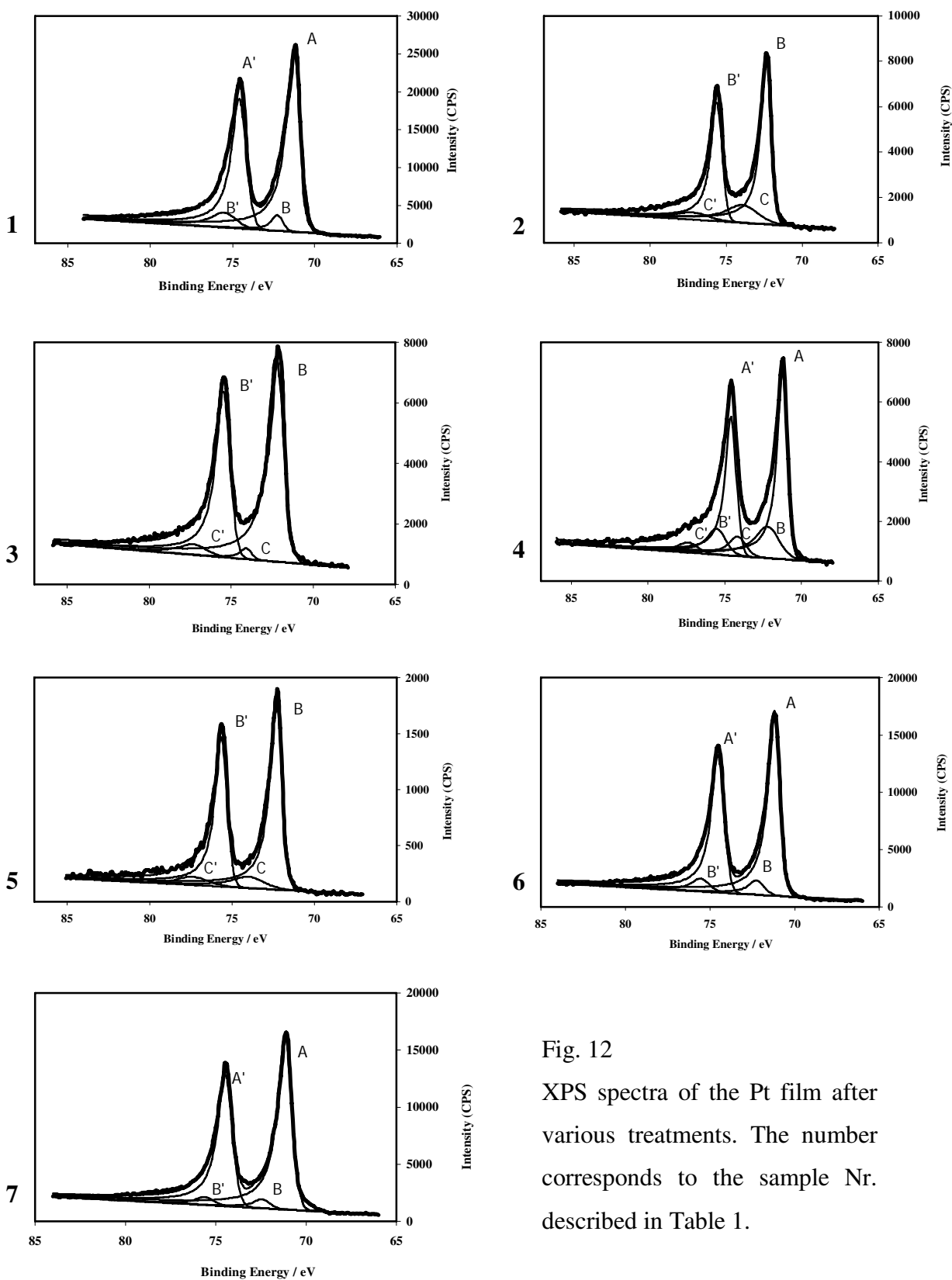
Fig. 12

XPS spectra of the Pt film after various treatments. The number corresponds to the sample Nr. described in Table 1.

5.4   Discussion

5.4.1   Open circuit measurements

Catalyst deactivation and reactivation

As illustrated in Fig. 2 and Fig. 3, high temperature treatment ($T > 525°C$) causes a dramatic deactivation of the catalyst in the given gas mixture ($O_2/C_2H_4 = 4$). Two possible causes are invoked to interpret this behavior. The first possible cause is the deposition of poisoning non-reactive carbon species (coke formation). This cause for the deactivation can however be ruled out for the following reasons. First, XPS surface analysis showed no significant carbon enrichment on Pt films in the deactivated state compared to the active state. Moreover, in literature, on silica supported Pt [2] and Pt foils [3, 4], it was reported that coke formation occurred only in the fuel rich domain ($O_2/C_2H_4 < 3$).

The other possible cause for the reported catalyst deactivation is the formation of platinum surface oxide species. Indeed, heating the YSZ supported Pt film in the slightly oxidizing gas feed ($O_2/C_2H_4 = 4$) may trigger the surface oxidation of Pt and, consequently, the drop of the catalytic activity. To support this suggestion, XPS measurements (Fig. 12 and Table 1) show that the deactivated Pt film, after the 600 °C heat treatment (shown in Fig. 3), features mainly platinum in the PtO state (sample 5). Note that an open circuit 600°C treatment in air also leads to an oxidized surface state (sample 2).

From a thermodynamic point of view, the formation of surface platinum oxide in these experimental conditions is possible. Indeed, as presented in chapter 2, the stability domain of surface Pt oxides has been determined experimentally by Vayenas et al. [5] for the identical reaction on a similar system, i.e. kinetic measurements of the catalytic oxidation of ethylene on YSZ supported Pt film. The given stability domain of surface Pt oxide is shown in Fig. 13. The black circles (a, b and c) represent the treatments preformed in the present work (temperature and gas mixture). They are all located in the oxide domain, but very close to the stability limit.

The Pt film preparation and the presence of YSZ may also have a significant influence on the stability domain of surface Pt oxide. The influence of the support is highlighted by Vayenas et al. [5], showing that the oxide stability domain of YSZ supported Pt films is extended to higher temperature compared to unsupported Pt wires. This could explain why the 600°C deactivation as evidenced in Fig. 3 has only been observed on YSZ supported Pt but not on Pt wires and Pt foils.
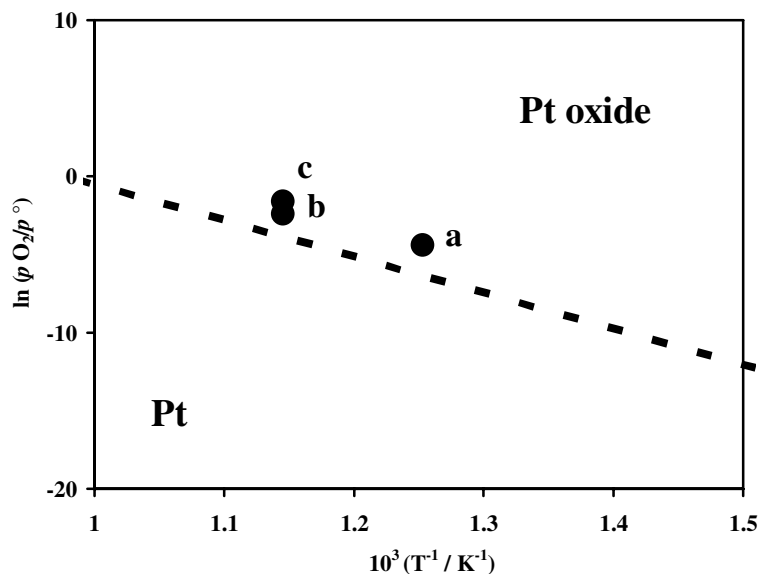
Fig. 13: Surface oxide stability domain of a platinum film deposited on YSZ [5]. The treatments mentioned in this work are represented by the circles (a) : 525°C in the reactive mixture, (b) : 600°C in the reactive mixture, (c) : 600°C in air. $p° = 100kPa$.

The catalytic rate oscillations observed in Fig. 2, Fig. 4 and Fig. 6 also supports the suggestion of the deactivation being caused by the oxide formation. Indeed, such oscillations are usually encountered in the transition region between two states, characterized by high and low rate. In particular, heterogeneous catalytic rate oscillations have often been found to occur near the surface oxide stability limit [5-13].

The very slow spontaneous reactivation transient shown in Fig. 4 indicates that, at 525°C in the given reactive gas, the deactivated state is metastable. Indeed, at infinite time, the catalytic open circuit rate is the same as before the deactivation (see Fig. 3), i.e. $r_0(\infty) = 150$ nmolO/s. XPS measurements after reactivation indicate that most of the surface is composed of metallic Pt (sample 6 in Fig. 12 and Table 1), confirming that oxidation causes the deactivation. The fact that the spontaneous reactivation takes days to reach a steady state indicates that the oxide formation/dissociation kinetics is very slow at this low temperature.

To summarize the catalytic measurements performed at open circuit in a constant gas mixture ($O_2/C_2H_4 = 4$), one could say that the observed catalytic activity bistability is caused by the influence of two opposing processes. One process is the oxidation of the

film surface, leading to deactivation. The other process is the reduction, leading to an active state. For the same gas composition, temperature is the key factor influencing which process takes the advantage. At 525°C, the very slow reactivation (Fig. 4) shows that the activating process slightly predominates over the opposed process (deactivation). The rate oscillations occurring at this temperature indicate that the opposed process is in competition. At 600°C however, the deactivating process has the total advantage. This is indicated by a very fast deactivation (Fig. 3) and no oscillations.

5.4.2 Closed circuit measurements

Electrochemically induced reactivation

The electrochemically induced reactivation experiment (Fig. 5) shows that the catalyst can be brought from its metastable deactivated state to its active state by the application of anodic polarization pulses. Indeed, by applying pulses, the steady state activity $r_0(\infty)$ can be reached within roughly 10 h instead of 72 h, in the case of spontaneous open circuit reactivation (Fig. 4).

It is shown in Fig. 5 that when polarization is applied, the rate increases as habitually observed in experiments of electrochemical promotion of catalysis (EPOC) [14-20]. The Λ values in the order of 200 (Fig. 5) indicates that the promotion is Non-Faradaic ($\Lambda > 1$) and the γ values greater than 1 show that there is permanent promotion (Fig. 5). As the pulse number increases, the open circuit steady state rate tends to $r_0(\infty) = 150$ nmolO/s and, consequently, γ tends to 1. Based on these observations, we expect the electrochemical promotion of the catalyst to be completely reversible (no permanent effect) if the initial rate is $r_0 = r_0(\infty)$.

This prediction is verified in Fig. 6, where, independently of the polarization duration t_{pol}, the long-term catalytic activity after current interruption goes back to the initial rate $r_0 = r'(\infty) = 150$ nmolO/s.

According to the sacrificial promoter mechanism of electrochemical promotion [20, 21], reviewed in chapter 2 of this work, anodic polarization produces $O^{\delta-}$ species via the reaction

$$O^{2-}(YSZ) \rightarrow [O^{\delta-}\text{-}\delta+]_{(Pt)}+2e^- \qquad 5.2$$
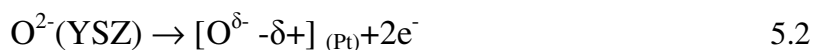
The species migrate along with its mirror charge δ+ and progressively cover the Pt/gas interface. They increase the work function of the metal [22] and consequently weaken the Pt-O bond of chemisorbed oxygen atoms O_{ad}. Bond weakening induces a lowering of the overall O_{ad} coverage, causing the process of oxygen intrusion into the platinum lattice to be less favorable. This causes a global destabilization of the surface platinum oxide. This process is thought to cause the fast catalyst reactivation shown in Fig. 5.

When no net current is applied (open circuit conditions), a small quantity of $O^{\delta-}$ back-spillover species is still present on the surface. They are called natural back-spillover species [20] and they could be the cause of the very slow spontaneous open circuit reactivation shown in Fig. 4.

XPS measurements indicate that mostly metallic platinum is found on the surface of the film after anodic polarization in air at 600°C and in the reactive gas at 525°C (samples 4 and 7, respectively). Cathodic polarization, however, has a deactivating effect because it causes the reaction 5.2 to be reversed (consumption of the back-spillover species). XPS showed that cathodic polarization does not destabilize the oxide (sample 3).

The effect of the back-spillover species (activating) can be seen as the process opposing the oxide formation process (deactivating) presented in the previous section (5.4.1).

A very similar behavior has been observed with YSZ supported Rh catalyst. It was found that oxidative treatment at high temperature caused the deactivation of the catalysis [13, 23]. Catalytic rate oscillations were also observed [11, 13] and were related to the presence of two surface states (metallic and oxide Rh) with very distinct catalytic activity. As in the present work, the activity of the deactivated (oxidized) catalyst was permanently enhanced by polarization (electrochemically induced reactivation). Similarly, the electrochemically induced reactivation was related to the oxide destabilizing effect of the back-spillover species.

Influence of the polarization duration t_{pol} on the catalytic rate transients
As postulated in the generally admitted sacrificial promoted model of EPOC [20, 21], the electrochemically produced back-spillover species is consumed both by reaction with ethylene and by desorption. When balance between electrochemical production and consumption is reached, the electro-promoted rate of reaction 5.1 reaches a steady state

and it remains roughly constant during the whole polarization period, meaning that no more alteration of the catalyst/gas interface occurs. However, Fig. 6 and Fig. 7 indicate that during this apparent steady state period, the polarization still alters the system. However, the alteration does not concern directly the gas exposed Pt surface. It must then occur at another location on the $O_{2(g)}$,Pt/YSZ system, "hidden" from the gas phase. The very fascinating feature shown in these figures is that the hidden alteration only affects the catalytic activity once the circuit is opened. It only affects the relaxation transient. The very long characteristic times implicated in this effect indicate that the hidden alteration is linked to very slow processes, even at high temperatures (up to 600°C).

In addition, comparing the relaxation transients in Fig. 6 and Fig. 7 suggest that the reverse alteration of both the catalytic surface and the hidden location are temperature activated. Indeed, at 600°C and at very long polarization times (t_{pol} = 11 h), the effect of the hidden promoter already vanishes at t_{relax} = 6.5 h, whereas a time twice as high (13 h) is needed at 525°C. The different kinetic behaviors between the visible and the hidden alteration allow their effects to be more distinctly perceived at 600°C than at 525°C. Indeed, at 600°C for long t_{pol}, when the current is switched off, the catalytic rate first reaches a minimum (almost the initial rate r_0) before rising to a maximum value (see arrow in Fig. 7). This indicates that the traditional back-spillover species, responsible for the promotion during polarization, is almost totally consumed when the effect of the hidden alteration appears.

The nature of the anodically produced hidden alteration

For a better understanding of the anodic polarization effect on the $O_{2(g)}$,Pt/YSZ system, techniques such as single and double step chronoamperometry, chronocoulometry, chronopotentiometry and programmed cyclic voltammetry were performed in absence of ethylene. The results were presented and discussed in chapters 3 and 4. They indicated that application of an anodic polarization on the $O_{2(g)}$,Pt/YSZ system caused short and long term charge storage in the form of Pt-O species.

$$Pt + O^{2-} \rightleftharpoons Pt - O + 2e^- \qquad\qquad 5.3$$

In particular, distinct peaks observed by linear sweep voltammetry measurements suggested that three Pt-O species were formed during the anodic treatment. The location of these species on the $O_{2(g)}$,Pt/YSZ system is schematically represented in Fig. 14. The first anodically produced Pt-O species was attributed to an oxygen monolayer formed at the Pt/YSZ interface (1 in Fig. 14). The amount of this species saturated at short polarization times (10 min), due to the very limited amount of storage sites at this interface. Located on a hidden interface, this species has no direct effect on the catalytic rate. The second Pt-O species was attributed to the back-spillover species $O^{\delta-}$ (2 in Fig. 14). As mentioned earlier, its location at the Pt/gas interface causes the electrochemical promotion of catalysis (EPOC). The amount of this species was found to saturate after about one hour of anodic polarization, in agreement with the polarization time needed to reach the promoted steady state in Fig. 6 and Fig. 7.
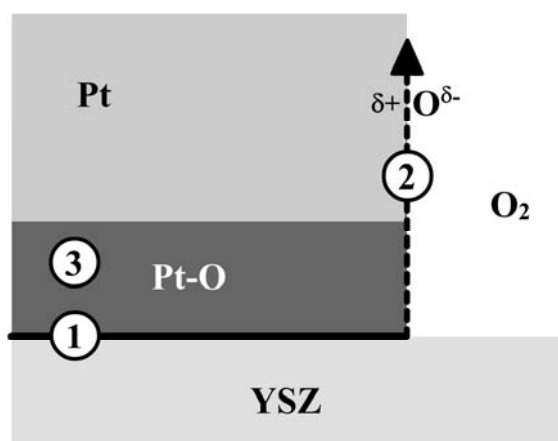
Fig. 14   Scheme of the locations of oxygen storage under anodic polarization according to the model proposed in chapter 4.

The third Pt-O species, appearing consecutively to the saturation of the first species, was attributed to the growth of the oxide layer toward the bulk of the Pt phase (3 in Fig. 14). The amount of this species did not saturate, even at long polarization time (t > 2000 min), indicating a very large charge storage capacity. The stored amount corresponding to this third peak was found to obey a $t^{1/2}$ kinetic law, typical for diffusion-controlled processes.

By comparing the results presented in this chapter and the model proposed in chapter 4, intriguing similarities are found. Indeed, in both chapters, it is evidenced that the anodic polarization produces oxygen species which accumulate on the $O_{2(g)}$,Pt/YSZ system.

Moreover, in both cases, there is a strong influence of the polarization duration and the effects are characterized by very large time constants. Considering the high experimental temperatures, this suggests very slow processes, such as solid phase diffusion.

Based on these similarities, we speculate that the results presented in these two chapters are linked. In other words, the anodic effects observed in catalysis experiments are caused by the anodic oxygen storage process at various locations of the system, as discussed in chapter 4 and schematized in Fig. 14.

It is important to note that catalysis experiments can only provide information on the state of the gas exposed platinum surface (catalytically active). For instance, the presence of $O^{\delta-}$ back-spillover species causes an increase of the catalytic activity, whereas the presence of oxides causes a deactivation. In contrast, electrochemical experiments can only provide information on the species that undergoes electrochemical reactions. This includes the $O^{\delta-}$ back-spillover species but also the species present at the Pt/YSZ interface.

Consequently, in agreement with the sacrificial promoter model, the increase in catalytic activity under anodic polarization is caused by the presence of $O^{\delta-}$ back-spillover species (2 in Fig. 14). In contrast, the effect of the polarization duration t_{pol} on the relaxation transients (see Fig. 6 and Fig. 7) is caused by the storage of oxygen at the Pt/YSZ interface and inside the Pt phase. Since these oxygen species are located away from the catalytically active surface, they do not modify the catalytic rate. However, somehow, they are revealed to the catalytic surface once the current is interrupted and once the back-spillover species are consumed. They can diffuse along the Pt/YSZ interface to the tpb and then alter the catalytically active surface. Indeed, as mentioned in chapter 2, the diffusion of oxygen atoms along the electrode/electrolyte interface has been reported in literature.

The cathodic peak in programmed voltammetry on the $O_{2(g)}$,Pt/YSZ system in the presence of ethylene (Fig. 8) indicates that the hydrocarbon does not prevent the oxygen storage process. In addition, the charge given by peak integration follows a $t_h^{1/2}$ law (Fig. 9), as reported in chapter 4, indicating a diffusion-controlled process. This supports the idea that the storage process involves either the strongly bonded $O^{\delta-}$ back-spillover species (2 in Fig. 14), the diffusion of oxygen into the Pt phase (3 in Fig. 14) or, more likely, the sum of both processes.

To interpret the effect of the prolonged anodic polarization on the relaxation transients (Fig. 6 and Fig. 7), the first approach could be to simply see the platinum as an oxygen

supplier for the oxidation of ethylene. Indeed, as mentioned in chapter 2, platinum oxide can play the role of the oxidant in the reaction of hydrocarbon oxidation [24].

This oxygen supplier function can be compared to the role of ceria in three-way catalysts. Indeed, in such systems, ceria is known to store oxygen when exposed to lean gas conditions (eq. 5.4) and play the role of oxidant for the combustion of soot and the oxidation of CO under rich gas conditions (eq. 5.5).

Lean: $$Ce_2O_3 + \tfrac{1}{2}O_2 \longrightarrow CeO_2 \qquad\qquad 5.4$$

Rich: $$CeO_2 + CO \longrightarrow Ce_2O_3 + CO_2 \qquad\qquad 5.5$$
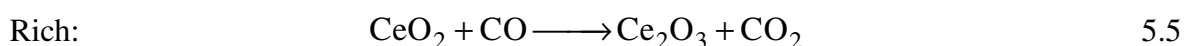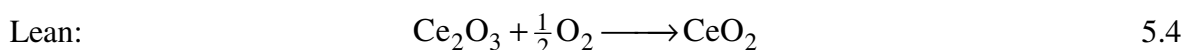
The major difference between the oxygen storing function of ceria and Pt-O in the present case is that the Pt-O species is produced electrochemically under anodic polarization rather than by exposition to a lean gas mixture.

Based on this idea, a similar mechanism is assumed involving oxygen storage under polarization and consumption of stored oxygen by the hydrocarbon during relaxation at open circuit.

$$Pt + O^{2-} \longrightarrow Pt-O + 2e^- \qquad\qquad 5.6$$

$$6\,Pt-O + C_2H_4 \longrightarrow 2\,CO_2 + 2\,H_2O + 6\,Pt \qquad\qquad 5.7$$

During the anodic polarization, oxygen species are stored inside the Pt electrode via the Pt/YSZ interface (storage location 3 in Fig. 14). This corresponds to reaction 5.6.

These Pt-O species, hidden from the catalytic surface, do not directly alter the catalytic rate. However, in parallel, the promoting $O^{\delta-}$ species are also anodically produced and back-spill over the gas exposed Pt surface (2 in Fig. 14), causing the catalytic rate increase. When the current is switched off, the $O^{\delta-}$ species are consumed by reaction with ethylene and a decrease in the catalytic activity is observed. The Pt-O species, located inside the Pt phase (3 in Fig. 14) diffuse in the solid and along the Pt/YSZ interface toward the tpb to the catalytic surface. It can then react with ethylene (eq. 5.7) to

contribute to the reaction observed after current interruption (relaxation transients). As discussed in chapter 4, the diffusion of oxygen in Pt is known to be a very slow process. This may explain the very long relaxation transients seen in Fig. 6 and Fig. 7.

Because the Pt-O species are produced electrochemically, it is straightforward to calculate the maximum amount of oxygen that could be stored electrochemically, according to reaction 5.6. Indeed, using Faraday's law, one determines the amount of oxygen N_F passing through the cell during the total polarization period t_{pol} (eq. 5.8)

$$N_F = I \cdot t_{pol} / 2F \qquad\qquad 5.8$$

where I is the current passing through the cell during the polarization.

In consequence, N_F corresponds to the amount of oxygen atoms which could be stored at the $O_{2,(g)}$ Pt/YSZ system with a 100% charge storage yield (CSY = 100%).

In fact, the real amount of stored oxygen must represent only a fraction of N_F because the majority of the oxygen passing through the cell desorbs in the gas phase as O_2. Indeed, it has been found in chapter 4 that the charge storage yield (CSY) is in the order of a few percents. In addition, in presence of ethylene, a fraction of the oxygen passing through the cell is consumed in the catalytic reaction.
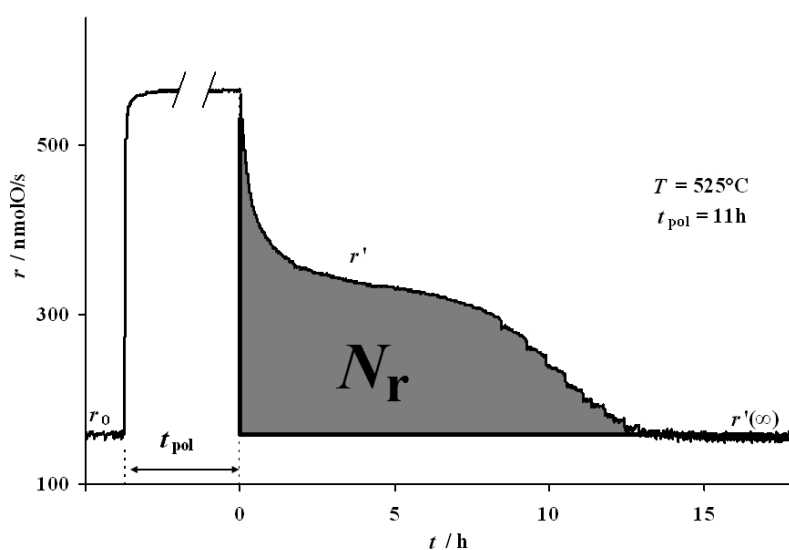
Fig. 15   Graphic representation of the integrated amount of oxygen N_r involved in the catalytic reaction after current interruption

The amount N_r of oxygen species consumed via reaction 5.7 after the current interruption can be calculated by integrating the area between the relaxation transient curve and the base line given by the unpromoted catalytic rate (see Fig. 15).

Define the oxygen storage efficiency Λ_{OS} as the ratio between the amount N_r of oxygen consumed by reaction with ethylene and the amount of electrochemically stored oxygen assuming a CSY = 100%.

$$\Lambda_{OS} = N_r / N_F \qquad\qquad 5.9$$

Λ_{OS} represents the faction of oxygen, electrochemically stored during t_{pol}, which is found to react with ethylene once the polarization is switched off. If the catalytic r' rate enhancement, after current interruption, is simply due to the consumption of the stored Pt-O species, the maximum Λ_{OS} value should be $\Lambda_{OS} = 1$. This would correspond to the ideal case, where all the oxygen passing through the cell is stored (CSY = 100%) and reacts later with ethylene.

Fig. 16   Effect of the polarization time t_{pol} on the oxygen storage efficiency Λ_{os} (as defined by eq. 5.9) at 525°C and 600°C. $pC_2H_4 = 0.25$ kPa, $pO_2 = 1$ kPa.

Fig. 16 shows the Λ_{OS} values in function of t_{pol} for $T = 525°C$ and for $T = 600°C$. The Λ_{OS} values all exceed 1, for $T = 525°C$ as for $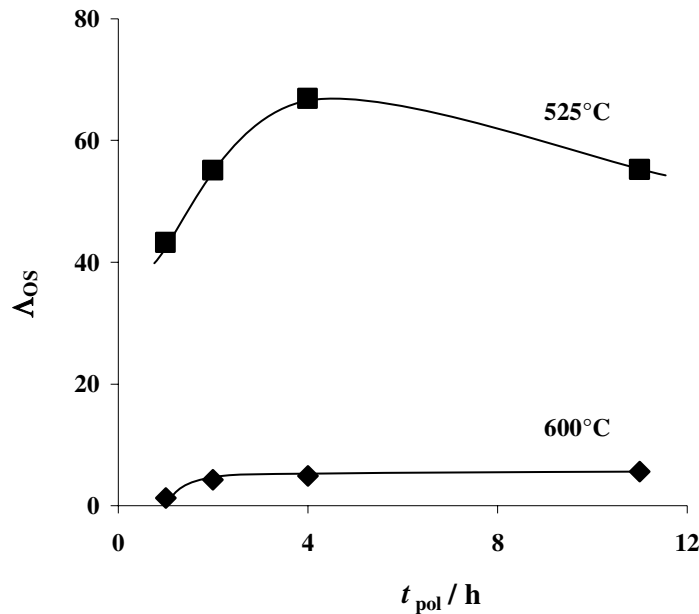T = 600°C$. This indicates that the r' rate enhancement after current interruption is not simply due to the consumption of the hidden Pt-O by ethylene (eq. 5.7). This implies that the oxygen involved in the reaction with ethylene during the r' rate enhancement is oxygen originating from the gas phase, as in the model of EPOC. The improved reactivity of these oxygen atoms must then be caused by an effect identical to that of the $O^{\delta-}$ back-spillover species.

Based on this deduction, the following scenario is proposed to interpret the fascinating rate transients shown in Fig. 6 and Fig. 7. The application of the anodic polarization causes the flooding of $O^{\delta-}$ back-spillover species over the gas-exposed surface, in agreement with the promoter mechanism of EPOC. However, in parallel, the anodic polarization produces another type of promoter, which is stored away from the metal/gas catalytically active interface. It is stored at the metal/solid electrolyte interface and spreading into the platinum bulk (3 in Fig. 14). These locations are "hidden" from the catalytic reaction. Therefore, they do not cause an apparent activity change. Once the current is switched off, the "visible" $O^{\delta-}$ back-spillover species, present at the gas-exposed surface, are consumed by reaction with ethylene. This causes a relatively rapid catalytic activity drop. The consumption of the "visible" back-spillover creates a concentration gradient, dragging the "hidden" promoters toward the tpb.
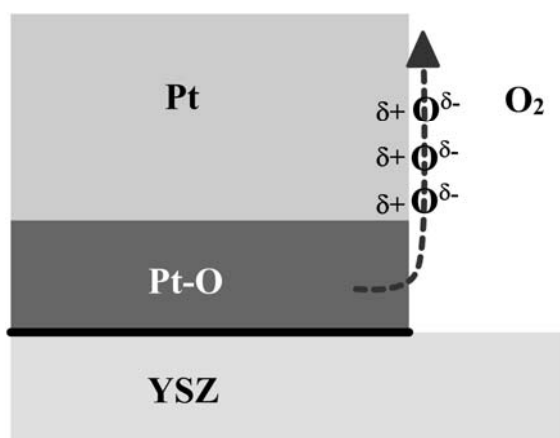

Fig. 17   Path of the anodically produced hidden promoters (3 in Fig. 14) after current interruption.

The diffusion path of the oxygen species is schematized in Fig. 17. The diffusion through Pt is very slow, even at high temperature (Fig. 7). This causes the hidden promoter to appear very slowly. Much time is then necessary to consume all these hidden promoters. Therefore, the high catalytic activity can be maintained even hours after the polarization has been switched off. Finally, when all hidden back-spillover species have been consumed, the catalytic rate goes to its initial value (r' (∞) = r_0).

5.5   Conclusions

In this chapter, the platinum sputtered catalyst film deposited on an YSZ pellet is found to exhibit two different states, an inactive and an active state, toward the catalytic ethylene oxidation reaction. As evidenced by XPS measurements and in agreement with the thermodynamic data for the given system, the inactive (deactivated) state is attributed to surface platinum oxide formation, occurring at T > 550°C in a slightly oxidizing reactive atmosphere (O_2/C_2H_4= 4). Decreasing the reaction temperature to 525°C triggers a slow reactivation of the catalyst and several days are necessary to reach its active state, with most of the catalyst being in its metallic state. The catalyst activity recovery is greatly accelerated by the application of anodic potential pulses. As postulated by the back-spillover mechanism of electrochemical promotion of catalysis, anodic polarization produces an oxide destabilizing species $O^{\delta-}$ that back-spills over the metal/gas surface, weakening the chemisorptive Pt-O_{ad} bond strength. This species is also known to be present, but to much smaller extent, under open circuit conditions. Under cathodic polarization, this species is not produced and no activation is observed.

Anodic polarization of the catalyst in its open circuit steady state (active catalyst) causes a reversible promotion. However, the polarization duration, t_{pol}, is found to have a great influence on the relaxation transient, large t_{pol} causing catalytic rate enhancement even hours after switching off the current. This long-term effect is linked with the oxygen storage processes occurring under long anodic polarization times, as presented in chapter 4. To support this idea, linear sweep voltammetry evidenced that the oxygen storage also occurs in the presence of ethylene, with the same $t^{1/2}$ kinetic law as found for the oxygen storage process. Based on the results presented in the present chapter, the rate enhancing effect of long polarization times is due to oxygen storage occurring at a location, hidden from the gas. When the current is switched off, the hidden oxygen species appear and

cause the enhancement. The obtained values of oxygen storage efficiency, Λ_{OS} greater than 1, evidence that the rate enhancement after current interruption is not simply due to ethylene oxidation by these oxygen species. Consequently, these hidden oxygen species must have a promoting role on the reactivity of the other chemisorbed reactants. They may have the same promoting role as the $O^{\delta-}$ species, responsible for the electrochemical promotion of catalysis under closed circuit. In summary, long anodic polarization times cause the storage of hidden species, away from the catalytic surface. Therefore, they do not cause the promotion of catalysis during the polarization period. However, when the polarization is switched off, these hidden species appear and cause long term promotion of the catalytic activity.

5.6 References

1   G. M. Bancroft, I. Adams, L. L. Coatsworth, C. D. Bennewitz, J. D. Brown, W. D. Westwood, Anal. Chem. 47 (1975) 586

2   N. L. Wu, J. Phillips, J. Appl. Phys. 59 769

3   N. L. Wu, J. Phillips, J. Catal. 113 (1988) 383

4   N. L. Wu, J. Phillips, J. Phys. Chem. 89 (1985) 591

5   C. G. Vayenas, J. N. Michaels, Surf. Sci. 120 (1982) L405

6   M. Baer, M. Falcke, C. Zuelicke, H. Engel, M. Eiswirth, G. Ertl, Surf. Sci. 269-270 (1992) 471

7   K. Krischer, M. Eiswirth, G. Ertl, Surf. Sci. 251-52 (1991) 900

8   M. M. Slin'ko, N. I. Jaeger, Studies in Surface Science and Catalysis 86 (1994)

9   C. G. Vayenas, B. Lee, J. Michaels, J. Catal. 66 (1980) 36

10   I. V. Yentekakis, S. Neophytides, C. G. Vayenas, J. Catal. 111 (1988) 152

11   E. A. Baranova, A. Thursfield, S. Brosda, G. Fóti, C. Comninellis, C. G. Vayenas, Catal. Lett. 105 (2005) 15

12   C. G. Vayenas, C. Georgakis, J. Michaels, J. Tormo, J. Catal. 67 (1981) 348

13   E. A. Baranova, Chemical and Electrochemical Promotion of Supported Rh Catalyst, Thesis Nr. 3245, EPFL, Lausanne (2005)

14   J. Nicole, C. Comninellis, Solid State Ionics 136-137 (2000) 687

15   S. Wodiunig, V. Patsis, C. Comninellis, Solid State Ionics 136-137 (2000) 813

16   S. Wodiunig, C. Comninellis, J. Europ. Ceram. Soc. 19 (1999) 931

17   D. Tsiplakides, J. Nicole, C. G. Vayenas, C. Comninellis, J. Electrochem. Soc. 145 (1998) 905

18   G. Foti, V. Stankovic, I. Bolzonella, C. Comninellis, J. Electroanal. Chem. 532 (2002) 191

19   J. Nicole, D. Tsiplakides, C. Pliangos, X. E. Verykios, C. Comninellis, C. G. Vayenas, J. Catal. 204 (2001) 23

20   C. G. Vayenas, S. Bebelis, C. Pliangos, S. Brosda, D. Tsiplakides, Electrochemical Activation of Catalysis: Promotion, Electrochemical Promotion, and Metal-Support Interactions (Kluwer Academic / Plenum Publishers, New York, 2001)

21   D. Tsiplakides, S. Balomenou, A. Katsaounis, D. Archonta, C. Koutsodontis, C. G. Vayenas, Catal. Today 100 (2005) 133

22   J. Fleig, J. Jamnik, J. Electrochem. Soc. 152 (2005) E138

23   G. Foti, O. Lavanchy, C. Comninellis, J. Appl. Electrochem. 30 (2000) 1223

24   C.-B. Wang, H.-K. Lin, S.-N. Hsu, T.-H. Huang, H.-C. Chiu, J. Molec. Catal. A 188 (2002) 201

CHAPTER 6

General discussion, conclusions and perspectives

In this final chapter, the main innovative results obtained in the present work are reviewed and the principal conclusions are drawn. This PhD thesis continues the investigations started several years ago in the "NEMCA group" of Prof. Comninellis at the EPFL. It focuses on the electrochemical promotion of catalysis on YSZ supported Pt films for the oxidation of ethylene. It has been shown that the Pt film exhibits various activities depending on the oxidation state of its surface. Anodic polarization has been found to enhance dramatically the reactivation process of the film, similarly to the so-called "permanent EPOC" effect, reported for Rh and IrO_2 catalysts. The enhanced reactivation is related to the oxide destabilizing effect of the anodically produced $O^{\delta-}$ back-spillover species. In addition, for the first time, electrochemical promotion of ethylene oxidation on YSZ supported Pt was observed at temperatures up to 600°C. Very intriguing catalytic relaxation transients were observed after prolonged anodic polarization times. Indeed, it was found that enhanced catalytic activity was maintained for up to 10 hours after current interruption. This phenomenon is suggested to be related to the results obtained by electrochemical techniques on the $O_{2(g)}$,Pt/YSZ system. Indeed, these techniques evidenced that prolonged anodic polarization periods cause the storage of Pt-O species at various locations of the electrode, some of which are hidden from the gas phase. Subsequently, we have proposed an original model postulating that hidden promoter species are produced during the prolonged anodic polarization and appear when the current is interrupted, leading to a time extended promotion.
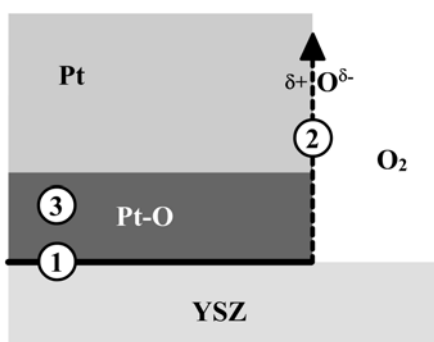
6.1   General discussion

As reviewed in chapter 2 of this work, literature reports that a vast variety of oxygen species can be found on platinum, depending on parameters such as the temperature, the surrounding gas and the preparation mode of the sample. These oxygen species consist of the chemisorbed oxygen originating from the gas phase and various types of platinum oxides. In cases where platinum is deposited on the YSZ solid electrolyte (the $O_{2(g)}$,Pt/YSZ system), its polarization leads to the electrochemical production of other oxygen species. In particular, the back-spillover $O^{\delta-}$ species is known to be produced under anodic polarization. In addition, anodic polarization generates various other oxygen species, accumulating at diverse geometric location of the $O_{2(g)}$,Pt/YSZ system or desorbing into the gas phase as O_2.

Considering the apparent complexity of the subject, it was decided that the investigations should concentrate on the identification of the oxygen species reported to coexist on the $O_{2(g)}$,Pt/YSZ system. In particular, the studies should focus on the oxygen species being present on the gas exposed Pt surface, as they have a great impact on the catalytic activity of the Pt film.

As reported in literature, the formation of surface Pt oxides usually leads to a deactivated state, compared to clean Pt [1-4]. Given the experimental temperature and oxygen partial pressure, thermodynamic values allow predicting the state of the Pt surface. However, it has been seen that the preparation method and the type of support of the Pt sample can have a great influence on the oxide stability domain. In particular, oxides have been reported to be more stable on YSZ supported Pt films than on unsupported Pt wires. This example illustrates that, despite extended studies on the interactions between platinum and oxygen, the issue of platinum oxide is still ambiguous and matter to discussion.

The anodically produced $O^{\delta-}$ back-spillover species is another oxygen species expected to have a remarkable impact on the catalytic activity of the Pt film. Indeed, as postulated in the theory of EPOC, its presence on the gas exposed Pt surface causes the alteration of the metal work function. Consequently, this modifies the binding strength of the adsorbed reactants, changing the overall catalytic activity. Literature on the electrochemical promotion of catalysis reports remarkable modifications in activity for a vast variety of

reactions on very diverse catalytic materials. Our laboratory reported cases where the electrogenerated modification of the activity was not totally reversible, leading to so-called "permanent EPOC" [5-7]. This effect was related to different stable or metastable states of the catalyst, which could be achieved via electrical polarization. In particular, it was found that deactivated oxidized rhodium catalysts could be reactivated by prolonged anodic polarization. The electrochemically assisted catalyst reactivation was explained by the oxide destabilizing effect of the $O^{\delta-}$ back-spillover species, in agreement with the theory of EPOC. In the present work, particular importance was given to the study of permanent EPOC on the $O_{2(g)}$,Pt/YSZ system and the role of metastable surface states.

Measurement of the catalytic activity is a key tool for the study of the gas exposed Pt surface state. However, in order to identify the oxygen species present on the $O_{2(g)}$,Pt/YSZ system, one must also consider the other interfaces and phases. Indeed, literature mentions that oxygen species are also found at the Pt/YSZ interface and in the Pt phase [8-11]. Electrochemical techniques can be used to investigate the presence and behavior of oxygen species if they can take part in redox reactions, i.e. if they have access to electrochemical reaction sites (ERS). Electrochemical techniques are well-suited for the study of the $O_{2(g)}$,Pt/YSZ system because they give in situ data on the state of the electrochemically active sites.

In chapter 3 of this work, the technique of cyclic voltammetry has been chosen to characterize the electrochemical response of electrodes prepared via three different methods (sputtering, thermal decomposition and screen-printing). Cyclic voltammetry (CV), known to be a sensitive electrochemical method, appeared as a useful tool to identify the behavior and the nature of the Pt/YSZ contact, an interface that is unavailable to non-destructive surface analysis techniques. As expected, the voltammogram shape was highly influenced by the microstructure and the chemical state of the electrode. In addition, as expected the microstructure, observed by scanning electron microscopy (SEM), was found to depend greatly on the preparation technique.

A pseudocapacitive behavior, characterized by one or two cathodic peaks and an anodic wave, has been distinctly observed in the cyclic voltammogram of the electrodes treated at high temperature (> 1000°C) and the non-porous sputtered electrodes (compact film).

However, heat treatment of the sputtered electrode at 700°C in 20 kPa O_2 resulted in a porous structure, featuring a non-pseudocapacitive behavior.

The charge obtained by integration of the cathodic peak in the cyclic voltammogram of non-porous sputtered electrodes tended to the value of a PtO monolayer. This suggested that the peak corresponds to the reduction of an anodically formed oxide monolayer at the Pt/YSZ interface.

Based on the preliminary studies, the cermet electrode was chosen for additional experiments, for the following reasons:

- Its cyclic voltammogram features two distinct cathodic peaks, indicating the reduction of two different species. Little is known about the second peak because it has been rarely reported and no unanimous interpretation has been given.

- Literature on the electrochemistry of cermet electrodes is less abundant than on non-cermet films.

- Cermet electrodes take more importance with the increasing interest in the field of gas sensing and fuel cells.

The additional electrochemical measurements have been reported in chapter 4 of this work. Various techniques, originally developed for liquid electrochemistry, have been adapted to study the effect of polarization on the $O_{2(g)}$,Pt/YSZ system. These are single and double step chronoamperometry, chronopotentiometry, cyclic voltammetry, chronocoulometry, steady state polarization and impedance spectroscopy. It is worthwhile to note that the chronoamperometry and chronopotentiometry results are completely innovative given that these techniques are hardly ever reported in literature for the $O_{2(g)}$,Pt/YSZ system.

The results of all these techniques support the same conclusion. They demonstrate that under anodic polarization, two parallel reactions take place. The first reaction is the oxygen evolution (eq. 6.1)

$$O^{2-}{}_{(YSZ)} \longrightarrow \frac{1}{2}O_{2(gas)} + 2e^- \qquad\qquad 6.1$$
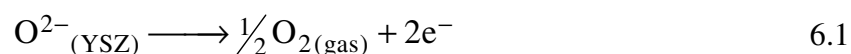
This reaction gives rise to a steady state current under a constant applied potential E_{WR}.

The other reaction is the oxygen storage (oxygen injection) (eq. 6.2).

$$Pt + O^{2-} \longrightarrow Pt - O + 2e^- \qquad\qquad 6.2$$
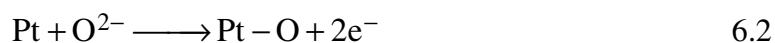
The anodic reaction stores charge on the $O_{2(g)}$,Pt/YSZ system in the form of Pt-O species. Consequently, it gives rise to a time dependent current under a constant applied potential E_{WR} (as in chronoamperometry). It is thought to be responsible for the pseudocapacitive behavior of the electrode, e.g. the peaks in cyclic voltammetry.

Linear sweep voltammetry measurements indicated that applying an anodic potential E_h during a time period t_h causes the storage of three types of Pt-O species. Then, by sweeping the potential linearly toward negative values, these species were successively reduced, giving rise to cathodic current peaks (see Fig. 1). This result, reported for the first time for the $O_{2(g)}$,Pt/YSZ system, suggests that the oxygen storage (injection) and the oxygen release (ejection) produces Pt-O species of different natures, characterized by distinct kinetic behaviors.
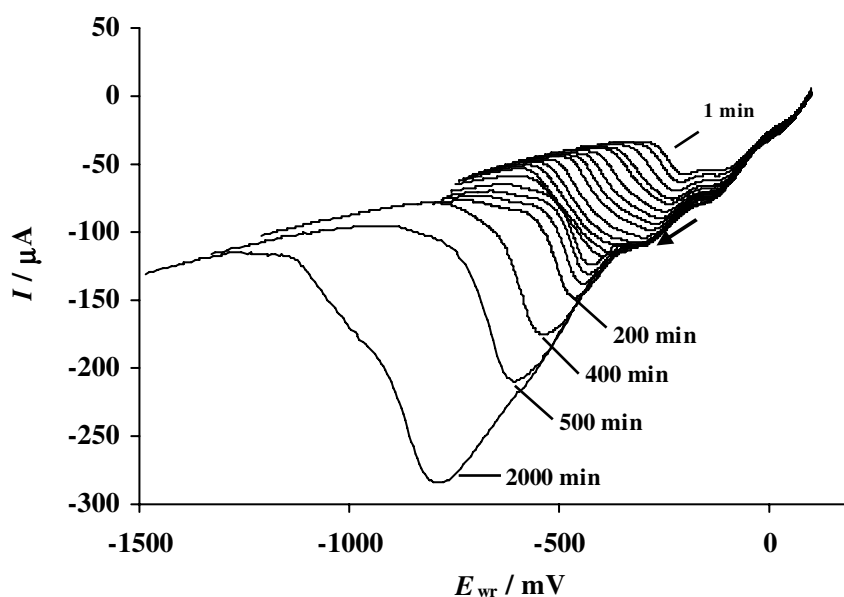

Fig. 1   Voltammogram of the $O_{2(g)}$,Pt/YSZ system. Effect of the holding time, t_h, at $E_h = 100\,\text{mV}$ on the first cathodic scan. $T = 450°C$, $pO_2 = 20\,\text{kPa}$, $\nu = 10\,\text{mV/s}$.

Based on the saturation and kinetic characteristic of each peak, these three species were attributed to Pt-O species being stored at three different locations on the electrode:

1) the first peak was characterized by a fast growth. It saturated after a few minutes at a low storage value. Corresponding to the storage of oxygen at a location easily available for the electrochemical reaction, it has been attributed to the build-up of an oxide monolayer at the Pt/YSZ interface, in agreement with the interpretation usually found in literature (1 in Fig. 2).

2) the second peak was characterized by a slower growth. It saturated after roughly one hour at a level higher than the first peak. Corresponding to oxygen storage at a location which is not directly available to the electrochemical reaction, it has been attributed to the storage of Pt-O species along the gas exposed Pt surface via the tpb (2 in Fig. 2). It is worthwhile to note that this species may alter the Pt gas exposed surface, i.e. the site of the catalytic reaction. It is related to the $O^{\delta-}$ back-spillover species, responsible for the electrochemical promotion of catalysis.
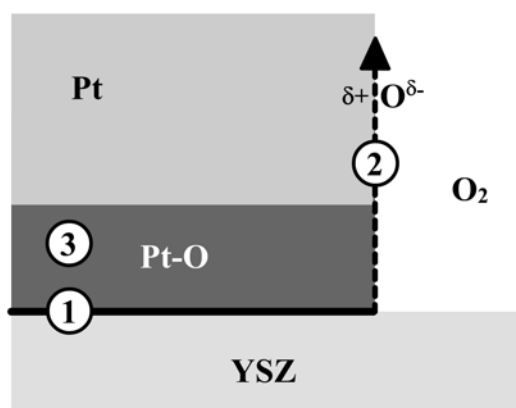
Fig. 2   Scheme of the locations of the oxygen storage processes under anodic polarization according to the model proposed in chapter 4.

3) the third peak is characterized by a very slow growth, with a $t^{1/2}$ kinetic law, which is typical for diffusion controlled processes. The amount of this species has not been found to reach saturation, even at very long polarization times (> 2000 min), indicating that it must be stored in a phase rather than at an interface. It has been attributed to the diffusion of oxygen atoms into the bulk of the platinum electrode via the Pt/YSZ interface (3 in Fig. 2).

In chapter 5 of this work, ethylene was added to the supplied gas mixture ($O_2/C_2H_4 = 4$), causing its catalytic oxidation by oxygen. Indeed, platinum is known to be a very good catalyst for this reaction. However, the catalyst film, deposited on the YSZ pellet, was found to exhibit two different states, an inactive and an active state, with respect to the catalytic reaction. As evidenced by XPS measurements and in agreement with the thermodynamic data for the given system, the inactive (deactivated) state has been attributed to the formation of surface platinum oxide at $T > 550°C$. Decreasing the reaction temperature to $525°C$ caused the slow spontaneous reactivation of the catalyst and several days were necessary to reach the active state, where most of the catalyst was present in its metallic state, according to XPS data.

The catalyst activity recovery could be accelerated by the application of anodic potential pulses. In agreement with the mechanism of EPOC, this was explained by the oxide destabilizing effect of the $O^{\delta-}$ species. Indeed, the anodically produced species back-spills over the metal/gas surface, weakening the Pt-O bond strength. The observed electrochemically assisted recovery of catalytic activity is very similar to the "permanent EPOC" reported on YSZ supported Rh films, also interpreted by the oxide destabilizing effect of $O^{\delta-}$ [12].

When anodic polarization was applied to the catalyst in its stable active state, a reversible promotion was observed at temperatures as high as $600°C$, which is remarkable given that electrochemical promotion on this system is reported to be limited to around $450°C$ [7]. In these experiments, the polarization duration, t_{pol}, was found to have a great influence on the relaxation transient after the current interruption. This effect, reported for the first time on the $O_{2(g)}$,Pt/YSZ system, is illustrated in Fig. 3. Large t_{pol} caused a catalytic rate enhancement even hours after switching off the current. This long-term effect was thought to be linked with the oxygen storage processes occurring under long anodic polarization times, as presented in chapter 4. This is supported by linear sweep voltammetry experiments, which evidenced that the oxygen storage also occurs in the presence of ethylene, with the same $t^{1/2}$ kinetic law as found in oxygen atmosphere.

Based on these results, the open circuit rate enhancing effect of long polarization times was attributed to oxygen storage occurring at a location hidden from the gas (i.e. no influence on catalysis). When the current is switched off, the hidden oxygen species

appear and cause the long term enhancement. This "hidden promoter" model is evidenced by oxygen storage efficiency values Λ_{OS} greater than 1. This demonstrates that the rate enhancement after current interruption is not simply due to ethylene oxidation by these oxygen species. Consequently, these species are thought to have the same promoting role as the $O^{\delta-}$ back-spillover species, responsible for the electrochemical promotion of catalysis under closed circuit.
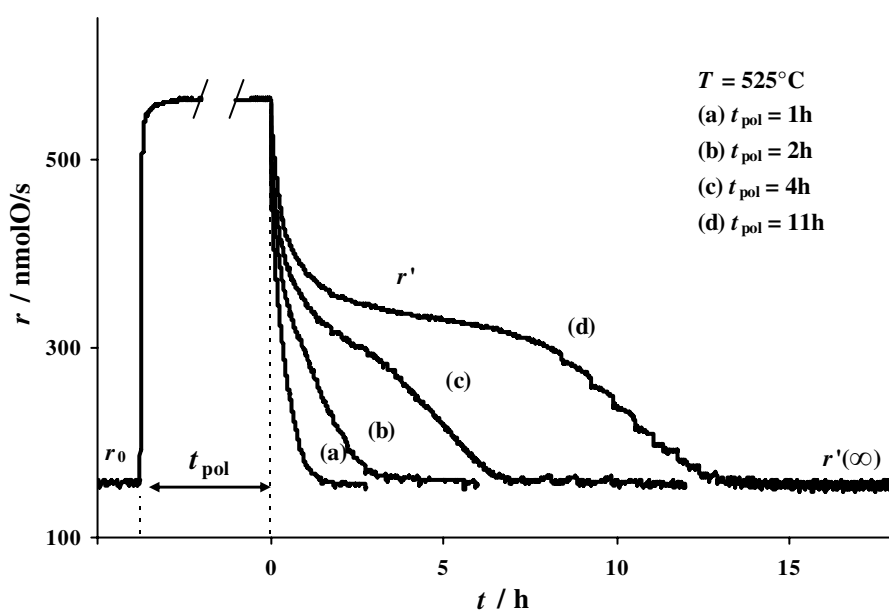
Fig. 3   Effect of the polarization time t_{pol} on the rate transient of EPOC. $T = 525°C$, $pC_2H_4 = 0.25$ kPa, $pO_2 = 1$ kPa.

6.2   Conclusions

In this work, the $O_{2(g)}$,Pt/YSZ system has been studied by a variety of electrochemical techniques and by two ex situ surface analysis techniques (SEM and XPS). The catalytic activity of the system has been also investigated using the reaction of ethylene combustion. The most relevant results are summarized:

-        We have evidenced the great influence of the electrode deposition technique on the featured microstructure and on the electrochemical response given by cyclic voltammetry.

- Further electrochemical techniques suggested that, in parallel to the reaction of oxygen evolution, prolonged anodic polarization causes the storage of Pt-O species at various locations of the electrode, on the gas exposed Pt surface but also at other hidden phases and/or interfaces. These charging/discharging processes are responsible for the pseudocapacitive behavior of the electrode. Linear sweep voltammetry measurements indicated that, by application of an anodic potential, at least three types of Pt-O species were stored, following distinct kinetics. Based on the effect of the polarization time on the amount of the stored Pt-O species, they were attributed to three different locations on the electrode: 1) at the Pt/YSZ interface, 2) diffusing from the tpb toward the Pt/gas interface, 3) diffusing from the Pt/YSZ interface toward the bulk of the platinum electrode.

- It has been shown that the Pt film exhibited various activity states toward the catalytic oxidation of ethylene, depending on the oxygen species present at its surface. Oxides were found to cause deactivation, whereas anodically produced $O^{\delta-}$ species caused the reactivation via destabilization of the oxide, similarly to the so-called "permanent EPOC" effect. Anodic polarization also caused reversible electrochemical promotion of catalysis at unusually high temperatures (600°C). In addition, very intriguing catalytic relaxation transients were observed after prolonged anodic polarization times. Indeed, it was found that enhanced catalytic activity could be maintained for up to 10 hours after current interruption.

By discussing and combining these latter results, the related literature, the state of the art model of EPOC, and the results obtained by electrochemical techniques, we proposed an original model based on the processes of Pt-O charging/discharging at various locations of the $O_{2(g)}$,Pt/YSZ system.

According to this model, anodic polarization produces $O^{\delta-}$ back-spillover species, promoting the catalytic activity, in agreement with the mechanism of EPOC. In parallel, hidden oxygen species are stored at the Pt/YSZ interface and diffuse toward the Pt phase. When the polarization is switched off, these hidden oxygen species diffuse to gas-exposed surface and cause non-Faradaic promotion, as back-spillover $O^{\delta-}$ do. The large amount of stored charge and its slow diffusion controlled emergence causes the rate enhancement to last for hours.

As mentioned in chapter 2, the aim of this work was to clarify some ambiguous points in the phenomenon of EPOC, especially concerning the nature of the oxygen species present on the system and their effects on the catalytic activity, with special attention to the phenomenon of permanent promotion (P-EPOC). The aim has been reached in the sense that we have produced innovative results on the subject, bringing new elements of discussion to the model of EPOC, in particular, for the case of very long polarization periods.

6.3   Perspectives

-       From the practical point of view, the phenomena of the electrochemically assisted catalyst reactivation and the open circuit promotion by previously electro-generated hidden species, experienced and discussed in this work, are of major importance in applied devices such as the monolith electropromoted reactor (MEPR). Indeed, in these phenomena, polarization causes long lasting positive effects on the catalytic activity, even hours after current interruption. Moreover, the appropriate polarization process can reactivate, almost instantaneously, a deactivated Pt catalyst.

-       From a fundamental point of view, by the proposed model, this work brings new insight to the phenomenon. However, it focuses on EPOC experiments of YSZ supported Pt films in an invariant C_2H_4/O_2 gas mixture and on electrochemical techniques performed at a constant temperature. Studies in other experimental conditions electrodes of other preparations should be performed to generalize the intriguing long polarization time effects. This would help elucidate some points of the proposed model, bringing support or leading to its revision.

Recent experiments, carried out in our laboratory on YSZ supported film prepared by deposition of a Pt paste, confirmed the catalytic activity bistability of the Pt film caused by high temperature treatment in an identical oxidative mixture. Moreover, as in the present work, the activity recovery was induced by an anodic polarization. These recent results are an encouraging first step in the generalization of the effects, originally reported in this work, and give a first positive response to the model proposed.

-       Similarly, reproduction of these results should be done using electrodes of well-defined microstructure, such as microelectrodes. In addition, the effects of extended

anodic polarization should be studied with other electrode materials, other electrolytes and for various catalytic reactions.

- As for the techniques used, temperature programmed desorption (TPD) could be used to detect the various oxygen species produced at long polarization times and after interruption of the current.

- In addition, a broad study by electrochemical impedance spectroscopy (EIS) could be performed on the system after various polarization treatments. The variation of the parameters derived from EIS would help to interpret the effects of extended polarization.

- As mentioned in bibliography (Chapter 2), work function measurements of the catalytic surface gives key information on the species present. Such measurements on the catalyst in its different states could confirm the effect of very long polarization times.

- Extended strong polarization steps are commonly used to activate zirconia based gas sensors [13-15]. Although the activating mechanism of polarization is still unknown, it may be linked with the presence of Pt-O species. Indeed, it has been suggested that the presence of oxygen-containing species, such as oxides, on key sites of the electrode could lead to strong increase of the polarization resistance [13, 16]. The proposed model, dealing with the presence of various Pt-O species at different locations of the electrode may bring some elements of comprehension to the activating effect.

6.4   References

1   J. Dicke, H. H. Rotermund, J. Lauterbach, Surf. Sci. 454-456 (2000) 352

2   C. G. Vayenas, J. N. Michaels, Surf. Sci. 120 (1982) L405

3   C. G. Vayenas, B. Lee, J. Michaels, J. Catal. 66 (1980) 36

4   C. G. Vayenas, C. Georgakis, J. Michaels, J. Tormo, J. Catal. 67 (1981) 348

5   J. Nicole, D. T. Tsiplakides, S. Wodiunig, C. Comninellis, J. Electrochem. Soc. 144 (1997) L312

6   J. Nicole, C. Comninellis, J. Appl. Electrochem. 28 (1998) 223

7   C. G. Vayenas, S. Bebelis, C. Pliangos, S. Brosda, D. Tsiplakides, Electrochemical Activation of Catalysis: Promotion, Electrochemical Promotion,

and Metal-Support Interactions (Kluwer Academic / Plenum Publishers, New York, 2001)

8   Tsaofang Chao, K. J. Walsh, P. S. Fedkiw, Solid State Ionics 47 (1991) 277

9   A. Jaccoud, G. Foti, C. Comninellis, Electrochim. Acta 51 (2006) 1264

10   M. W. Breiter, K. Leeb, G. Fafilek, J. Electroanal. Chem. 434 (1997) 129

11   E. Varkaraki, Electrochemical promotion of an IrO2 catalyst for the gas phase oxidation of ethylene, Thesis Nr. 1455, EPFL, Lausanne (1995)

12   E. A. Baranova, Chemical and Electrochemical Promotion of Supported Rh Catalyst, Thesis Nr. 3245, EPFL, Lausanne (2005)

13   T. Kawai, N. Hayakawa, T. Yamada, US Pat. 5,433,830, Method of Activating Zirconia Oxygen Sensor, 1995

14   H. K. O. Yasushi, US Pat. 4,702,816, Oxygen concentration detection system 1987

15   Takao Murase, T. Yoshimura, US Pat. 5130002, Method of processing oxygen concentration sensor by applying AC current, and the thus processed sensor, 1992

16   S. Sridhar, V. Stancovski, U. Pal, Solid State Ionics 100 (1997) 17

List of symbols

1 List of acronyms

CE   counter electrode

CV   cyclic voltammetry

EIS   electrochemical impedance spectroscopy

EP   Electrochemical Promotion

EP_r reversible electrochemical promotion

EP_i irreversible electrochemical promotion

ERS   electrochemical reaction site

EPOC   electrochemical promotion of catalysis

M   metal

MEPR   monolithic electrochemically promoted reactor

NEMCA   non-Faradaic electrochemical modification of catalytic activity

P-EPOC   permanent electrochemical promotion of catalysis

RDS   rate determining step

RE   reference electrode

SE   solid electrolyte

SEM   scanning electron microscopy

SOFC   solid oxide fuel cells

tpb   triple phase boundary

TPD   temperature programmed desorption

WE   working electrode

XPS   X-ray photoelectron spectroscopy

YSZ   yttria stabilized zirconia (ZrO_2 doped with 8mol% Y_2O_3)

2   Roman symbols

Symbol	Meaning	Units
A	electrode geometric surface	m^2
a_O	oxygen activity	-
C_d	double layer capacitance	F
c_i	concentration of the species i	$mol\ m^{-3}$
D	diffusion coefficient	$m^2\ s^{-1}$
d	interatomic distance	m
E_h	holding potential	V
E_p	peak potential	V
E_{pre}	pretreatment potential	V
E_r	reversal potential	V
E_{WR}	potential difference between the working and the reference electrode	V
E^0	standard potential	V
F	Faraday constant	$96485\ C\ mol^{-1}$
f	frequency	Hz
I	current	A
I_p	peak current	A
I_R	current of the rate determining step	A
I_0	exchange current	A
i	current density with respect to the geometric surface area	$A\ m^{-2}$
K_i	equilibrium constant	-
k_i	rate constant	$m\ s^{-1}$
L_t	diffusion length	m
l_{tpb}	length of the three phase boundary	m
N	number of atom	-
n	number of electrons exchanged in the global reaction	-
p	partial pressure	Pa
p°	standard pressure	Pa
Q	charge	C
Q_{extra}	extra charge	C
R	ideal gas constant	$8.3145\ J\ K^{-1}\ mol^{-1}$

R_{ct}	charge transfer resistance	Ω
R_{chem}	resistance due to non-electrochemical processes	Ω
R_p	polarization resistance	Ω
R_{tot}	global electrode resistance	Ω
R_S	electrolyte resistance	Ω
r	number of electron exchanged during the RDS (in section 4.2.7)	-
r	rate of the catalytic reaction	molO s^{-1}
r_0	open circuit catalytic rate before polarization	molO s^{-1}
r'	open circuit catalytic rate after polarization	molO s^{-1}
T	temperature	°C, K
t	time	s
t_h	holding time	s
t_{pol}	polarization time	s
t_{pre}	pretreatment time	s
V_O	oxygen vacancy in lattice	
Z'	real component of impedance Z	Ω
Z''	imaginary component of impedance Z	Ω

3 Greek symbols

α	transfer coefficient	-
α_a	anodic transfer coefficient	-
α_c	cathodic transfer coefficient	-
β	charge transfer coefficient in the elementary electrochemical reaction	-
γ	permanent rate enhancement factor	-
$\overrightarrow{\gamma}$	number of electron transfer steps preceding the RDS	-
$\overleftarrow{\gamma}$	number of electron transfer steps following the RDS	-
η	overpotential	V
Λ	Faradaic efficiency	-
Λ_{OS}	oxygen storage efficiency	-
ν	potential sweep rate	V s^{-1}
ν	number of times the RDS step is repeated (in section 4.2.7)	-

ρ	catalytic rate enhancement factor	-
τ	time constant	s
φ	phase shift in impedance spectroscopy	-
φ	Galvani potential	V

4 Subscripts

ad   relative to an adsorbed species

charging   relative to the charging process (electrochemical oxygen storage)

discharging   relative to the discharging process (electrochemical oxygen release)

ss   relative to the steady state

JACCOUD Arnaud   28 (July 9th 1978)

Chez-les-Favez 1   Single

1610 Vuibroye (VD)   Swiss

Switzerland

+41 79 382 49 19

arnaud.jaccoud@a3.epfl.ch

EDUCATION AND PROFESSIONAL EXPERIENCE

- **PhD thesis** at the Swiss Federal Institute of Technology   2003-2006
  in Lausanne (**EPFL**)

  Subject: Electrochemical promotion of platinum catalysts for gas phase reactions

  (Application for fuel cells, catalysts, gas sensors)

- **Chemical Engineer** (Bachelor and Master Studies at the EPFL)   1998-2003

  Diploma work on the promotion of rhodium catalysts

- High School (Mathematics and Sciences) Lausanne   1995-1998

- Frankenmuth **High School MICHIGAN (USA)**   1994-1995

  Diploma with distinctions:

  High School's Honor Roll and **Exemplary Attendance**

PhD ACHIEVEMENTS AND ACQUIRED SKILLS

- Part time professor assistant for the teaching of undergraduates EPFL students
- Experience in the use of scanning electron microscopes

LANGUAGES

French:	Mother tongue
English:	Fluent (language of the PhD thesis and many public talks)
Spanish:	Fluent (4 months in South America)
German:	Good high school knowledge

Publications

A. Jaccoud, G. Fóti, R. Wüthrich and Ch. Comninellis, Effect of microstructure on the electrochemical behavior of Pt/YSZ electrodes, Topics in Catalysis, in press

A. Jaccoud, G. Fóti and Ch. Comninellis, Electrochemical investigation of platinum electrode in solid electrolyte cell, Electrochimica Acta, 51 (2006)1264-1273

Oral presentations

A. Jaccoud, G. Fóti and Ch. Comninellis, Electrochimie de l'interface Pt/YSZ/O$_2$, 2$^{\text{ème}}$ Workshop sur la promotion électrochimique de la catalyse, 24 June 2004, Université Claude Bernard Lyon (France)

A. Jaccoud, G. Fóti and Ch. Comninellis, Electrochemical regeneration of deactivated catalysts, 3$^{\text{ème}}$ Workshop sur la promotion électrochimique de la catalyse, 7 March 2006, Ecole des Mines, Nancy (France)

A. Jaccoud, G. Fóti and Ch. Comninellis, Electrochemical promotion of Pt catalysts for gas phase reactions, Ceramics Seminars, 18 January 2007, Department of Materials, NONMET – ETH Zurich

Posters

A. Jaccoud, G. Fóti, Ch. Comninellis, Utilisation de la voltamétrie cyclique en phase solide pour l'étude de la surface d'un catalyseur, Séminaire hors ville en chimie inorganique et génie chimique, Octobre 2003, Champéry, (Switzerland)

A. Jaccoud, G. Fóti, Ch. Comninellis, Etude de l'électrode O$_2$, Pt/YSZ, Journées d'électrochimie 2005, 5-8 July 2005, St-Malo (France)